2011

Sealing and cutting of PLA bio-plastic

Julius Vogel
Iowa State University

Sealing and cutting of PLA bio-plastic

by

Julius Vogel

A dissertation submitted to the graduate faculty
in partial fulfillment of the requirements for the degree of
DOCTOR OF PHILOSOPHY

Major: Mechanical Engineering

Program of Study Committee:

David Grewell (Co-Major Professor)
Sriram Sundararajan (Co-Major Professor)
Palaniappa A. Molian
Pranav Shrotriya
Michael R. Kessler

Iowa State University
Ames, Iowa
2011

Table of Contents

Abstract

Recently, there has been an increased interest in bio-based plastics due to environmental concerns as well as fluctuating oil and gas prices. Bio-based plastics, as defined here, are those plastics that are fully or partially produced from renewable feedstock. As with many products, sealing and cutting of semi-finished parts are required. This is particularly true with packaging applications, such as food packages, where there is a natural fit for bio-plastics because of the product's short life cycle (<1 year) and large amount of waste associated with this product (12.5 million tons of containers and packaging per year). In order to increase the acceptance of polylactic acid (PLA a starch derived bioplastic), its weldability and cuttability was studied in detail. Ultrasonic and heat welding, which are two common welding techniques in industrial applications, are examined in terms of weld strength, cycle time, and weld strength consistency. While the ultrasonic welding of PLA is very effective, heat welding is examined in great detail to find the activation energy for diffusion in such processes. In addition, the ultrasonic cutting that is often done simultaneously with ultrasonic welding processes is examined here too. The cuttability of PLA was studied by examining the cutting speed, the mechanical properties of the material after cutting as well as the surface of the cut. In addition, a new kind of cutting tool was developed that can cut and seal simultaneously. However, the manufacturing of products from bio-based plastics may result in more energy consumption, waste, and emissions than traditional plastics, which would reduce or eliminate the acceptance of PLA. In order to address this issue, a model was generated to examine the 'Carbon Footprint' of bio-plastics such as zein (a corn based protein polymer), soy protein isolate (SPI) (a soy bean based protein polymer), and polylactic

acid (PLA) which compares these materials to petroleum based plastics with similar mechanical properties and potentially similar applications, such as polyethylene (PE) and polystyrene (PS). The results show the energy consumption, greenhouse gas emissions, and costs during the life cycle steps of material production, manufacturing of plastic products, and the beneficial as well as non-beneficial effects of the end-of-life recovery processes of the considered materials.

Chapter 1: Background

1 Bio-plastics

Over the past decades, bio-based plastics have been in development and introduced in many applications/products. While the first polymers were produced from biomass feedstock, such as cellulose and natural rubber, they were progressively replaced by petrochemical polymers since the 1930's because of their superior properties, lower cost, and abundance. However, recently there has been an increased interest in bio-based polymers in many industries due to environmental concerns as well as rising prices for oil and gas. In principle, biodegradable polymers can also be manufactured from petrochemical raw materials, but bio-based polymers are defined here as polymers that are fully or partially produced from renewable feedstocks [1].

There are many driving forces encouraging the use of bio-based plastics, such as the previously mentioned environmental concerns. The limited volume and acceptance of landfill in densely populated areas, the negative image of plastic and plastic waste, which is considered as a threat to wildlife habitats as well as pollution of waters and landscapes are others. In addition, producing plastics from agricultural feedstock and agricultural surplus materials also promotes the creation of new jobs in rural areas and adds value to domestic industries.

There are different bio-based polymers and different ways to produce them. Starch or protein polymers are produced by modifying the molecular structure of their feedstock but leaving it intact to a large extend. In more detail, starch and proteins are natural polymers of polymerized sugar and amino acids monomers. By denaturing these natural

polymers with solvents (such as water, ethanol or glycerine), heat and shearing (such as in an extruder) it is possible to produce materials that can be plasticized and processed with conventional polymer processing equipment. The materials produced by following this approach are often used in disposable utensils.

Polylactic acid (PLA) can be produced by fermenting starch to lactic acid, which is then polymerized. Because this is one of the few commercially available bioplastics, it is detailed in a following section. Cellulose polymers have been used for decades in a wide range of applications. Cellulose acetate and cellulose nitrate are only some of the widely used cellulose based bio-plastics. Other bio-based plastics can directly be produced by microorganisms such as polyhydroxyalkanoate (PHA) or by genetically modified crops [2]. The use of agricultural products, such as soybean or other vegetable oils, to be polymerized to plastics or to be used for bio-based polyurethanes, thermoset plastics or bio-based foams has been widely demonstrated by researchers [3]. Another significant application for vegetable oil is its use as polyols, which are commonly produced from petrochemical feedstock. In the US, approximately 1.4 million tons of polyols are used annually with a market potential of soy-based polyols of 320,000-410,000 tons. The global market for bio-based polyols is estimated to be approximately 0.95-1.23 million tons per year [4]. However, some of these polymers have the advantage to be biodegradable while other bio-based plastics, such as bio-based thermosets, degrade very slowly. While this can be considered a disadvantage, because they need to be treated in landfill facilities, it can also be considered an advantage, because these material store carbon which was absorbed during the growth of the plants.

Ideally bio-plastics would have a zero carbon foot print. In more detail, the carbon cycle of bio-based materials is closed because the plants absorb the same amount of CO_2 during

their growth as the material releases when it decomposes. However, the carbon cycle for slowly degrading bio-based plastics results in CO_2 absorption from the atmosphere, because the rate of CO_2 fixation during the growth of the plants is higher than the rate of CO_2 released to the atmosphere when the material decomposes.

2 Polylactic Acid (PLA)

Polylactic acid (PLA) is a biodegradable polymer derived from lactic acid made from 100% renewable resources such as sugar beets, wheat, corn, or other starch-rich crops. The starch is hydrolyzed to depolymerize the polymers into sugar. In the case of sugar beets the sugar is extracted directly. This sugar is then used to propagate microbes for the production of lactic acid. The lactic acid is polymerized either by condensation or by a ring opening process [5]. By controlling the purity of the monomer it is possible to produce polymers with a wide range of molecular weight. Compared to petrochemical polymers, PLA is environmentally friendly ("green") as the carbon cycle of the material is relatively closed. That is to say, the same amount of CO_2 that is produced during decomposition of PLA is trapped during the growth of the plants of the raw material for PLA. It is not truly carbon neutral as there are petrochemical feedstocks consumed during the production of the crops, namely in transportation, fertilizing and other unit operations for its production. In addition, PLA does not contribute to landfill as it is biodegraded within a year [6] when composted.

Polylactic acid is typically transparent, rigid, and exhibits mechanical properties similar to many petroleum based polymers. For example, it has a tensile strength of approximately 70 MPa and a modulus of elasticity of 3.6 GPa; similar to PET, which has a tensile strength of 60–80 MPa [7] and a modulus of elasticity of 2.1–3.1 GPa. In

addition it has a density of 1.25 g/cm^3, which is lower compared to PET having a density of 1.35–1.38 g/cm^3. It is relatively resistant to moisture and solvents such as oil and grease and has relatively high vapor barrier properties. Depending on its formulation, it can be made rigid or flexible and can have a melting point between 130 °C and 220 °C. The molecular weight of PLA varies between 100,000 to 300,000 Daltons. As for polymers in general, strength, viscosity, melt temperature, and glass transition temperature all increase with molecular weight due to decreasing relative motion of the polymer chains as they become longer. However, with increasing molecular weight the ease of processing is to expect to decrease [8].

PLA can be amorphous or semicrystalline depending on its stereochemistry and thermal history. The building blocks of PLA (lactic acid monomer) can have two arrangements, L-lactic acid or D-lactic acid. Three arrangements are possible for the lactide, L-, D-, and meso-lactide with glass transition temperatures of 61 °C, 46 °C, and 53 °C, respectively. The simplest form of PLA is the isotactic homopolymer poly(L-lactide) PLLA or the poly(D-lactide) PDLA. However, the most common commercial polymers of PLA are copolymers of L-lactide with small amounts of D- and meso-lactides [8, 9]. These co-monomers introduce distortions in the natural conformation of PLA and defects in its crystalline structure, which decreases the melting temperature, reduces the obtainable degree of crystallinity, and lowers the crystallization rate. Because PLA has a relatively slow crystallization rate, it can be quenched to a quasi-amorphous state and crystallinity can be increased by annealing. In addition, by heating PLA between its T_g and the cold crystallization temperature T_{cc} (95 ºC–105 ºC), the polymers can undergo stress induced crystallization. Stretching PLA sheets promotes gradual crystallization and application of

stretching in transverse directions causes destruction of the semicrystalline structure while generating a second population of oriented but poorly ordered PLA crystals [5].

For amorphous PLA the glass transition temperature is approximately 58 °C and for semicrystalline PLA, melt temperature (T_m) ranges between 130 and 230 °C. Both transitions at T_g and T_m are dependent on the polymer composition, thermal history, and molecular weight. A reduction in the glass transition temperature of PLA can be achieved under mechanically constrained conditions, where the polymer is prevented from shrinking during cooling. This constrained crystallization process increases the free volume of the amorphous phase of the polymer, which depresses glass transition while the crystallinity increases [6].

Due to its relatively high cost, PLA was initially used only for medical applications, such as temporary implants, controlled drug release applications, and medical sutures. Recent improvements in its fermentation technology have lowered its production costs, making it more attractive for industry. Today it is sold for approximately $2.64/kg and used for a large number of applications such as bags, cups, bottles, films, and food packaging. Approximately 70% of the PLA produced is used for packaging applications [9]. Because it can be formed into fibers using a melt spinning process, it is also used for non-wovens. Common processing methods for PLA include extrusion, injection molding, thermoforming, film extrusion, and blow molding [8, 10, 11]. Major producers of PLA in the US and worldwide are Nature Works with an annual production of 150.000 tons and Hycail from the Netherlands with 50.000 tons.

3 Welding and Cutting of Plastics

Welding is an important step in the manufacturing of plastic products. It is used in a wide range of applications; from plastic pipelines and water vessels to small parts, such as electronic switches. It is common to classify welding processes by the method of heat generation. In general it is either internal or external heat that promotes molecular mobility and welding. Typically, the processes that generate heat internally are faster compared to those processes that rely on heat from external sources because they are limited by thermal diffusion.

While heat tool welding is a rather slow process, as it relies on external heat, ultrasonic and vibration welding rely on internal heat generated by surface or molecular friction. While there a wide range of methods for joining plastics, it is common to use ultrasonic and impulse welding to join films. During ultrasonic welding, mechanical vibrations at frequencies between 20 – 40 kilohertz (kHz) and an amplitude between 20 – 100 micrometers peak to peak ($\mu m_{p\text{-}p}$), are applied to the parts to be joined. The heat generation by the cyclical deformation of the thermoplastic material is highest at the interface of the parts to be joined because of surface asperities. Ultrasonic welding equipment usually includes the following components: (1) ultrasonic converter, (2) booster, and (3) sonotrode. The converter produces an axial mechanical vibration which can be increased or decreased by the booster. When the assembly of the three parts moves down, the horn transfers the vibrations to the part. In impulse welding, one or two heated bars/elements are pressed against the surfaces of the films to be welded until the films melt and bond at the faying surfaces whereby temperature, time, and pressure are the main process parameters.

However, the basic welding steps are (a) surface preparation, (b) heating, (c) pressing, (d) intermolecular diffusion and (e) cooling. The two weld methods studied here will be heat and ultrasonic welding [6, 7].

In many applications, such as the welding of individual plastic bags from continuous films, the welded parts need to be cut to bring it into their final shape.

Ultrasonic cutting is a process similar to ultrasonic welding with the same functional parts. However, two configurations are possible: 1. the horn is the cutting knife/edge and typically vibrates at a frequency of 20 – 40 kHz, heating the substrate during the cutting and simultaneously sealing the edges; 2. the anvil has the shape of a knife and the horn has a flat surface. During the ultrasonic vibration the horn applies a cycle stress ("hammering") on the part placed between horn and anvil and cuts it thereby.

Because welding and cutting are two subsequent procedures in some industrial applications, the ultrasonic cutting process of plastic films was analyzed here in great detail. In addition, a method that allows to seal and cut films simultaneously in the same process step was invented and tested for its applicability.

4 Life Cycle Assessment (LCA)

The life cycle assessment (LCA) has become a very important tool for engineers to measure the environmental performance of a product or service. It is a holistic environmental and energy audit for new processes, for new or redesigned products that are meant to meet new environmental criteria and focuses on the entire life of a product from raw material acquisition to final product disposal [11, 12].

Through a LCA it is possible to calculate and report the ecological impact associated with a product covering all stages of its life. By providing these data, a LCA has become a key input in decision making processes to identify and steer future industrial as well as socioeconomic processes [12, 13]. While there are ISO standards detailing how to precisely to conduct an LCA (ISO 14040 – 14050), the method used here will be according to ASTM D 7075 - Standard Practice for Evaluating and Reporting Environmental Performance of Biobased Products.

The LCA is usually completed in 4 steps. In a brief summary these are:

Definition of Goal and Scope

The first step of the LCA includes a clear and unambiguous statement of the purpose of the study. It defines its system boundaries in a way that the goal will be fulfilled. After choosing the functional unit of the LCA, all included process flows can be normalized to the amount of material required to fulfil its stated task.

Life Cycle Inventory

In the life cycle inventory the process flow across the system boundary of the LCA will be identified and quantified. Often, the unit operations involve energy in- and outputs. However, only the most elementary flows that cross system boundaries shall be included in the LCA. Internal flows for product production shall not be included.

Life Cycle Impact Assessment

The environmental impacts are calculated by the formula

$$\text{Impact Index}_j = \Sigma\, m_i * P_{j,i}$$

Where: j = impact category (for example Global Warming); i = category indicator (for example CO_2); Pj,i = factor of conversation of *i* to reference indicator equivalent

According to the ASTM standard there are 11 impact categories which can be found in the standard's appendix.

Life Cycle Interpretation

After identifying and quantifying the process flows and calculating the impact indices, the findings of the life cycle assessment can be converted into specific statements or recommendations.

5 Research Questions

The question this dissertation will answer is whether bio-plastics have the potential to replace existing materials without resulting in any ecological, technical, or economical disadvantage.

The research questions of this work can be summarized in three topics.

Can PLA (and to what degree) be welded using existing weld techniques such as ultrasonic and heat welding (impulse welding) and what happens to the material structure after welding?

Can the weld process be modelled based on fundamental considerations of polymer chain movement and diffusion and can predictive equations, such as an Arrhenius equation, be used to calculate the degree of welding for unknown parameters?

What are environmental and socio-economical impacts of bio-plastics? Does it make sense to replace established materials with new upcoming bio material such as PLA?

References

[1] M. Patel, C. Bastioli, L. Marini, E. Würdinger, Environmental assessment of bio-based polymers and natural fibers

[2] J.K. Pandey, A.P. Kumar, M. Misra, A.K. Mohanty, L.T. Drzal, R.P. Singh, J. Nanosci, Nanotech, 5, 497-526 (2005)

[3] R.P. Wool, X.S. Sun, Bio-based polymers and composites, Academic Press (2006)

[4] POLYOLS MADE FROM VEGETABLE OIL AND THEIR PPLICATIONS, A Thesis presented to the Faculty of the Graduate School, University of Missouri-Columbia, KIRAN K. YERRAKONDREDDYGARI

[5] D.W. Farrington, J. Lunt, S. Davies, and R.S. Blackburn, Biodegradable and sustainable fibers "Polylactic Acid Fibers", Blackburn, Leeds (2005), 192-196

[6] A. Mohanty A, M. Misra, L. Drzal, Natural Fibers, Biopolymers and Biocomposites, Taylor & Francis, 2005, 0-8493-1741-X

[7] T. Oswald, E. Baur, S. Brinkmann, K. Oberbach, E. Schmachtenberg, International Plastics Handbook, Hanser Publications, Munich Germany (2006)

[8] A. Harper, Modern Plastics Handbook, McGraw-Hill Professional, New York (2000)

[9] Ploylactide, Biologisch abbaubare Kunststoffe aus nachwachsenden Rohstoffen, Sven Jacobsen

[10] B.L. Deopura, R. Alagirusamy, M. Joshi and B. Gupta, Polyesters and polyamides, Woodhead Publishing (2008)

[11] European Science and Technology Observatory, Institute for Prospective Technological Studies, Techno-economic feasibility of large-scale production of bio-based polymers in Europe, EUR 22103 EN

[12] J. Bendal, R. Narayan, Life Cycle Ana1ysis: A Marketing Nightmare, Presented at Cellulose '91, New Orleans, Louisiana, (1991) ;Conference Proceedings

[13] Position Paper Life Cycle Assessment of Bioplastics e.V., European Bioplastics

Chapter 2: Ultrasonic and impulse welding of polylactic acid films

David Grewell - Department of Agricultural and Biosystems Engineering, Iowa State University

Julius Vogel – Department of Mechanical Engineering, Iowa State University

Michael R. Kessler - Department of Materials Science and Engineering, Iowa State University

Dietmar Drummer - Institute of Polymer Technology, University of Erlangen-Nuernberg

Markus Menacher - Institute of Polymer Technology, University of Erlangen-Nuernberg

A paper published by the Society of Plastics Engineers (SPE) *Polymer Engineering & Science Journal*

1 Introduction

Polylactic acid (PLA), a biodegradable polymer derived from lactic acid, is made from 100% renewable resources such as sugar beets, wheat, corn or other starch-rich crops. The starch from the feedstock is extracted through a range of mechanisms and hydrolyzed into fermentable sugars to produce lactic acid. The lactic acid is polymerized either by a condensation reaction or through a ring opening process [1]. By controlling the purity of the monomer it is possible to produce polymers within a wide range of molecular weights.

Polylatic acid is typically transparent, rigid and exhibits mechanical properties similar to many petroleum based polymers. For example, PLA has a tensile strength of approximately 70 megapascals (MPa) and a modulus of elasticity of 3,600 MPa; similar to polyethylene terephthalate (PET) which has a tensile strength of 47 MPa and a modulus of elasticity of 3,100 MPa [2]. In addition, PLA has a density of 1.25 g/cm^3 which is approximately 8% lower than PET. Polylatic acid is relatively resistant to moisture and solvents such as oil and grease and has high vapor barrier properties. Depending on its formulation, it can be made rigid or flexible and can have a melting point between 130 and 230 degree Celsius (°C). The molecular weight of PLA can vary between 100,000 to 300,000 Daltons. As with other polymers, the strength, viscosity, melt temperature and glass transition temperature of PLA increase with molecular weight due to increased molecular entanglement. In addition, with increasing molecular weight the ease of processing decreases [3].

Amorphous PLA has a glass transition temperature (T_g) of approximately 58 °C and, for semicrystalline PLA, a melt temperature (T_m) between 130 – 230 °C. Both transitions at T_g and T_m are dependent on the polymer composition, thermal history and molecular weight. A reduction in the glass transition of PLA can be achieved under mechanically constrained conditions, where the polymer is prevented from shrinking during cooling. This constrained crystallization process increases the free volume of the amorphous phase of the polymer which depresses the glass transition while the crystallinity increases [4].

Compared to petrochemical polymers, PLA is environmentally friendly because a similar amount of carbon dioxide is trapped during the growth of the plants from which PLA is derived as produced during its decomposition. In addition the energy consumption and emission generation during its production is significantly lower than for most

commercially available thermoplastic polymers. Also, PLA does not contribute to excessive landfill waste because it is biodegraded within a year [4,5]. PLA is used for a large number of applications such as bags, cups, bottles, films and food packaging. Approximately 75% of all PLA is used for packaging applications. Common processing methods for PLA include extrusion, injection molding, thermoforming, film extrusion and blow molding [6].

Because most applications cannot be molded as a single part, joining of sub-components is often required. While there are a number of methods for joining plastics, it is common to use ultrasonic and impulse welding to join films. During ultrasonic welding, mechanical vibrations at high frequencies between 20 – 40 kilohertz (kHz) and low amplitude, typically between 20 – 100 micrometers peak to peak ($\mu m_{p\text{-}p}$), are applied to the parts to be joined. The heat generated by the cyclical deformation of the thermoplastic material is highest at the interface of the parts to be joined because of surface asperities. Ultrasonic welding equipment includes three functional components: (1) ultrasonic converter, (2) booster and (3) sonotrode (see FIG. 1) and once coupled together are referred to as the stack assembly. The converter produces an axial mechanical vibration which can be increased or decreased by the booster. The horn transfers the vibrations to the part. Typically the stack assembly is engaged with the parts with a pneumatic system. The force of engagement can vary during the weld cycle and affects weld strength, as well as weld time for a given energy setting [7,8].

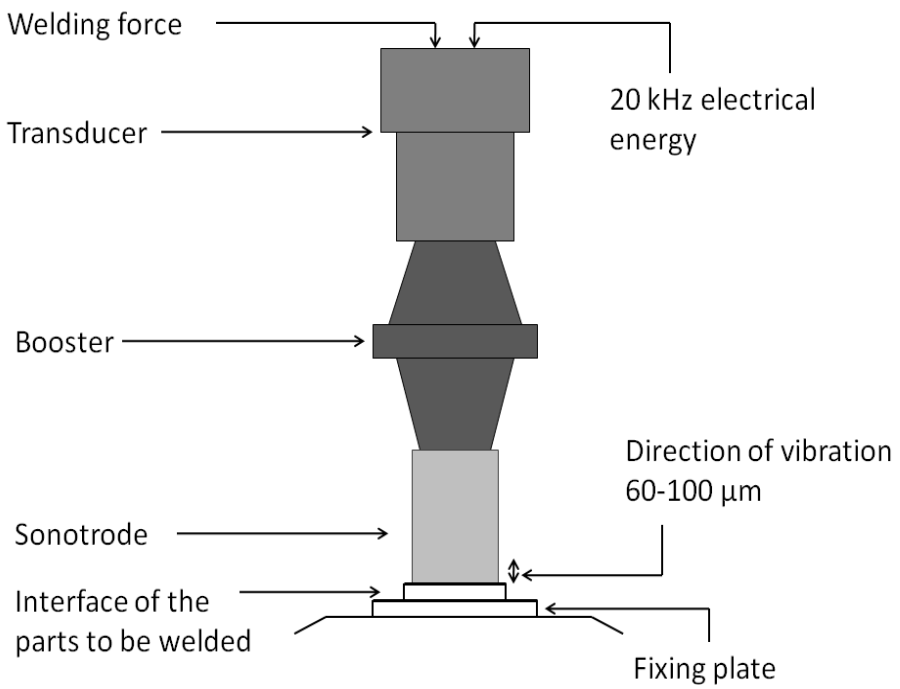

FIG. 1 Schematic drawing of an ultrasonic welding machine

Ultrasonic welding of thermoplastics was studied by many researchers. Benatar et al. studied energy dissipation and heating rates in near-field ultrasonic welding [9]. The temperature distribution for various energy directors in ultrasonic welding was studied by Suresha et al. [10]. Benatar and Cheng [11] developed a model for wave propagation in viscoelastic materials to predict vibration amplitude experienced at the joint interface. Proper joint design, which typically includes energy directors and shear joints for welding of rigid applications, was examined by Grewell et al. [12].

In impulse welding, one or more electrically heated bars/elements are pressed against the surfaces of the films to be welded until the films melt and bond at the faying surfaces. Temperature, time and pressure are the main process parameters [13]. Most common impulse welders use a nickel-chromium heating element with a small thermal mass that is heated quickly with electrical current, while the heating time can be as short as 2 seconds

(s) or below. Once the element(s) applies sufficient heat to promote bonding, the energy is discontinued and the residual heat is quickly absorbed through thermal conduction by the thermal mass of the welding head to quickly cool. This allows the welding cycle to be completed within a relatively short period of time. With thicker samples it is common to utilize a dual heating head, where heating elements are placed on both sides of the films, to further reduce the cycle time [8].

To gain insight into the morphology induced by a welding process, differential scanning calorimetry (DSC) and polarized optical microscopy (POM) are common analytical methods. The glass transition, melting and crystallization temperatures of the plastics can be determined with DSC, and POM can reveal changes in the morphological structure of plastics with birefringent properties [14, 15]. Often it is useful to compare the morphology of base material samples and welded samples. In addition dynamic mechanical analysis (DMA) can be used to characterize a material's loss and storage moduli and damping behavior.

Although processing technologies of PLA such as extrusion, injection molding, foaming and fiber spinning were studied in great detail by Lim et al. [16], no systematic study on the weldability of PLA films exists. Because PLA is the first commodity bio-polymer produced on a large industrial scale, the results of such a weldability study are industrially relevant. Because PLA has widely different processing conditions compared to traditional petrochemical plastics, such as low processing temperatures of 100 °C, slow crystallization rates [5], and high moisture sensitivity during processing [16], we theorized that its weldability may be difficult. Thus, this paper examines the welding of PLA films by ultrasonic and impulse welding techniques as a precursor for future studies on this growing technology. The goal of this work is to demonstrate the welding of PLA

with ultrasonic and impulse welding and to connect weld strength to the key processing parameters.

2 Materials and Methods

The material used was a biaxially oriented film (Evlon®) provided by Bi-Ax International Inc. (Ontario, Canada) and manufactured from a Nature Works (Minnetonka, MN) PLA with film thicknesses of 25, 40, 100, 200, 254 and 305 μm. These films were manufactured with a calendering process followed by stretching in the transverse direction to promote orientation to a desired thickness. It is important to note that stretching PLA films promotes crystallization and stretching in the transverse directions destructs this crystallinity while generating a second population of oriented but poorly ordered PLA crystals [4].

The impulse welding system used was an America International Electric (Whittier, CA) type AIE 200-C (260 Watt) impulse sealer with a sealing length of 22 centimeters (cm). The welding time was varied from 0.5 to 4 sec in 0.5 and 1.0 sec intervals with constant weld forces determined by the springs within the welding head. The hold time was held constant at 3 sec. In order to characterize the welding process, a 36 gauge thermocouple (TC) type-K wire was placed at the edge of weld. The TC was located in the center of the heating element using an auxiliary sample near the edge of the test sample. The sampling rate of the digital data acquisition system was 10 kHz (kilo Hertz). Five replicate welds were made for each set of experimental parameters.

The ultrasonic welding system was a Branson 2000 (Danbury, CT) welding system operating at a frequency of 20 kHz. The experiment was conducted in a weld-time mode and the welding force was set to 145.5, 236.6 and 360 Newton (N). The trigger force was

set to 90% of the weld force [17]. The booster and horn had a gain of 1.5:1 and 2.66:1 respectively. Three amplitudes were examined: 48, 64 and 80 μm_{p-p} at the horn face, while the welding time was varied from 0.15 sec to 0.45 sec in 0.1 sec intervals for one selected amplitude. A flat surface anvil was used and the hold time was held constant at 2 sec in order to assure that the welds were fully cooled. Five replicate welds were made for each set of experimental parameters. In general a T-design of experiment was used and is detailed in Table 1.

Table 1 Experimental design of ultrasonic welding: 200, 254, 305 μm film thickness, 145.5 N weld force, *repeated for weld force of 236.6 and 360 N

	Weld Time [sec]			
Amplitude [μm_{p-p}]	0.15	0.25	0.35	0.45
48	x			
64	x*	x	x	x
80	x			

All DSC measurements were taken under nitrogen atmosphere at a heating rate of 5 ºC/min (ºC/minute) from room temperature to 190 ºC. Samples for DSC characterization were cut from virgin films, from films annealed at 90 ºC for 90 min (annealed films), from films at the weld zone and from films at the weld zone that were subsequently annealed. The annealed films were slowly cooled to room temperature at a cooling rate of -1 ºC/min after the isothermal treatment. All DSC samples were between 6.5 – 11 mg (milligrams). Because ultrasonic welding has much higher heating rates, peak

temperature and cooling rates compared to impulse welding, only ultrasonic welds were studied with the DSC characterization to investigate changes in the material morphology.

Dynamic mechanical analysis of the PLA films was completed with a TA Instruments model Q800 DMA with a gas cooling accessory. Rectangular sample films with dimensions of 21.43 × 4.45 × 0.254 mm (millimeters) were tested in the film tension configuration at an oscillation frequency of 1 Hz and amplitude of 10 μm at a heating rate of 3.75 ºC/min.

Tensile testing of the welded films was completed according to ASTM (American Society of Testing and Materials) D 638 and ASTM 3163 with a modified sample geometry using an Instron (Norwood, MA) model 4500 load frame with a 5 kN load cell at a crosshead speed of 10 mm/min. The sample geometry used in this study is defined by ASTM D 638 and the tests were completed in a lap shear joint configuration according to ASTM 3163. In more detail, films in a lap shear configuration with an overlap of 2.3 mm were welded with impulse welding and ultrasonic welding. After welding, the samples were cut to a standard tensile test specimen with dimensions detailed in FIG. 2 and FIG. 3.

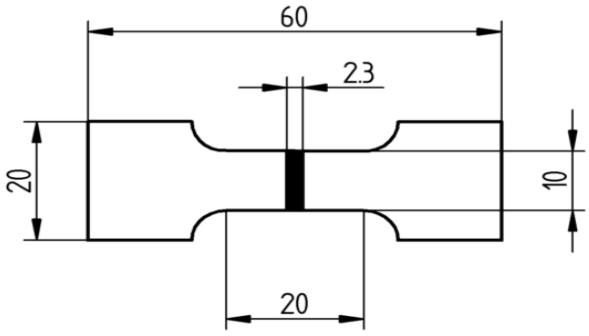

FIG. 2 Dimensions (mm) of tensile test samples for ultrasonic welding

The various gauge lengths (20 and 60 mm) were used in order to match the griping mechanisms for the various thicknesses. Samples of similar geometries were also cut from virgin films (not welded) for base material references.

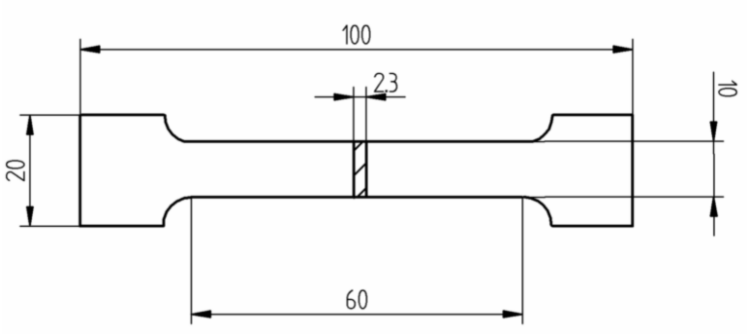

FIG. 3 Dimensions (mm) of tensile test samples for impulse welding

3 Results and Discussion

3.1 Base Material Characterization

FIG. 4 shows the storage and loss moduli and tan δ as a function of temperature from DMA of the base material. It is seen that the T_g of PLA (as measured by the onset drop in the storage modulus) is approximately 61 ºC which is in good agreement with the published T_g of the poly-L lactide (PLLA) polymer (61 ºC) [5]. The motivation of measuring the T_g was due to observations during impulse welding (to be detailed in following sections) that showed PLA could be welded at surprisingly low temperatures (~ 75 ºC).

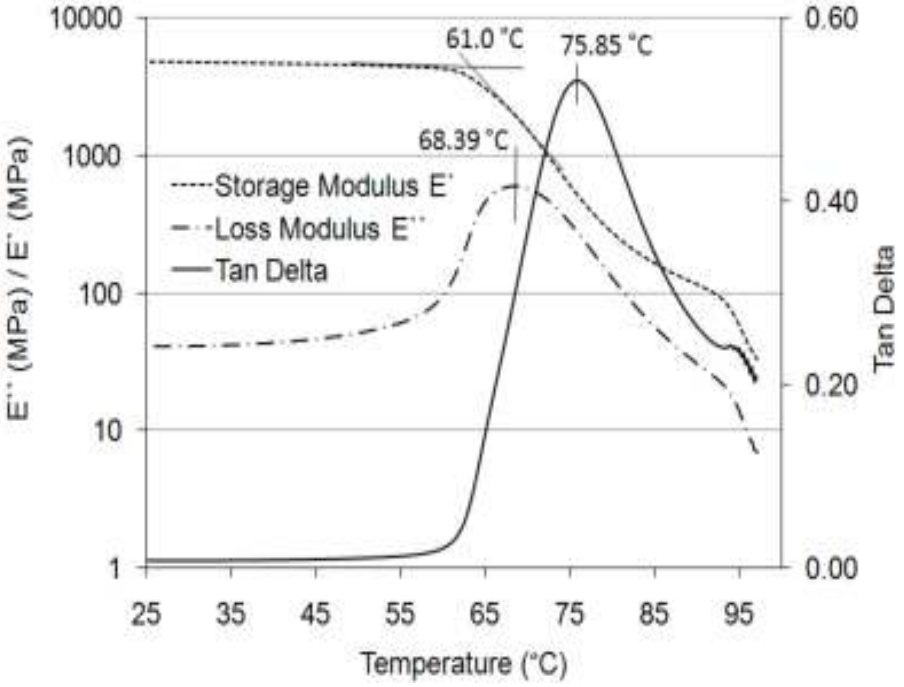

FIG. 4 DMA test results for PLA

For film thickness of 25 and 40 μm the measured failure load was 23 and 35 N, corresponding to a tensile strength of 92 and 88 MPa, while it was approximately 78 MPa for film thicknesses of 100, 200, 254 and 305 μm, which is in agreement for the published tensile strength of PLA [2]. The higher tensile strength for the thinner samples may have been due to higher retained molecular orientation resulting from faster cooling rates through the thickness.

3.2 Impulse Welding

The weld factor (failure load of the welded samples divided by the failure load of the base material) of impulse welded films is shown as a function of weld time in FIG. 5. It is seen that weld factors slightly above one are measured. While a weld factor greater than one is counter intuitive it has been report by others and is believed to be due to geometric factors during loading [18].

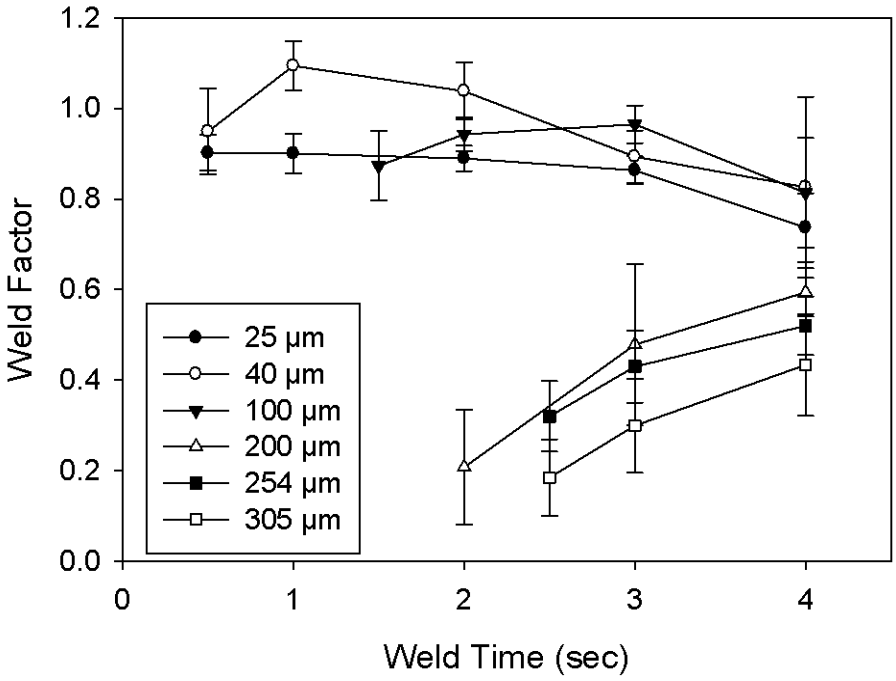

FIG. 5 Tensile test results of impulse welded films

FIG. 6 shows the peak temperature during impulse welding as a function of heating time for the various sample thicknesses. The peak temperature is proportional to weld time and inversely proportional to sample thickness and in general the temperature at the weld was above T_g (61 ºC). This data is presented for reference purposes of the thermal history at the faying surface and not intended for interpretation of interfacial welding (healing). With a film thickness of 100 µm, the measurements of the temperature for weld times less than 1.5 sec are not reported because no welds were produced. It is important to note that during the heating, both squeeze flow, wetting and molecular diffusions are simultaneously occurring all leading to the welding process [14, 19].

Welding typically requires interfacial temperatures well above T_g, while this paper reports welding at temperatures slightly above the T_g, at approximately 75 ºC in less than a one sec.

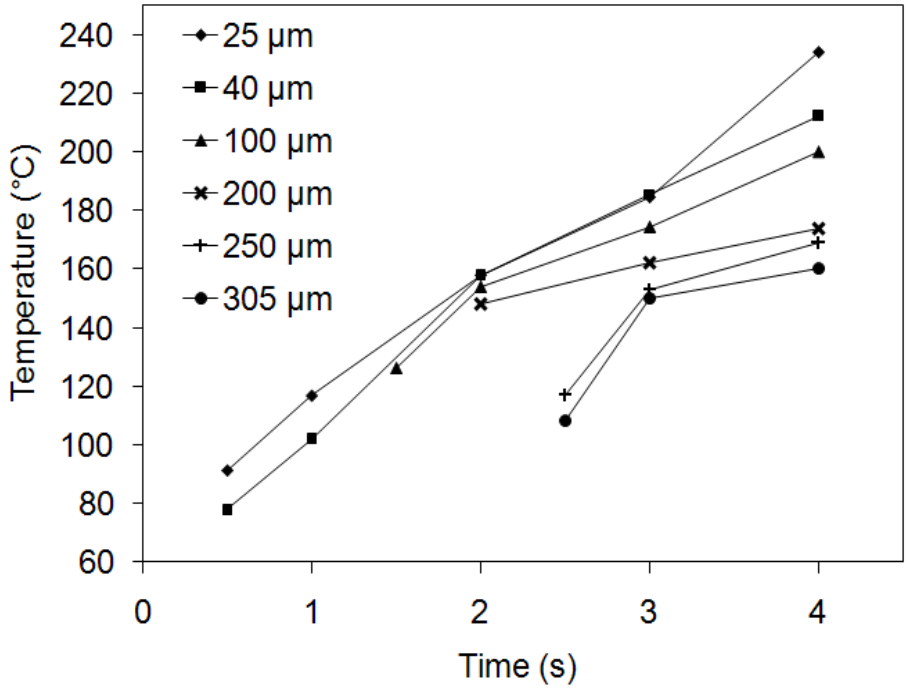

FIG. 6 Peak temperatures during impulse welding

Because of this counter intuitive observation, the relation between welding molecular structure needs to be reviewed. It was reported by Ljunberg et al. [20] that the minimum weld temperatures for constant heat welding of PLA films with a thickness of 20 and 40 µm at 65 ºC is possible with a welding time of 60 sec which is disproportionally high compared to the short weld times of 2 - 4 sec used in this study. It is believed that high strength welds occurred at these relatively low temperatures because of the low degree of polymerization of PLA. The published molecular weight of PLA ranges between 100,000 – 300,000 Daltons. Because the repeat unit of lactic acid has a molecular weight of 72 Daltons [5], the degree of polymerization is between 1,400 to 4,166. In contrast, the degree of polymerization of a common semicrystalline polymer such as polyethylene for which the weld temperature must be well above T_g for effective fusion bonding, can range between 100 – 250,000 Daltons [21]. Because of the relatively low degree of polymerization for PLA it is believed that fusion occurs slightly above T_g. In addition,

Wool [22] proposed that "polymer entanglement" is inversely proportional to increasing molecular weight. It was shown, that interfacial fracture energy is dependent on weld time and molecular weight as:

$$G_{lc}(\mathrm{t}) \sim t^{r/4} M^{-s/4} \qquad [1]$$

where: G_{1c} - interfacial fracture energy

t - weld time

M - molecular weight

r, s = 2 in case of interface fracture dominated by disentanglement (experimental determination)

Thus, it is believed that welding for PLA can occur at temperatures near T_g, because of low degree of polymerization. It is also important to note that while there was evidence of a frozen layer at the faying surfaces (detailed in the following section through optical microscopy images), which would be highly amorphous, and may contain lower molecular weight species. It is possible that the surfaces of the films had a disproportionally high amount of low molecular weight species, which could also explain the welding of the samples in a short period of time at relatively low temperatures.

In FIG. 5 the error bars correspond to ±1 standard deviation. As defined in Eq. 1, failure load of the weld is generally proportional to welding time. However, it is not possible to distinguish this relationship between strength and time in FIG. 5 as full parent material strength is achieved at the shortest possible weld times (0.5 sec) of the impulse welding machine. It is seen that with a film thickness of 100 μm, a weld time of 1.5 sec is required to result in measurable fusion, and to produce maximum weld factor, a weld time of two sec is required. With a thickness of 25 μm a weld time of 0.5 sec is sufficient to promote fusion to reach a weld factor of 1, and for 40 μm a weld time of 1 sec is required

to achieve a maximum strength. For a film thickness of 100 μm, three sec of weld time is required to achieve a weld factor near one. It is also seen that with extended weld times for film thicknesses of 100 μm or less, the strength tends to decrease. This is the result of excessive squeeze flow resulting in reduced film thickness. The results also indicate that the welding process is relatively robust in that weld strength is not adversely affected over a relatively wide range of weld times. For example, near base material weld strengths can be achieved with a fluctuation of ± 1 sec of the optimum weld time. It also seen that for film thicknesses of 200 μm and great, the maximum weld time of the impulse welding machine (4 sec) was not sufficient to produce significantly strong welds and the weld factor was less than 0.6.

3.3 Ultrasonic Welding

FIG. 7FIG. 7 shows the weld factor for three film thickness welded with ultrasonics with a weld time of 0.15 sec and a weld amplitude of 64 μm_{p-p} as a function of weld force. Weld factor is generally proportional to weld force and this is most likely due to better coupling of the horn to the samples which promotes better heating and fusion of the samples. Thinner samples are not reported because the repeatability of thinner films resulted in larger standard deviations than those seen in FIG 7. It is believed that the inconsistency in the weld factor with the thinner films is due to the criticalness in horn/fixture alignment [23].

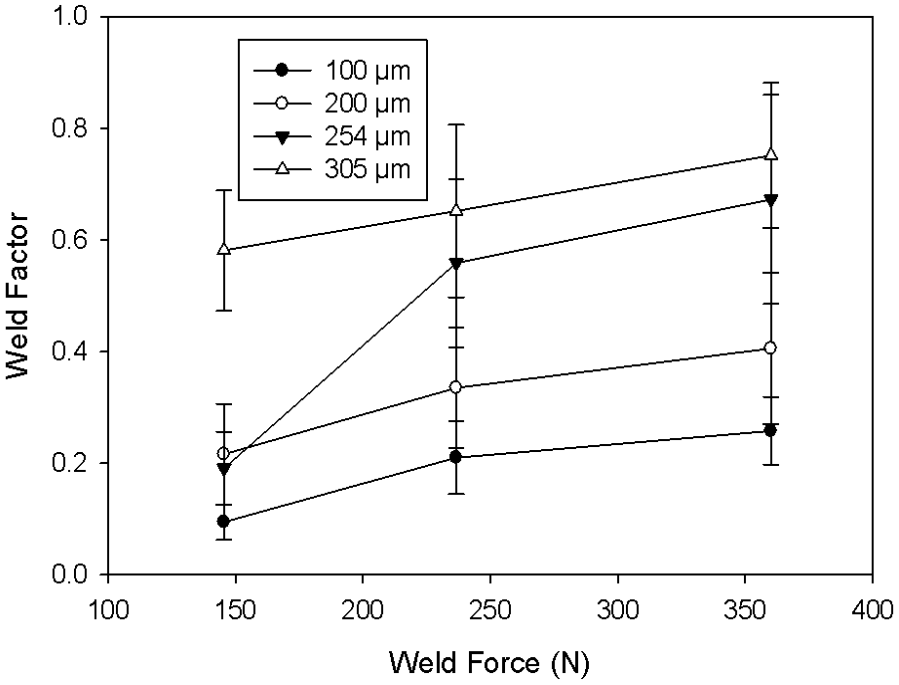

FIG. 7 Weld factor for increasing ultrasonic welding force, weld amplitude = 64 µmp-p, weld time = 0.15 sec

The weld factor was generally proportional to weld amplitude as seen in FIG.8. It is expected that weld strength increases with amplitude since volumetric heating during ultrasonic welding is proportional to strain squared (ε_0^2) as defined in Eq. 2 [8] where ω is angular frequency and E" is the loss modulus.

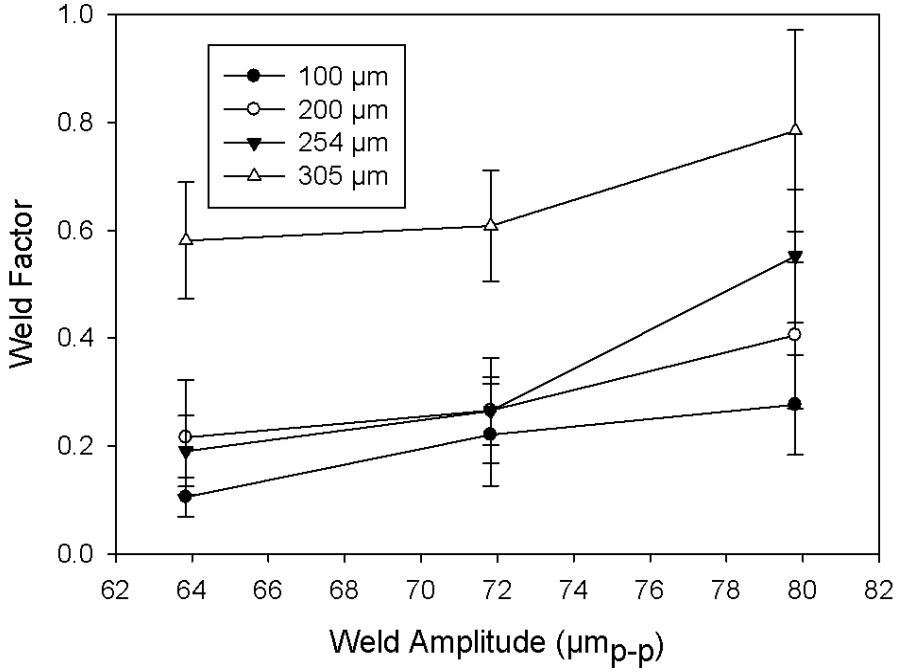

FIG.8 Weld factor for increasing amplitude, weld force = 145 N, weld time = 0.15 sec

In this case the induced strain is proportional to amplitude and is often assumed to be the amplitude divided by the energy director height, or in this case, the height of the asperity peaks.

$$\dot{Q}_{avg} = \frac{\omega E'' \varepsilon_0^2}{2} \qquad [2]$$

FIG. 9 shows that the weld factor is generally proportional to weld time and that most thicknesses can be bonded with a weld factor near one. However, with excessive heating (longer welding times), there is a decrease is strength due to over-heating and excessive squeeze flow. It is important to note that with ultrasonic welding the maximum failure load of the weld was 180 N for 200 µm films at 0.35 sec, 198 N for 254 µm films at 0.35 sec, and approximately 275 N for 305 µm films at 0.25 sec weld time.

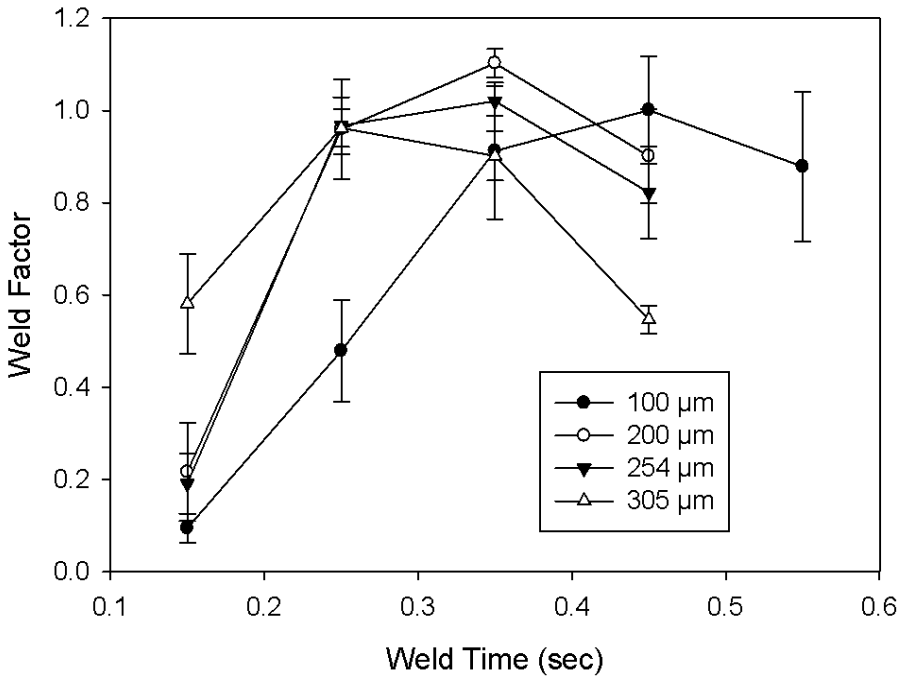

FIG. 9 Weld factor for increasing weld time, weld force = 145 N, weld amplitude = 64 μm_{p-p}

FIG. 10 and FIG. 11 show micrographs of the weld zone of samples with a thickness of 305 µm and welded at a weld force of 145.5 N and weld times of 0.15, 0.25 and 0.35 sec at two magnifications.

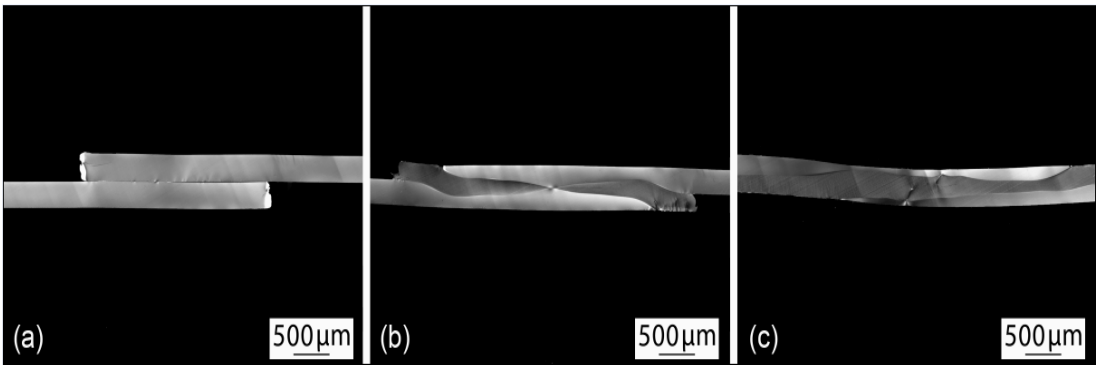

FIG. 10 Micrographs of ultrasonic welded PLA films, 305 µm thickness, detailing weld line and squeeze flow (left: welded 0.15 sec, center: welded 0.25 sec, right: welded 0.35 sec)

With a weld time of 0.15 sec both films are individually distinguishable and maintain their original thickness. However, with a weld time of 0.25 sec the thickness of the two films is reduced as a result of melting and squeeze flow.

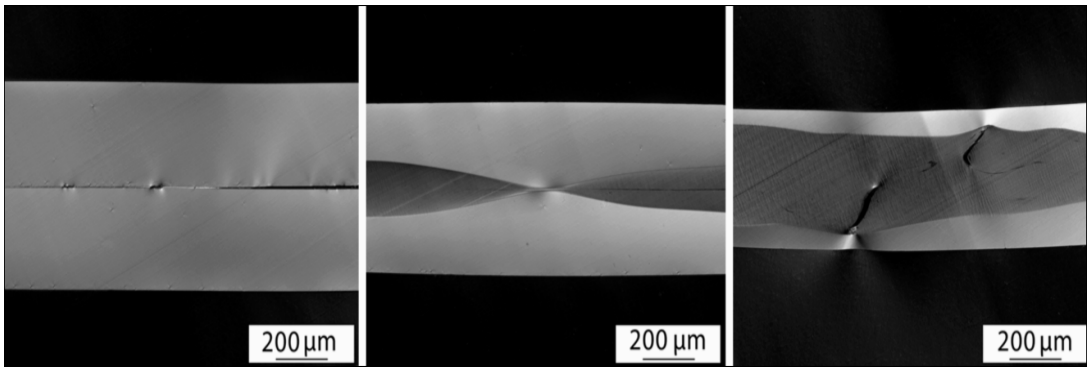

FIG. 11 Micrographs of ultrasonic welded PLA films, 305 µm thickness, detailing weld zones and crack formation in the weld line (left: welded 0.15 sec, center: welded 0.25 sec, right: welded 0.35 sec)

It is interesting to note that the squeeze flow has a distinctive appearance compared to the base material. It is believed that the change in appearance is due to a loss of orientation as a result of melting. It is also seen than at the center of the weld, there is little squeeze flow at 0.25 sec while at 0.35 sec the entire weld zone appears to be fully melted. There is no clear explanation for the apparent stagnation region in the center of the weld at 0.25 sec.

The voids in the images at 0.35 sec may be due to mechanical impact of the horn or thermally induced out-gassing of water during welding and may be the reason that the weld factor decreases with increasing weld time as shown in FIG. 9.

3.4 Heat Treatment of PLA

Table 2 shows the failure load of samples from bulk material and welded samples (ultrasonic process only) of PLA and annealed PLA. The samples were welded for 0.35

sec with a weld amplitude of 64 μm_{p-p} and a weld force of 445 N. The film thickness was 254 μm. After annealing, the failure load of both welded and bulk materials increased by approximately 10%. The melt enthalpy (ΔH_m), which correlates to the area of the melting peak in the DSC, is reported in Table 2. In addition, the degree of crystallinity (Table 2) was obtained by dividing the enthalpy of melting of the semicrystalline material (from integrating with respect to time the melting endotherm from the DSC trace) divided by the enthalpy of melting of completely crystalline PLA (ΔH_c = 93.1 J/g) [16]. It was found that the degree of crystallinity was 25% suggesting, that welding could occur below T_m. The integration for the melt enthalpy was completed between the onset of melting at approximately 134 ºC to complete melting at 154 ºC. It is seen that there is a difference between the four samples with the welded sample having a lower melt enthalpy. This suggests that there is less crystallinity in the welded part of the samples and that annealing did promote crystallization to a certain degree.

Table 2 Tensile load, melt enthalpy of ultrasonically welded samples, annealed and neat material, PLA-neat: material as received, PLA annealed: heat treated material

PLA	Degree of crystallinity [%]	Deviation [%]	Load [N]	Deviation [N]
neat	25.06	1.65	205	6
annealed	25.77	1.28	222	14
welded	18.34	1.13	170	30
weld.+anneal.	28.16	1.61	186	23

In addition, FIG. 12 and FIG. 13 show images of samples that were annealed after welding.

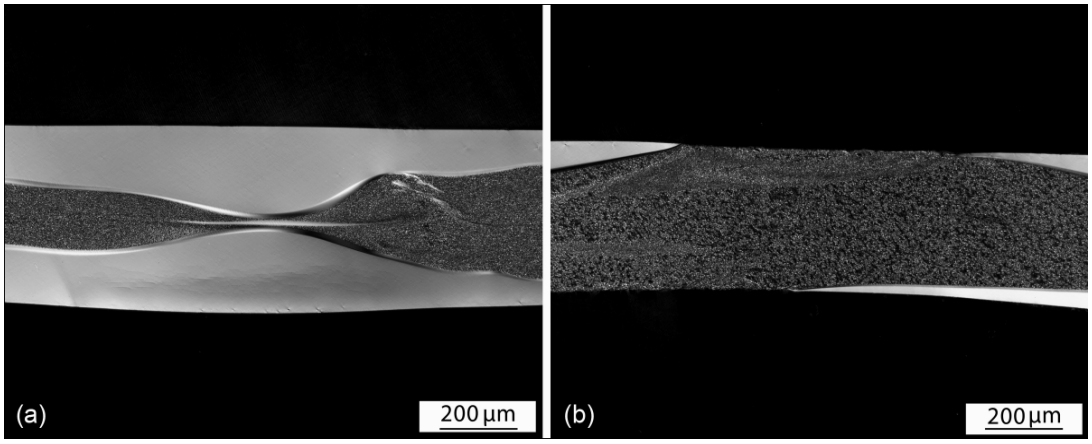

FIG. 12 Micrographs of ultrasonic welded PLA films, 305 µm thickness, detailing change of morphology in the weld after annealing for 90 min at 90 °C (left: welded 0.25 sec, right: welded 0.35 sec)

The morphology in the POM images show spherulites in the weld zone that do not appear in the images of the weld samples that were not annealed. Such growth of spherulites is in good agreement with the higher crystallinity observed in the DSC scans as well as a higher weld factor.

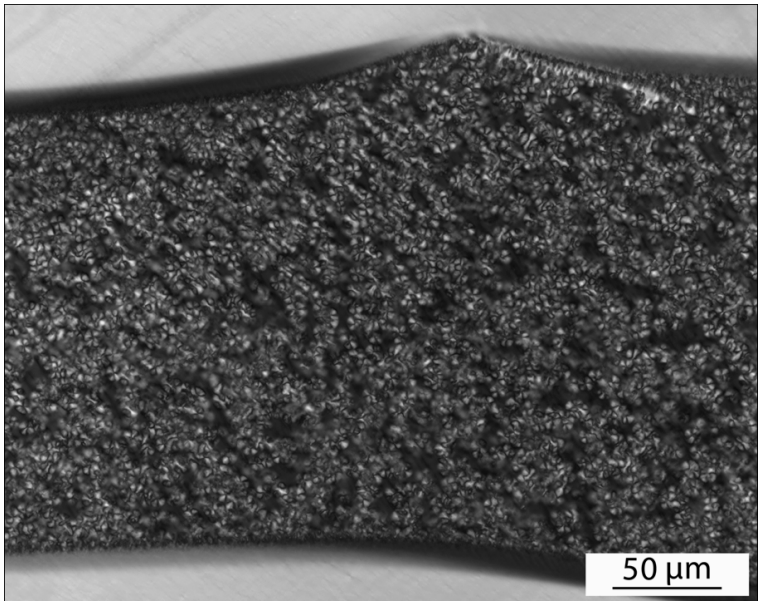

FIG. 13 Micrograph of ultrasonic welded PLA film, 305 µm thickness, weld time 0.35 sec, detailing change of morphology in weld line after annealing

FIG. 14 shows the results of the DSC measurements. All four samples show a glass transition temperature at approximately 61 ºC. The two samples that were not annealed above their glass transition temperature, 'PLA neat' and the 'PLA welded' show an endothermic peak immediately following the glass transition temperature. Such endothermic peaks, attributed to enthalpic relaxation or physical aging, are commonly seen during the glass transition relaxation on heating in glassy polymers that have been held for an extended period below T_g [24, 25]. This enthalpic relaxation is "erased" in the two samples that were annealed above the glass transition temperature.

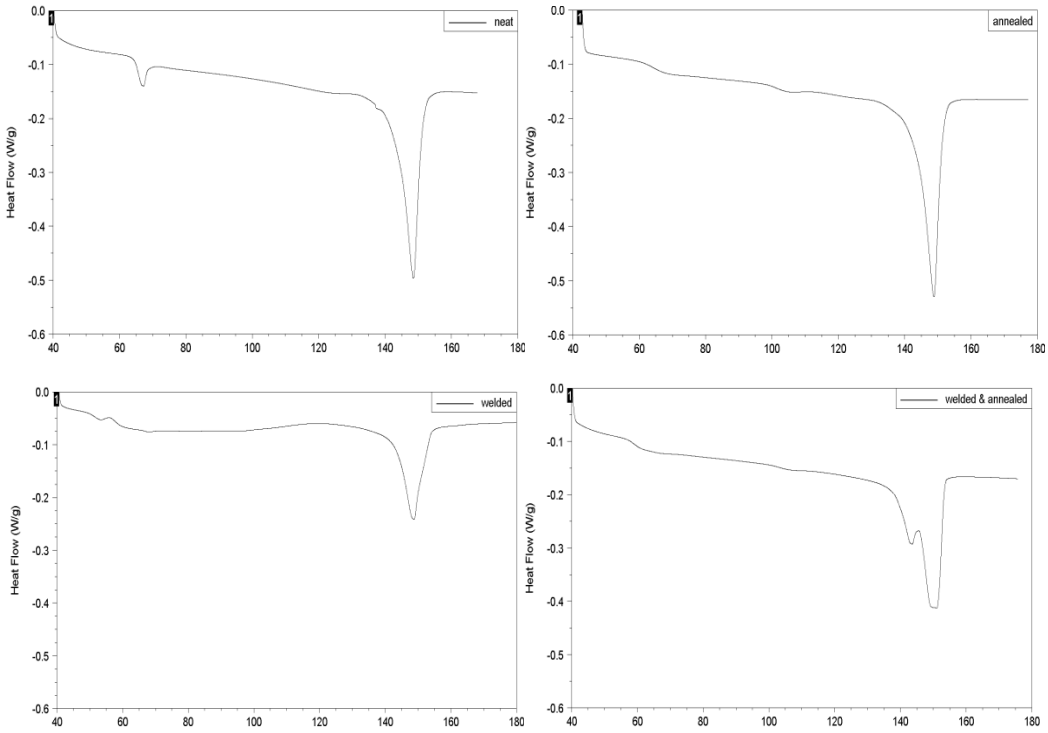

FIG. 14 DSC measurements of welded, annealed and pristine PLA samples, heating rate 5°C/min, horizontal axis: Temperature (°C)

Annealing the material above T_g for 90 min and cooling it slowly at a constant rate of approximately -1 ºC/min, allows the material to crystallize above T_g and return to a state

of the lower free energy in preferred regular conformations, resulting in a higher failure load for the samples [26].

The annealed samples also exhibit a second 'second order transition' at approximately 110 ºC. It is hypothesized that this transition indicates the presence of the so called 'Rigid Amorphous Fraction' which can appear in semicrystalline polymers after annealing. This third phase starts vitrifying when the crystallization process in a semicrystalline material is almost completed [27].

4 Conclusions

In impulse welding, it was shown that increasing the weld time initially caused an increase in the failure load. However, once a limit in the heat input into the weld was surpassed, the strength of the PLA films starts to decrease. Impulse welding of PLA films can be completed at cycle times as low as 0.5 sec and even lower for film thicknesses at 25 μm. A weld time of 4 sec was too high and the failure load tends to decrease at these longer times due to squeeze flow.

Ultrasonic welding can be completed at cycle times as low as 0.15 sec at an amplitude of 68 μm_{p-p} and weld force of 145.5 N, resulting in a significant high weld strengths for PLA films with a thickness of 305 μm. At weld times lower than 0.15 sec the material does not fuse, indicating that the amount of heat generated is insufficient to adequately plasticize the polymer. At low weld times, the welding is inconsistent, which results in a deviation of up to 30%. However, with increasing weld times of 0.25 sec and more, the deviation decreases to less than 10%. Increasing the weld amplitude and weld force was effective to increase the failure load of the samples but did not eliminate the high deviation of the results.

Heat treatment of PLA films shows that annealing and the 'erased' physical aging increases the weld strength as well as the base strength of the material. It is also important to note that the annealing process allows the polymer chains to form spherulites in the weld zone that increase the crystallinity of the material. FIG. 13 highlights this interesting effect of growing spherulites in the weld zone of ultrasonic welded samples that were annealed. Further research should be done to examine the effect of growing spherulites on the physical properties of PLA as well as to examine why the spherulites appear only in the welded zone and not in the base material.

5 Acknowledgements

Acknowledgements go to Branson Ultrasonics Corporation for donation of welding equipment, Bi-Ax International Inc. for donation of PLA samples and the United States Department of Agriculture Bio-Preferred program for support of this work.

References

1. D.W. Farrington, J. Lunt, S. Davies, and R.S. Blackburn, Biodegradable and sustainable fibers"Polylactic Acid Fibers",Blackburn, Leeds (2005), 192-196.

2. T. Oswald, E. Baur, S. Brinkmann, K. Oberbach, E. Schmachtenberg, International Plastis Handbook, Hanser Publications, Munich (2006) 731.

3. A. Harper, Modern Plastics Handbook, McGraw-Hill Professional, New York (2000).

4. X. Ou, M. Cakmak, Polymer, 49, 24 (2008) 5344-5352.

5. A. Mohanty, M. Misra, L. Drzal, Natural Fibers, Biopolymers and Biocomposites "Polylactic Acod Technology", Taylor & Francis, Boca Raton (2005) 529-577.

6. A.P. Gupta, V. Kumar, Eur. Polym. J., 43 (2007) 4053–4074.

7. C.J. Nonhof, G.A. Luiten, Polym. Eng. Sci., 36, 9 (1996) 1177.

8. M. Kellomäki, P. Törmälä, J. Mater. Sci. Lett., 16, (1997) 1786 – 1789.

9. A. Benatar, R.V. Eswaran and S.K. Nayar, Polym. Eng. Sci., 29, 23 (1989) 1689-1698.

10. K.S. Suresh, M. R. Rania, K. Prakasan, R. Rudramoorthy, J. Mater. Process. Technol., 186, 1-3 (2007) 138-146.

11. A. Benatar, Z. Cheng, Polym. Eng. Sci., **29**, 23 (1989) 1699-1704.

12. D. Grewell, A. Benatar, J. Park, *Plastics and Composites Welding Handbook "Ultrasonic Welding",* Hanser Publications, Munich (2003).

13. D. Grewell, A. Benatar, *Polym. Eng. Sci.,* **48**, 5 (2008) 860-867.

14. T. Hatakeyama, F.X. Quinn, *Thermal Analysis, Fundamental Application to Polymer Science,* John Wiley & Sons Ltd., United Kingdom (1999).

15. C. Ageorges, L. Ye, M. Hou, Composites: Part A, 32, 6 (2001) 839-857.

16. L.T. Lim, R. Auras, M. Rubino, *Prog. Polym. Sci.,* **33**, 8 (2008) 820-852.

17. D. Grewell, *SPE ANTEC Proceedings,* Brookfield, CT, **54** (1996).

18. V.A. Kagan, C. Rothe, *SPE ANTEC Proceedings,* Brookfield, CT, **60** (2002) 1266–1274.

19. D. Grewell, A. Benatar, *Polym. Eng. Sci.,* **48**, 8 (2008) 1542-1549.

20. N. Ljunberg, T. Andersson, B. Wesslen, *J. Appl. Polym. Sci.,* **86**, 5 (2002) 1227-1234.

21. A.J. Peackock, *Handbook of Polyethylene, Structure Properties and Applications,* CRC Press, New York (2000).

22. R.P. Wool, *Polymer Interfaces, Structure and Strength,* Hanser Publications, Munich (1995).

23. S.S. Volkov, I.N. Garanin, Y.V. Khoplov, *Russ. Ultrason.,* **28**, 15 (1998).

24. M.R. Kessler, S.R. White, *J. Polym. Sci., Part A: Polym. Chem*, **40**, 14 (2002) 743-753.

25. G.B. McKenna, C. Booth, C. Price, *In Comprehensive Polymer Science,* Oxford, New York (1989).

26. A. Rudin, *The Elements of Polymer Science and Engineering,* Academic Press, San Diego (1999).

27. M.C. Righetti, E. Tombari, M. Angiuli, M.L. Di Lorenzo, *Thermochima acta,* **462**, 1-2 (2007) 15-24.

Chapter 3: Ultrasonic cutting of biodegradable polylactic acid (PLA) films

Julius Vogel, Iowa State University, Mechanical Engineering
Dr. David Grewell, Iowa State University, Agricultural and Biosystems Engineering

A paper published in the Society of Plastics Engineers (SPE) *Annual Technical Conference* (ANTEC), May 2011, Boston

Abstract

Ultrasonic cutting systems are often used with materials that are difficult to cut with standard mechanical systems such as shears. The cutting knife/edge typically vibrates at a frequency of 20 - 60 kHz, heating the substrate during the cutting and simultaneously sealing the cut edges. Polylactic acid (PLA) is relatively brittle compared to polyethylene terephthalate (PET), which has similar mechanical properties. This brittleness is problematic during mechanical cutting, which produces micro-cracks that further embrittle the material.

This study used an ultrasonic equipment which had a knife fixed to the anvil and a horn with a flat surface that engaged the knife. After cutting, the samples were tested for mechanical properties such as strength, toughness, and elongation and compared with samples that were cut by mechanical shearing, as well as optically examined for micro cracks. It was found that ultrasonic cut samples had higher toughness and strain to failure, and the edges did not have micro-cracks compared to samples cut with mechanical shears.

1 Introduction

In general, a wide range of methods can be used for cutting plastics or synthetic fibers. These can be mechanical, heated tool, plasma, laser, high frequency and water jet cutting. However, these cutting methods have the disadvantage of either requiring complex and/or expensive equipment, such as the case for laser cutting or degradation of the cut edge, such as the case for plasma or laser gas cutting. Ultrasonic cutting is a process that does not have many of these disadvantages and is therefore used in the industry to cut food products, parts from plastics and composite materials [1].

In ultrasonic cutting, the blade has a cutting edge that is oscillated at a frequency between 20 and 60 kHz. The parts to be cut are engaged with the cutting tools typically with a pneumatic system. In the case of continuous cutting, the cutting speed, defined as the rate of material that moves past the cutting tool, can be as high as 5 m/min. The oscillation of the horn applies a cyclic cutting force on the cutting tip. The cyclic stress at the cutting edge of the blade causes heating of the product, which significantly reduces the overall cutting force required to cut through the material. Unlike in conventional cutting, where the cutting edge has to apply sufficiently high compression and shear that causes a tensile/shear failure at the crack tip, in ultrasonic cutting the blade vibrates continuously which enables the blade to “slide through” the material with considerably lower forces [2]. If excessive amplitudes and/or pressures are used the heat generated by friction and hysteresis can cause localized degradation of the polymers [3].

By using high-speed cameras, it was shown that during ultrasonic cutting the material appears to fracture/cut when the cutting tool impacts the surface. The cutting speed increases with increasing amplitude, frequency, and static force, and decreases with decreasing material hardness and brittleness [4]. In addition, the cutting speed (speed at

which the tool translates through the sample) also depends on the dimensions and shape of the cutting tool. As previously mentioned, the application of ultrasonic vibration results in a decrease of the static force required for plastic deformation to occur. It was shown in some experiments that the static force required to cut materials can be reduced by 85% by using ultrasonics. This increase in plastic deformation of the material can be attributed to a change in the distribution and mobility of dislocations and/or to thermal effects in the ultrasonic field caused by energy dissipation [4].

The cutting arrangement used for this study is shown in Figure 1 and has three functional parts, which are (1) transducer, (2) booster, and (3) horn. Once coupled together they are referred to as the stack assembly. The transducer converts a 20 kHz electrical voltage into a 20 kHz mechanical vibration (or other ultrasonic frequencies). The booster increases the mechanical vibration and transfers it into the horn. The workpiece is fixed between the horn and cutting blade. When the stack assembly engaged the part, the ultrasonic vibration started and the horn cut the part. It is important to note that the blade (sharp edge) can be located either on the horn or the anvil assuming inertial effects are ignored. In practice, this assumption is often applied so that the sharp edge can be placed on the anvil so that tooling design/production can be reduced. That is to, because the sharp edge has to be re-sharpened during maintenance, and the horn has to be designed to resonant at the stack frequency, it is advantageous to have the cutting edge on the anvil instead of the horn.

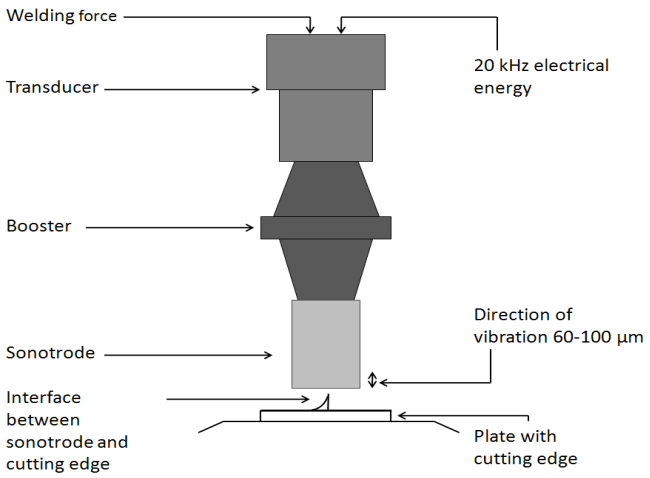

Figure 1 Ultrasonic cutting assembly

It is theorized, that because shear cutting leads to micro-cracks during the cutting and because ultrasonic cutting heats the material at the edge up to its melting temperature and 'heals' the cut edge, this will result in improved mechanical performance of the material.

2 Materials and Methods

The ultrasonic machine was configured in a ground detect mode, meaning that the ultrasonic vibration stopped when the horn physically touched the blade of the fixture. After cutting, the samples were removed and tested for their tensile strength.

The ultrasonic cutting was done with a Branson Ultrasonic 2000 Welding System (Danbury, CT) using a booster and horn with a gain of 1.5:1 and 2.66:1, respectively. The trigger force was set to 90% of the weld force [5]. The cutting time was measured as the time from the beginning of the vibrational movement of the horn until the cutting cycle was interrupted by the ground detect. The cutting speed (average) was calculated by dividing the sample thickness by the total cutting time as reported by the power supply. The films used for the experiments to measure the cutting speed had a thickness of 200, 250 and 300 µm. Cutting parameters were the force applied by the horn on the samples to

be cut and the vibrational amplitude. The width of the samples was chosen to be the width of the cutting horn (40 mm). Cutting was repeated six times at each machine setting and the cutting time was reported as the average of the six measurements. For selected data experimental conditions, the depth of cut was measured as a function of cutting time. In addition, the effect of ultrasonic cutting was studied on the weld strength of ultrasonic welded samples and how the strength of ultrasonic cut samples compare to samples cut by simple shearing. The dimensions of the lap shear joint geometry that was used for testing the mechanical properties of the welded and cut samples are shown in Figure 2. The ultrasonic cutting was completed along the neck region of the tensile test bar, to make sure that the ultrasonically cut edge was exposed to the maximum appearing stress.

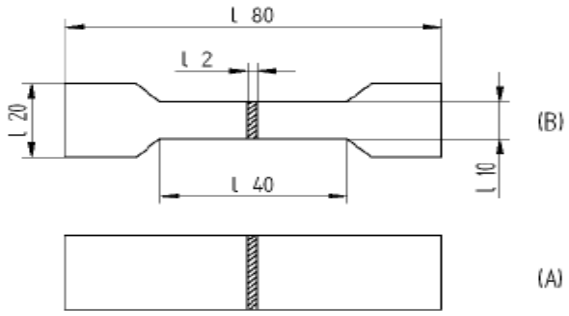

Figure 2 Dimensions (mm) of tensile test samples for ultrasonic welding; (A) sample dimensions after welding, (B) sample dimensions as tested

Welding was completed at a weld force of 170 N, a weld amplitude of 48 μm_{p-p} and a weld time of 0.2 s. After welding, six samples were cut using a scissor and six were cut with the ultrasonic cutting device and tested for their mechanical strength in the tensile direction. Testing of the welded films was completed according to ASTM D 638 with a modified sample geometry using an Instron (Norwood, MA) model 4500 load frame with a 5 kN load cell at a crosshead speed of 10 mm/min. The results of the tensile testing were reported as the weld factor, which is the failure load of the samples divided by the

tensile strength of the base material. The base material strength that was tested by using samples cut out from the base material.

3 Results and Discussion

Figure 3 shows the results for the log of the ultrasonic cutting speed as a function of static pressure. As expected, with increasing pressure the cutting and separation of the PLA films is more effective because of increased ultrasonic coupling and higher material displacement rates [7]. It is important to note that the because of the synergetic effects of better coupling, high squeeze flow, higher temperatures and shear thinning, the cutting speed increase as a exponential function of static force.

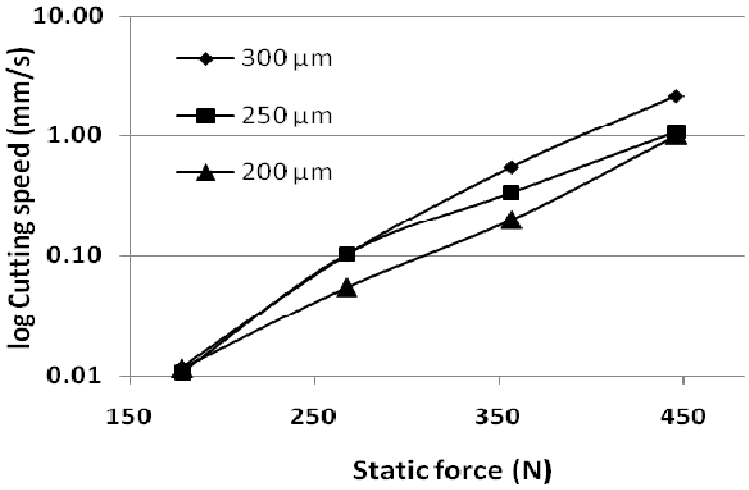

Figure 3 Cutting speed for increasing static force and three film thicknesses

A similar effect was observed for increasing vibrational amplitude. Figure 4 shows that the cutting speed increases from approximately 0.01 mm/s at 32 μm_{p-p} amplitude to 1 mm/s for 305 μm thick films, and approximately 0.5 and 0.2 mm/s for 250 and 200 μm thick films at 80 μm_{p-p} amplitude, while the static force was constant at 178 N. The time

to melt the PLA film is inversely proportional to the amplitude squared, which explains the exponential increase of the cutting time in this case.

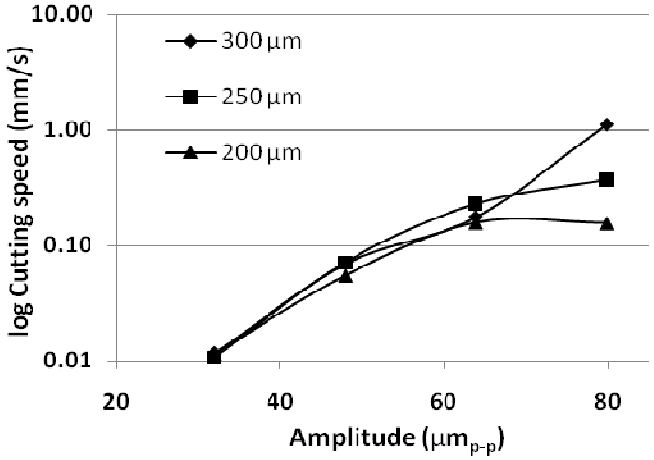

Figure 4 Cutting speed for increasing vibrational amplitude and three film thicknesses

The depth of cut as a function of cutting time is shown in Figure 5 for 305 µm thick films for the various vibrational amplitudes and static forces that were studied. One observation is a logarithmic relation between the relative penetration depth, (depth of cut/thickness of the film) and time. The velocity (slope of the curves) is highest at the start of the cutting process and slowest at the end of the cutting process with a transition in between.

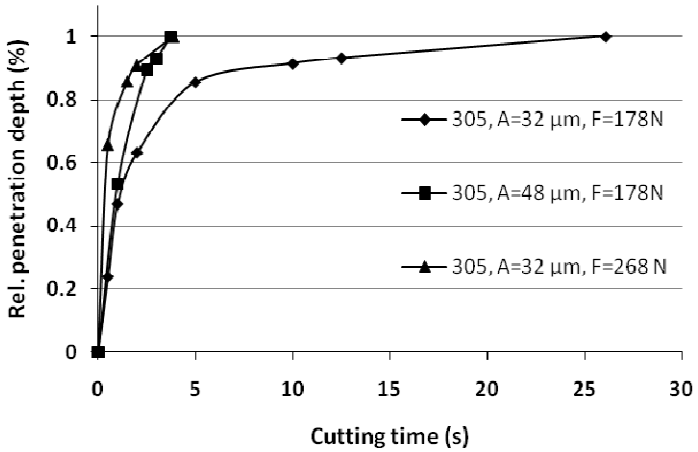

Figure 5 Depth of cut for increasing cutting time

However, while the transition from a fast cutting speed to a slow cutting speed is very distinct for the lowest cutting force and amplitude, it is less distinct when these parameters increase. It is believed that this is related to heat flow into the cool anvil and horn and loss of heat generation. In more detail as the cutting progresses, the total volume of plastic between the anvil and horn decreases and the amount of heat being generate decreases. In addition, as the cutting interface (cutting edge near sharp knife edge of anvil) approaches the horn, the distance between the heat source (namely at the knife edge) decreases allowing more of the generated heat to flow not only into the cool anvil but also into the cool horn. As this distance becomes very small near the end of the cutting cycle, at the lower force and amplitude, there is insufficient heat generation within the sample to overcome the heat loss. Thus, a relatively long cutting cycle is requried until sufficient heat is generated (conducted from the plastic) in the horn and anvil to allow the final cutting distance to be translated.

Such a change in the propagation speed of the cut also indicates a transition of the material properties resulting in a change in the cutting velocity that can be attributed to the change in the elastic properties of thermoplastic materials. With increasing temperatures, the material goes through a range of thermal transitions. At low temperatures, the Young's modulus of semicrystalline materials stays constant in the range of ca. 10^9 Pa. With further increasing temperatures, the modulus will at first slowly decrease and then rapidly decrease at the glass transition temperature (T_g). For polymers with a high amorphous part, the modulus will stay at the so called "rubbery plateau" which is usually in the order of 10^6 Pa until it will again rapidly drop when the temperature further increases. The appearance of this rubbery plateau is due to molecular entanglements of the polymer chains that prevent slippage. Therefore the modulus will

stay relatively high above the glass transition temperature [8]. Assuming that because of the heat generated during the ultrasonic interaction of the horn with the workpiece, the material will undergo these transitions which will result in different cutting velocities in each of the thermal states. Such a transition from a fast cutting speed to a low cutting speed, that resembles an exponential decay in the cutting speed, can be explained with the rubbery behavior of PLA in a temperature range between T_g and the cold crystallization temperature T_{cc}, where the material will exhibit a relatively high viscosity that enables it to endure high stresses while it shows little or no plastic deformation [9].

Figure 6 shows the results for the tensile test of samples which were cut ultrasonically and by shearing. While the maximum tensile stress are similar for both cutting methods the strain, as well as the toughness of the samples, increases significantly when the samples are cut with ultrasonics.

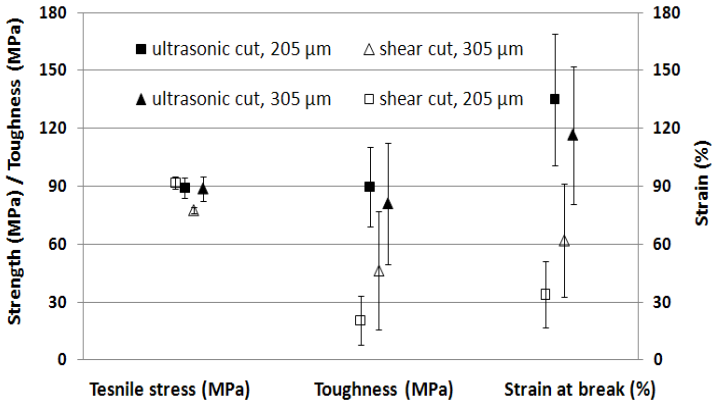

Figure 6 Stress, strain and toughness for tensile test samples cut through shearing and cut ultrasonically

Figure 7 shows SEM images of the cut edge at magnifications of 50x and 150x. During the scanning the sample was held in the fixture so that the electron beam is directed on

the cut edge. The direction of ultrasonic cutting is in the positive horizontal direction from left to right.

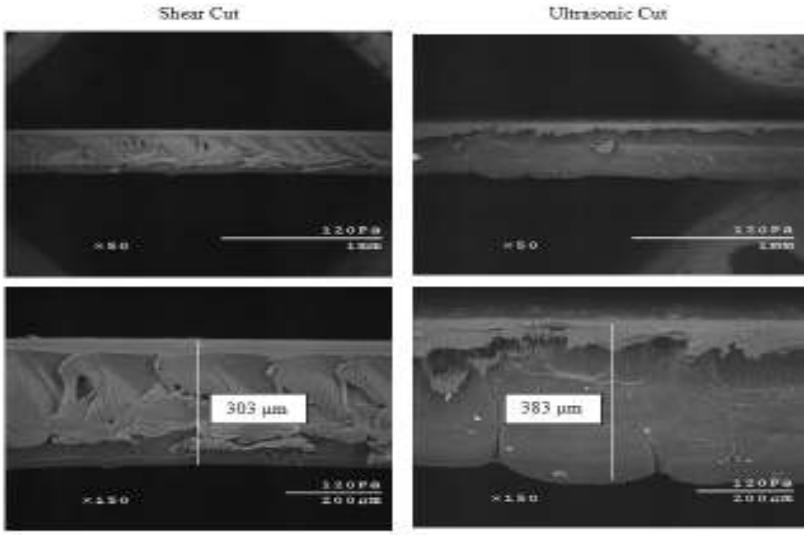

Figure 7 SEM images of cut edge of shear cut (left) and ultrasonically cut (right) samples showing a view normal to the cut edge at magnifications of 50x and 150x

The scanning showed that ultrasonically cut samples have a more homogeneous “smooth” surface on the cut edge as compared to the shear cut samples which have a more irregular edge. In addition, the cut edge of ultrasonically cut samples examined from the view on the plane surface on the sample shows “swellings” where the cutting blade interacts with the sample which is shown in Figure 8. This swelling is a result of the heating and melting of the plastic during the ultrasonic cutting that accumulates the molten material at the cutting blade. However, because the blade is not perfectly parallel to the horn, some sections of the sample are fully cut while others need to be separated forcefully which causes the cleavage burrs which are observed. In addition, Figure 8 shows that shear cutting leaves traces of deformation that starts from the cut edge and propagates in a 45° angle into the sample center, while this is not seen with samples cut with ultrasonics. It is assumed that because the shear fracture propagates from left to right with forces acting

from top to bottom, in this case of mechanical cutting, the effect of cutting will cause different fracture modes in the material as compared to the ultrasonic cutting that locally heats and separates the films thereby.

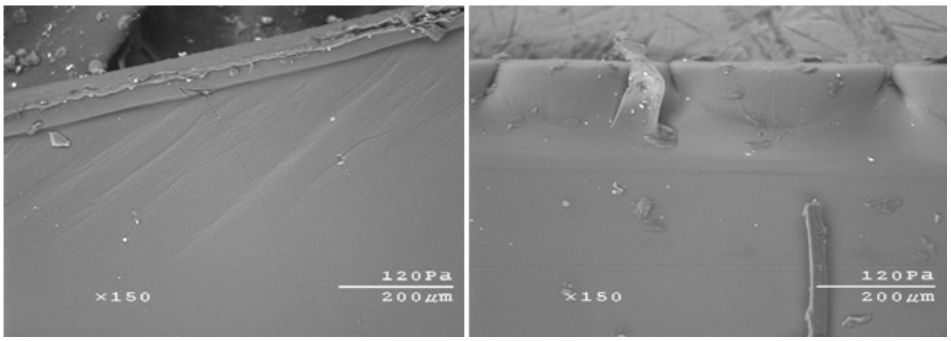

Figure 8 SEM images at 150x magnification of ultrasonic cut (right) and shear cut (left) samples

Figure 9 shows images of the cut edge of samples cut with ultrasonics and shearing after the samples were tested in the tensile mode. The images were taken at the necking zone of the samples where the thinning appears in the cross sectional area as a result of necking. These images show that the surface of the edge does not significantly change when the cut is made with mechanical shearing while there are obvious stretch-marks seen on the edge of the ultrasonically cut sample. The structures with the swelling at the edge of the samples, as seen in Figure 7 and Figure 8, are stretched in the tensile direction. The surface features that appear as globular accumulations of material are oriented into “lines” that continue along the axis of tensile elongation. This stretching of the globules into lines would explain why the samples can be exposed to more deformation before fracture appears, while the shear cut samples would fracture with less deformation because the shearing leaves a more irregular surface that is prone to growth of micro-cracks.

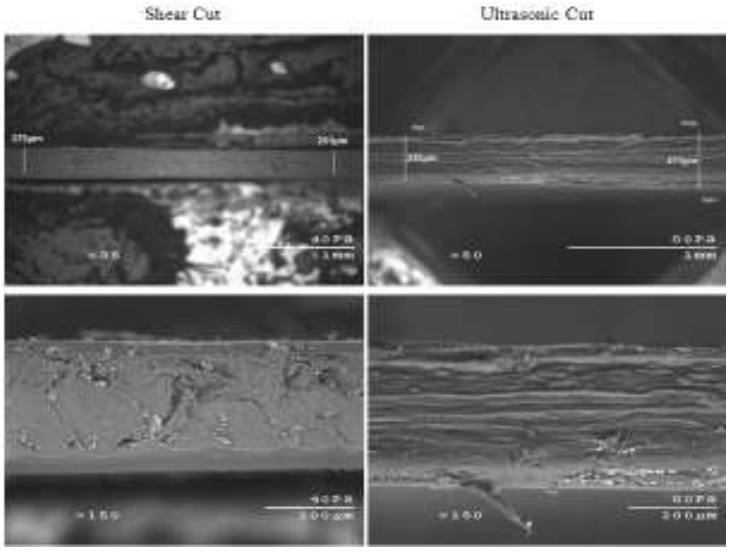

Figure 9 SEM images at 50x and 150x magnification of ultrasonic cut (right) and shear cut (left) samples after tensile test

Figure 10 shows the failure load of ultrasonic welded samples that were cut into the testing dimensions by shearing and by using ultrasonics. It is seen that ultrasonic cutting significantly increased the failure load of welded samples. This can be explained as the ultrasonic vibration caused sufficient friction, and thereby heat, to melt the welded zone of the two layers that were in contact with the blade. As a result, fusion bonding of the cut edge was more effective which resulted in the increased failure load. A disproportional high variation in the results of ultrasonically welded PLA films was observed here, which is probably due to incomplete welding in the overlap area as well as the brittle nature of PLA. However, such a high variation is not uncommon for PLA films welded at short weld times and has already been reported in other publications [11].

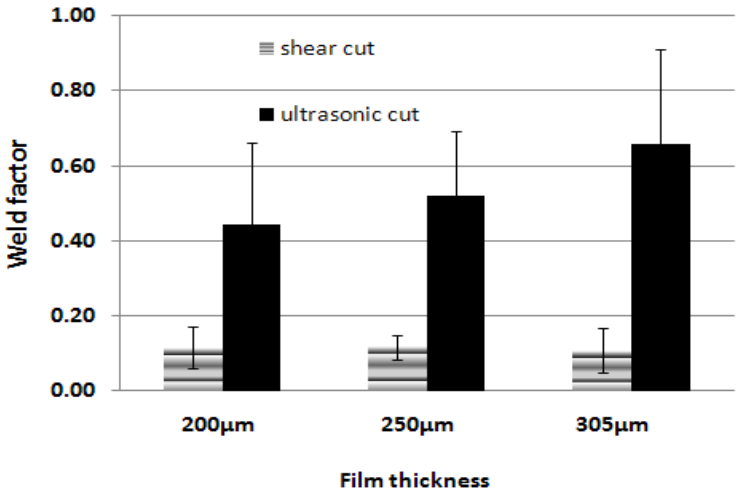

Figure 10 Failure load for welded samples cut with scissors and cut ultrasonically for three film thicknesses

Conclusions

Ultrasonic welding equipment can be used for cutting biodegradable films of PLA with cutting speed as high as 1 mm/s. The cutting speed was increased by almost two orders of magnitude by increasing the static force from 178 to 446 N. The effect of increasing amplitude was similar. For thinner films the cutting speed was lower while it was faster for thicker films. Further increase in amplitude did not substantially increase the cutting speed.

Ultrasonic cutting of welded samples can increase the failure load of the weld because the heat generated during the cutting melts and fuses the film layers more effectively in the zones where the cutting blade touches the film interface. Ultrasonic cutting is also advantageous in terms of tensile strain at break and toughness and can ‘conserve’ more of the potential strength and deformation of the material compared to shear cutting methods.

Acknowledgements

Acknowledgements go to Branson Ultrasonics Corporation for their donation of equipment, Bi-Ax International Inc. for donation of PLA samples, and the Iowa State University Center for Crops Utilization Research (CCUR). In addition, much appreciation and thanks to the USDA Bio-Preferred Program for funding this work.

References

1 S.S. Volkov, D.V. Sannikov, Russian Ultrasonics, Ultrasonic Cutting of Polymer Materials, 31 **5** (2001)

2 T.J. Mason, J.W. Povey, Ultrasound in Food Processing, Blackie Academic& Professional, London (1998)

3 D.H. Buckley, Polymer Science and Technology, V5b, **6**, pp 601, New York (1974)

4 V.K. Astachev, V.I. Babitsky, Ultrasonics in Processes and Machines, Springer Publications, Berlin Heidelberg (2007)

5 D. Pelton, Evlon Product Information Data Sheet, BI-AX International Inc, Ontario Canada

6 D. Grewell, SPE ANTEC Proceedings, Brookfield, CT, 54 (1996)

7 L.D. Rozenberg, Physical Principals Of Ultrasonic Technology, Plenum Press, New York (1970)

8 J.R. Fried, Polymer Science and Technology, Prentice Hall PTR, New Jersey (1995)

9 X. Ou, M. Cakmak, Polymer, **49** (2008).

10 J.D. Kim, E.S. Lee, Int. J. Adv. Manuf. Tech. (1996) **12**, pp 78-86

11 J. Vogel, D. Grewell, K. Haubrich, SPE ANTEC proceedings (2009), pp 306-310

Appendix to Chapter 3:

Tool for simultaneously cutting and sealing plastic films

Ultrasonic ‘seal-cutting’ is a common process in the industry to cut and simultaneously seal films, nonwovens or fibers. However, because the cutting blade seals only in that section where it interacts with the anvil and the material, this method has the disadvantage that the seal strength is rather weak. The cutting blade creates only a seal-line which can easily tear and is it inadequate for products that require a high seal strength.

In other applications, sealing and cutting are two different manufacturing operations that are typically designed to occur subsequently on different equipment. These manufacturing operations can be used to produce plastic bags from continuous plastic films or similar products.

This invention uses a new ‘seal-cut’ method. The existing state of technology is, that the ultrasonic machine with its functional parts, which are the converter, booster and sonotrode applies an ultrasonic vibration on the interfaces that need to be joined, or on the parts that need to be cut. The ultrasonic vibration creates heat that melts the parts locally allowing them to fuse in the case of welding, or to separate when cutting is required. In ultrasonic welding and cutting, the parts to be joined or cut are placed between the horn and anvil and two configurations are possible for cutting. Either the horn has the shape of a blade or the horn is flat and the anvil has a blade attached. However, in either configuration the created seal strength is relatively weak or it requires two operations to seal and cut.

The issue this technology solves is, that it can produce a relatively high seal strength while it cuts simultaneously or it can perform sealing and cutting in the same process step. Unlike the existing seal-cut technology this tool produces a weld area instead of a weld line. As it can be seen in Figure 1, the weld anvil of the tool is rigid and has a flat surface. When the ultrasonic horn travels down and starts the vibration, the films between horn and anvil are heated and thereby fused. At the same time the blade can move with the frequency of the ultrasonic vibrations. However, there will be some resistance to the motion of the horn by the springs that hold the blade. This creates heat at the tip of the blade, softening the material which enables it to separate the films.

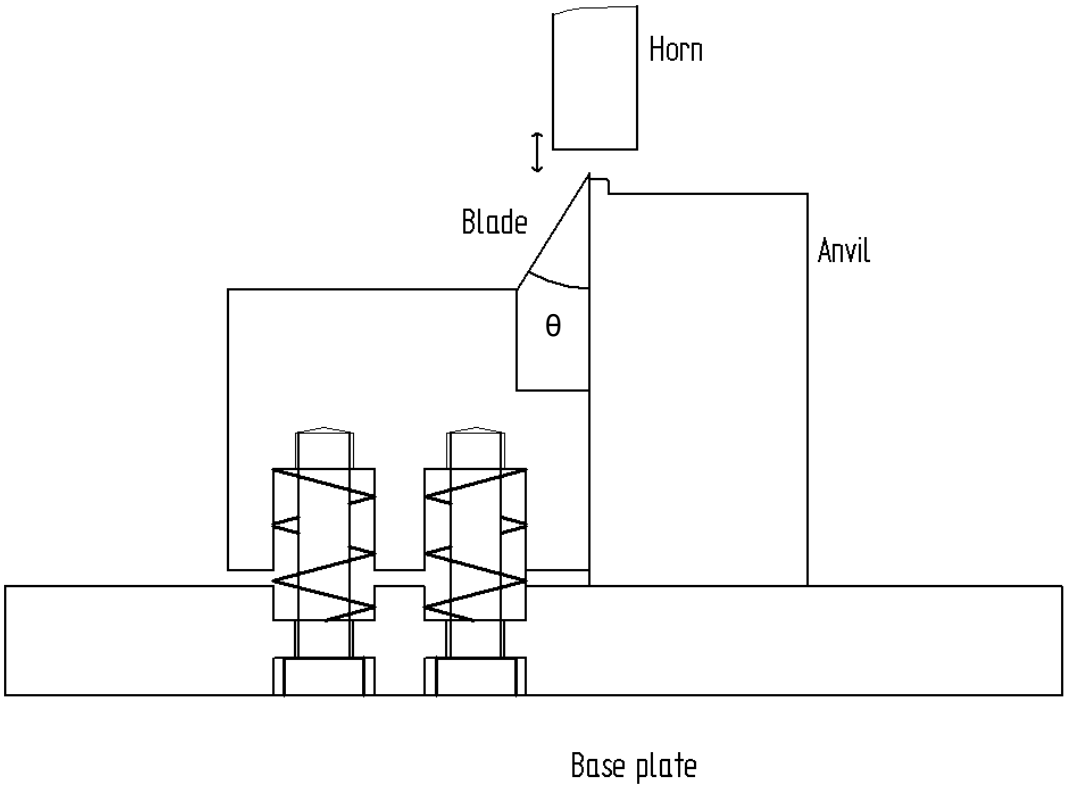

Figure 1 Ultrasonic seal-cut tool, θ - cutting angle

The invention here is, that the blade is designed in a way that it can 'float' during the ultrasonic vibration, avoiding a rigid contact between blade and horn but providing sufficient friction and cutting force to melt and separate the material. As it is shown in Figure 1, the weld anvil and cutting blade are arranged adjacent, so the tool creates the seal and cuts at the at the edge of the seal. The blade has to 'float', because the tip of the blade needs to be elevated above the anvil and a rigid contact between blade and horn has to be avoided because that would mechanically flatten the edge when the horn hammers on the blade. The advantages of this tool configuration include the generation of a relatively strong weld while simultaneously cutting the sample. In addition, this invention can reduce the required equipment. In case that sealing and cutting are done on two different machines here only one machine is required to finish both operations.

Results:

Initial experiments were completed on thin films made from polylactic acid (PLA). Two overlapping films were welded and simultaneously cut and then tested on a tensile testing machine. The geometry of the tested films and the test method are shown in Figure 2 and Figure 3.

Figure 2 shows the shape of the films after welding. The cut line and seal area are created simultaneously and are directly adjacent to each other.

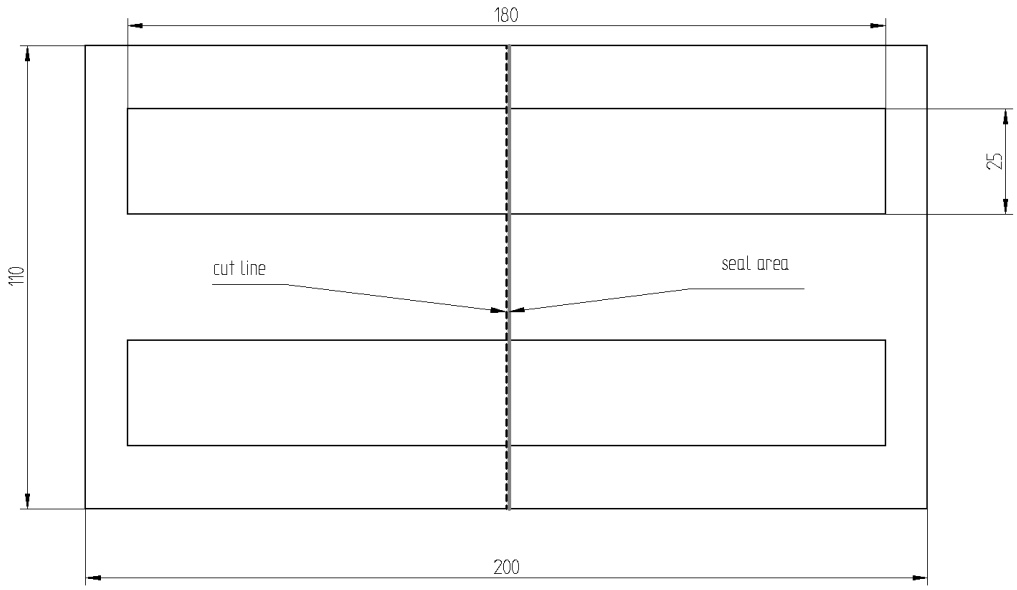

Figure 2 Geometry of tested films (all dimensions in mm)

Figure 3 shows the details of the tensile strength tests. Because the experiments were conducted for increasing the parameters weld time, weld amplitude and weld force, starting at the lowest possible parameter setting, the cutting was not fully complete at the lower parameters. Thus, a cutting efficiency was calculated according to *Eq. 1*.

$$\eta = 1 - \frac{\sigma}{\sigma_0} \qquad (1)$$

where: η – cutting efficiency
σ – strength of the cut sample
σ_0 – strength of the base material

After measuring the cutting efficiency, the sample, was tested in the peel mode to measure the seal strength. The seal strength was the measured force to tear the sealed films apart and converted to a seal strength per unit length.

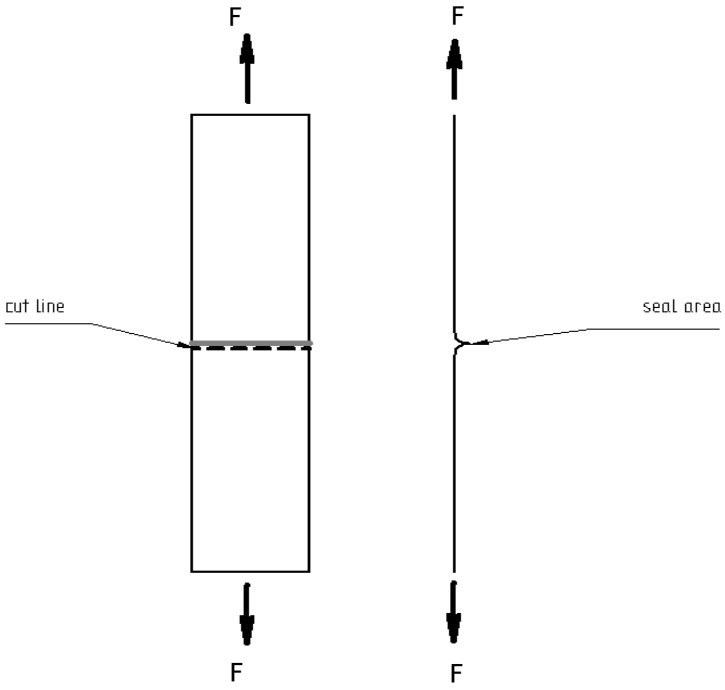

Figure 3 Test method left: testing cutting efficiency; right: testing seal strength

Some representative results of the testing are shown in Figure 4. It can be seen that the cutting efficiency is strongly affected by the cutting angle. While it is approximately 80% at 356 N cutting force and 100% cutting amplitude at a cutting angle of 32°, its approximately 100% at the same parameters and a cutting angle of 20°. The seal strength is comparable for both angle configurations with approximately 4 N/cm.

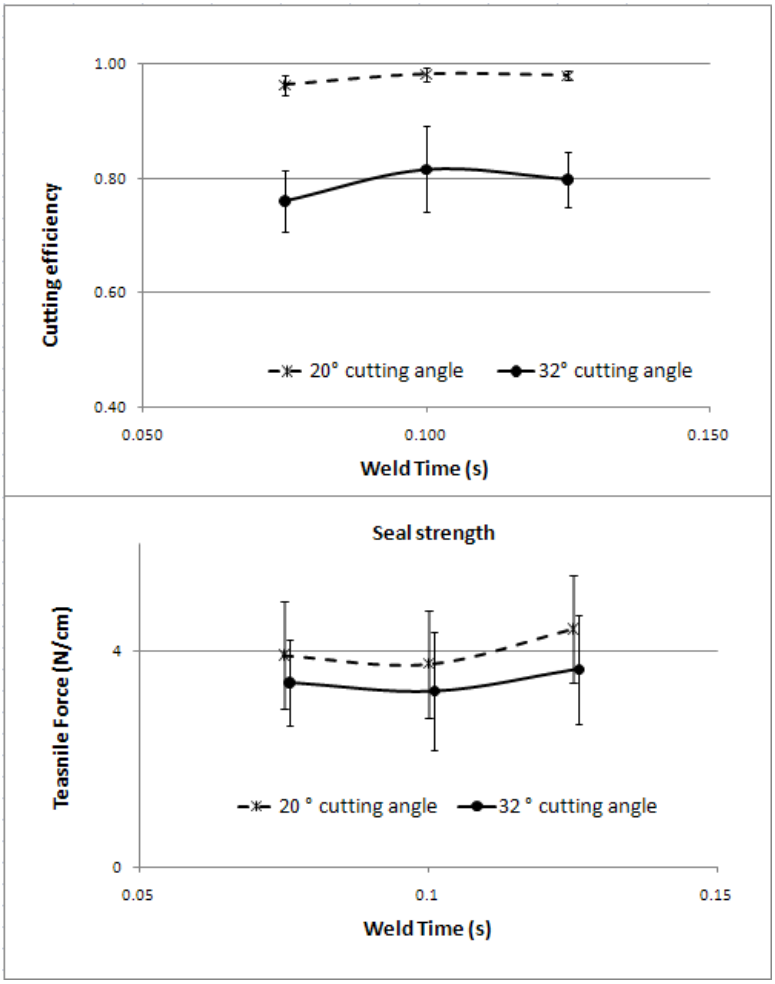

Figure 4 Results for testing cutting efficiency and seal strength

These results demonstrate that the designed tool can be used for simultaneous sealing and cutting, having the advantage that the two manufacturing operations sealing and cutting can be done in the same cycle. Possible applications are packaging for products such food product.

Chapter 4: Activation Energy for Diffusion and Welding of PLA Films

A paper to be submitted to the Society of Plastics Engineers (SPE) *Polymer Engineering & Science Journal*

Abstract

The bonding of polylactic acid (PLA) films was investigated for a broad range of temperatures and contact times above the glass transition temperature in a lap shear joint geometry using an impulse welding system.

It was observed that interfacial strength was linearly dependent to the fourth root of welding time until it approached the bulk material strength. Using models based on reptation theories the interfacial strength of lap shear welds was estimated based on thermal histories. In more detail, the activation energy for interfacial healing and self diffusion coefficient were calculated based on shear strength measurements of samples welded with well defined thermal histories. The parameters were then used to predict interfacial strength with varying temperature histories.

1. Introduction

Molecular diffusion (interfacial healing) occurs during the welding of plastics when two polymer surfaces are brought into contact above their glass transition temperature (T_g). At this temperature the polymer chains diffuse across the contact area (faying surface) until the interface is indistinguishable from the bulk material and the polymer-polymer interface disappears, while the mechanical strength of the bond increases until it reaches the bulk material strength. Such healing is important not only in polymer welding, but

also in many other polymer processing areas such as extrusion, casting or molding, where individual polymer pellets are formed into larger shapes. It is also important during the impregnation of polymer coated fibers with a thermoplastic resin, as well as the consolidation of individual plies of thermoplastic resin composites and during the crack healing in polymeric materials [1, 2, 3].

Interfacial healing was also observed below T_g for material combinations such as polystyrene/poly(phenylene oxide) (PS/PPO) and PS/PS [4]. This healing process can be subdivided into several stages. These are surface rearrangement, surface approach, wetting, diffusion and randomization. The driving force for such a mixing of polymer chain segments is the increase in entropy of the polymer chains at the interface. The parameters of such autohesion processes are contact time, temperature and pressure at the interfaces [5].

In this study the diffusion behavior during welding of polylatic acid (PLA) films was studied. Polylactic acid is a biodegradable polymer derived from lactic acid and made from 100% renewable resources such as sugar beets, wheat, corn or other starch-rich crops. The starch from the feedstock is extracted by a range of mechanisms and hydrolyzed into fermentable sugars to produce lactic acid. The lactic acid is polymerized either by a condensation reaction or through a ring opening process [6]. Polylatic acid is typically transparent, rigid and exhibits mechanical properties similar to some petroleum based polymers. For example, PLA has a tensile strength of approximately 70 MPa and a modulus of elasticity of 3.6 GPa; similar to PET (polyethylene terephthalate) which has a tensile strength of 60 - 80 MPa [7] and a modulus of elasticity of 2.1 – 3.1 GPa. In addition, PLA has a density of 1.25 g/cm^3 which is approximately 8% lower than PET. Polylatic acid is relatively resistant to moisture and solvents such as oil and grease and

has high vapor barrier properties. Depending on its formulation, it can be made rigid or flexible and can have a melting point between 130 °C and 220 °C. The molecular weight of PLA varies between 100,000 to 300,000 Daltons. As with other polymers, the strength, viscosity, melt temperature and glass transition temperature of PLA all increase with molecular weight due to increased molecular entanglement and decreased molecular movement. However, with increasing molecular weight the ease of processing is expected to decrease [8].

1.1 Effect of Contact Time on Autohesion

In order to re-establish the bulk material strength at polymer interfaces or the virgin material strength during crack healing or welding, the chains need to diffuse a distance to cross the physical separation. The time to achieve a significant level of interpenetration of the polymer chains during a welding process with a sufficiently high strength can be called the welding time t_w. It can be estimated that the average diffusion-distance $\langle x \rangle$ of a polymer chain in the bulk material follows Einstein's diffusion-equation [9] which can be applied to the polymer motion through diffusion and is given by

$$\langle X \rangle^2 = 2Dt \qquad (1)$$

where D is the self diffusion coefficient. The mechanism by which autohesion occurs can be attributed to the two characteristics of high molecular weight polymers, which are a random chain network and flexible macromolecules that are able to move within the bulk material. Figure 5 shows a schematic of the autohesion process for an amorphous polymer, assuming no flow is needed to match the surfaces to each other. At the initial contact in Figure 5 (a) the surfaces are brought in intimate contact but no adhesion is

seen. Figure 5 (b) shows the autohesion represented by D_{Au} (degree of autohesion) which ranges between 0 and 1, after some contact time above T_g. Some of the polymer chains have penetrated the surfaces of the touching parts, which is due to free chain movement that results from increased molecular free volume at the elevated temperatures. With increasing contact time the penetration depth of the diffusing polymer chains, as well as the number of chains crossing the interface increases, resulting in more entanglements and higher interfacial strength. In Figure 5 (c) at a contact time of $t=t_{\infty}$, the healing process can be considered complete as the interface disappears and strength as well as morphology are not distinguishable from the bulk material [9]. Some argue, that it is sufficient when the center of mass of a molecule has diffused a distance of approximately equal to its radius of gyration to achieve full adhesion or complete healing [10].

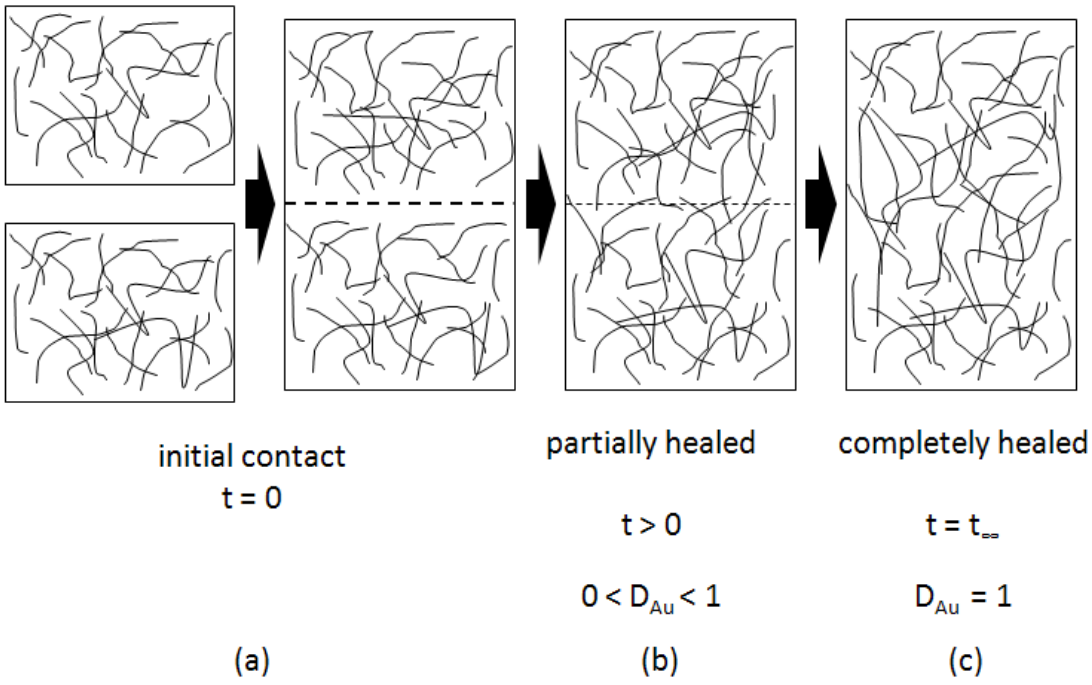

Figure 5 Physical picture of autohesion of an amorphous material

Two methods are reported to test the autohesion phenomenon [9], which are (1) radioactive doping of the polymer chains and measuring the rate of diffusion of the tracers and (2) mechanical testing of the strength of the interface. The later one will be the method employed in this work.

Using the mechanical strength-testing method, it is assumed that the interface structure at any time during the welding is related to the bulk material structure by the fourth root of the weld time t_w [5]. According to de Gennes [4], the average interpenetration depth $\langle X \rangle$ of a polymer repeat unit in a symmetric polymer interface is given by:

$$\left\langle X(t_w) \right\rangle = X_0 \left(t / t_\infty \right)^{\frac{1}{4}} \qquad (2)$$

where X_0 is the distance after a reptation time t_∞. In the reptation model the polymer motion is described as a serpentine movement of the chains within a tangle of the surrounding chains. Each chain is considered to be embodied in a tube-like surrounding and executes movements along the tube axis by thermal energy [11].

This model of polymer chain diffusion across interfaces predicts the cohesive strength of the interface is proportional to the fourth root of the weld time $(t_w)^{1/4}$, assuming no flow is needed for the interfaces to be in intimate contact. The time dependency of the interface strength during welding can be expressed as the ratio of a cohesive strength at a weld time t_w and the cohesive strength when the strength becomes independent of the processing time at t_∞ [9] as it is defined in Eq. (3).

$$D_{Au} = \frac{A_u(t,T)}{A_{u,\infty}(t_\infty, T)} \tag{3}$$

The strength of autohesion A_u depends on the contact time of the interfaces t_w and the temperature of the material. However, Jud [12] reported that the degree of autohesion can be represented by an Arrhenius law of diffusion as defined in Eq. (4).

$$D_{Au}(T) = D_0 \exp\left(-\frac{E_a}{RT}\right) \tag{4}$$

where R is the universal gas constant (8.3144 J $mol^{-1}K^{-1}$), T is the absolute temperature, E_a is the activation energy of diffusion and D_0 is a diffusion constant. The degree of autohesion in Eq. (4) can be written as:

$$D_{Au} = D_{Au\,0} + K(T)t^{1/4} \tag{5}$$

where D_{Au0} is the initial degree of autohesion due to surface attraction of the interfaces. The variable $K(T)$ is a temperature dependent parameter that represents the temperature dependent slope of D_{Au} when it is plotted as a function of the fourth root of the weld time and D_{Au0} is the intersection with the ordinate. In more detail, $K(T)$ is the product of a proportionality constant K_0 times the self diffusion coefficient of the Arrhenius as seen Eq. (6):

$$K(T) = K_0 * \exp\left(-\frac{E_a}{RT}\right) \tag{6}$$

With equation (5) and (6) the degree of autohesion D_{Au} can be written as

$$D_{Au} = D_{Au_0} + K_0 * \exp\left(-\frac{E_a}{RT}\right) * t^{\frac{1}{4}} \quad (7)$$

By plotting the natural logarithm of *K(T)* as a function of the inverse temperature, the slope of the graph is proportional to the activation energy of diffusion and the intersection of the graph with the ordinate is the proportionality factor K_0, Eq. (8)

$$\ln\left(K(T)\right) = \ln\left(K_0\right) - \frac{E_a}{RT} \quad (8)$$

Because the degree of autohesion D_{Au} is temperature dependant and assuming there is no autohesion before the weld process starts ($D_{Au0} = 0$) the degree of autohesion can be calculated as:

$$D_{Au}\left(T, t_w\right) = \sum_{t=0}^{t=t_w} K_0 * \exp\left(-\frac{E_a}{R * T}\right) * \Delta t^{\frac{1}{4}} \quad (9)$$

where E_a and K_0 can be determined experimentally [13].

The autohesive strength of an interface at any time less than t_∞ has been observed to be lower at the low temperature condition than at a higher temperature condition. That occurs because higher molecular mobility at higher temperatures allow more diffusion at the given time period. However, as well as higher temperatures cause faster diffusion rates allowing the polymer chains to penetrate interfaces easier it is also easier to pull the polymer chains and to separate interfaces [9].

1.2 Effect of Contact Pressure on Autohesion

The degree of autohesion increases asymptotic with pressure until it reaches a maximum at the so called 'saturation pressure' for a given temperature and time. A further increase in pressure does not result in any increase of autohesive strength. This behavior can be explained with an increasing contact area for increasing pressure. Once the interfaces are in full intimate contact after the surfaces have rearranged and deformed a higher pressure will have less of an effect on the autohesive strength [9].

1.3 Time Temperature Superposition

The time temperature superposition method can be used to gain information how a material will behave under certain conditions at fixed temperatures and different times. This information can be gained from the so called shift factor a_T. In case of a linear time temperature relationship the shift factor can be considered as the ratio of a time t_r for the material to reach a certain state at a reference temperature T_r to the time t to reach the same state at a different temperature T [14] as seen in Eq (10).

$$\log\ a_T\ =\ \log\left(\frac{t}{t_r}\right) \tag{10}$$

In more detail the time temperature superposition theory defines that a material property E at any time and temperature is the same as it is at a reference time and temperature as seen in Eq (11).

$$E(t,T)\ =\ E(t_r,T_r) \tag{11}$$

The shift factor depends on the temperature and can be estimated with an Arrhenius type equation assuming a constant activation energy [15, 16]:

$$\log a_T = \frac{E_a}{R}\left(\frac{1}{T} - \frac{1}{T_{ref}}\right) \tag{12}$$

where E_a is the activation energy of diffusion, R is the ideal gas constant, T is the given temperature and T_{ref} is a reference temperature.

2 Materials and Methods

Polylactic acid (PLA) films with a thickness of 100 μm from Evlon®, produced by Nature Works (Minnetonka, MN) were used in this study. The glass transition temperature and melting temperature which were determined with a TA Instruments Q20 DSC using a heating rate of 5°C/min. The results are shown in Figure 6.

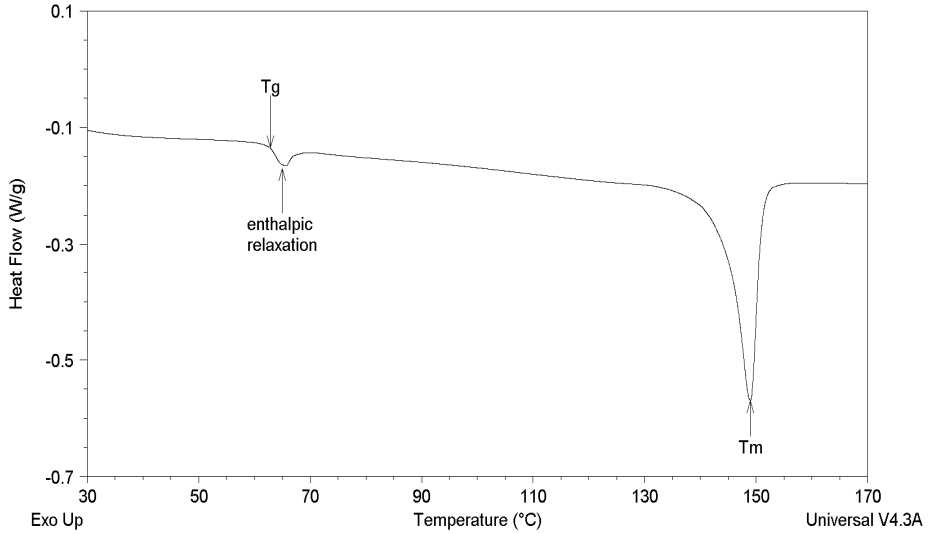

Figure 6 DSC scan of Evlon®, PLA heating rate 5°C/min

The impulse welding system and the dimensions of the samples used in this study for welding the PLA films are shown in Figure 7. When the welding head is, which is shown in Figure 7 (a) closed, a DC constant current increased the temperatures of the heating elements and held the temperature at a relatively constant value during the welding cycle. A thermocouple (TC-type J) connected to a digital data acquisition system (sample rate of 1000 Hz) was placed in an auxiliary sample between the heating elements close to the overlap area of the tested samples to measure the temperature during the welding cycles. At a time of (t_w-*1s)* a heat exchanger circulated chilled (approximately 20 C) water through water channels in the welding head. The water channels were placed closely to the heating element to assure rapid cooling of the welded samples. Films with a lap shear configuration with an overlap of 4.8 mm were welded and tested using an Instron (Norwood, MA) model 4500 load frame at a crosshead rate of 10 mm/min. Six duplicate samples were produced and tested for each set of experimental parameters. The failure load was used to estimate the average shear stress in the weld which was calculated as the applied force at failure divided by the overlap area. It is important to note that the pressure on the overlap was approximately 0.33 MPa, to provide a satisfactory contact between the two surfaces while keeping the pressure as low as possible to prevent reduce the impact on the degree of autohesion measurement. The sample dimensions are detailed in Figure 7 (B). The welding the samples were cut to a modified standard tensile test bar according to ASTM D 638.

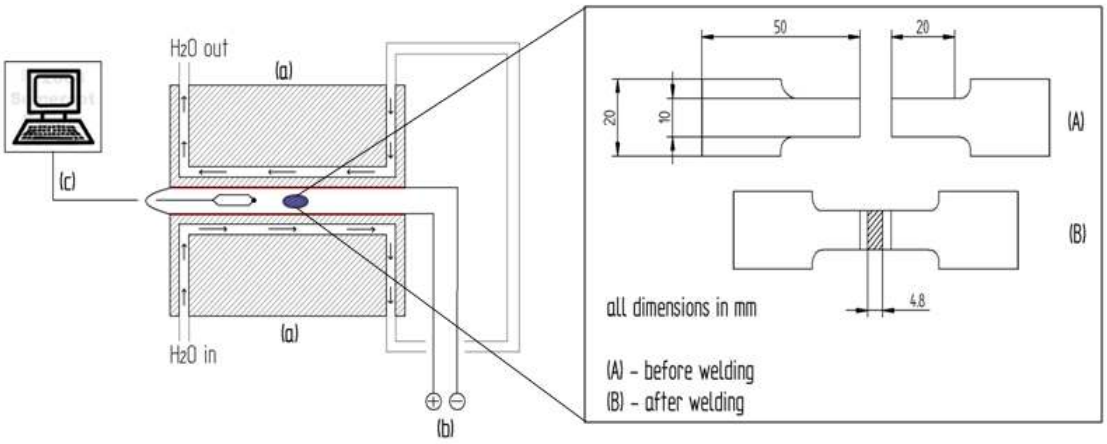

Figure 7 left: setup for impulse welding (a) welding head, (b) Nichrome heating elemnts connected to a DC power supply, (c) digital data acquisition system; right: sample dimensions

3 Results and Discussion

3.1 Effect of Contact Time and Temperature

Figure 8 shows the temperature profiles during welding for the data used for the calculation of the activation energy (relatively constant temperatures). Only those temperature profiles that reached a relatively steady state condition (similar to a top hat profile) were used to estimate the coefficients in Eq. 8. A steady state temperature was reached, at welding times greater than 10 s at 135 °C and for welding times greater than 15 s – 20 s a steady state was reached at 120 and 130 °C. In more detail, referring to the temperature profiles for 135 C, the thermal cycle for the 5 s weld, varied too much to be consider a steady temperature. It is important to note that at lower temperatures the measured degree of autohesion was not linearly increasing with the fourth root of the weld time while at higher temperature the degree of autohesion was $D_{Au}=1$ before a steady state in the temperature could be achieved. In these experiments the pressure was held constant at 0.33 MPa.

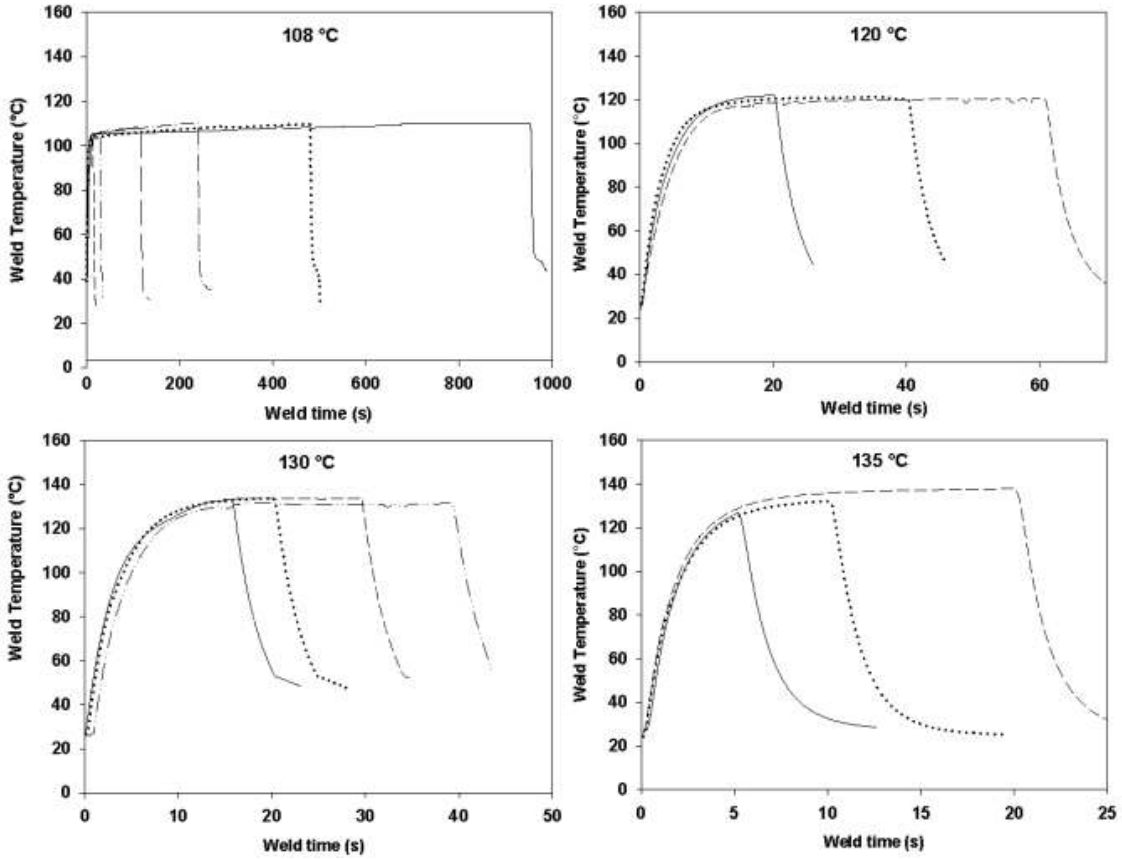

Figure 8 Temperature measurements during welding at pressure 1

Because the temperature history does not show a perfect ‘flat hat’ profile, the weld time is calculated as it is schematically shown in Figure 9. The beginning of the weld time is the intersection of the linearly increasing temperature profile with the extension of the constant weld temperature and the end of the weld time is the point when the weld temperature starts decreasing.

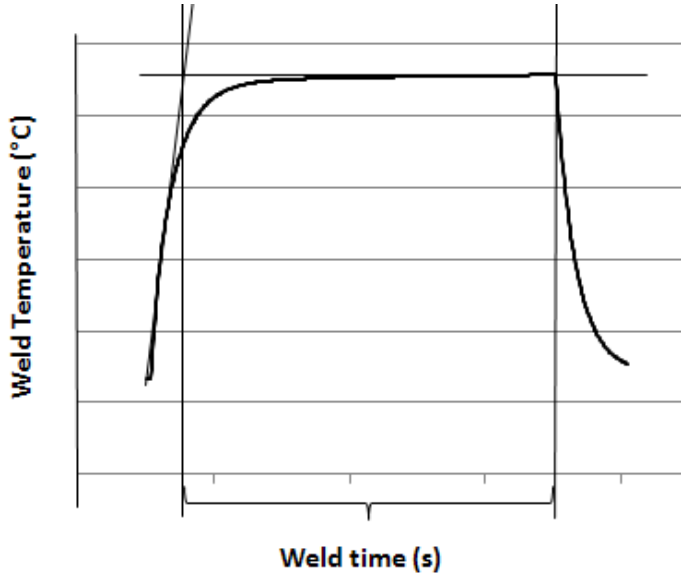

Figure 9 Construction of the contact time from weld temperature profiles

With the maximum shear strength of 1.83 MPa, the degree of autohesion (D_{Au}) as a function of the fourth root of the weld time is calculated as detailed in Eq. 3 and from the slope shown in Figure 10. In more detail, slopes of the trend lines can be used to determine the temperature depended *K(T)* of Eq. 6. Because the shear strength develops linearly with the fourth root of the weld time, it can be considered as diffusion limited [4, 9, 10].

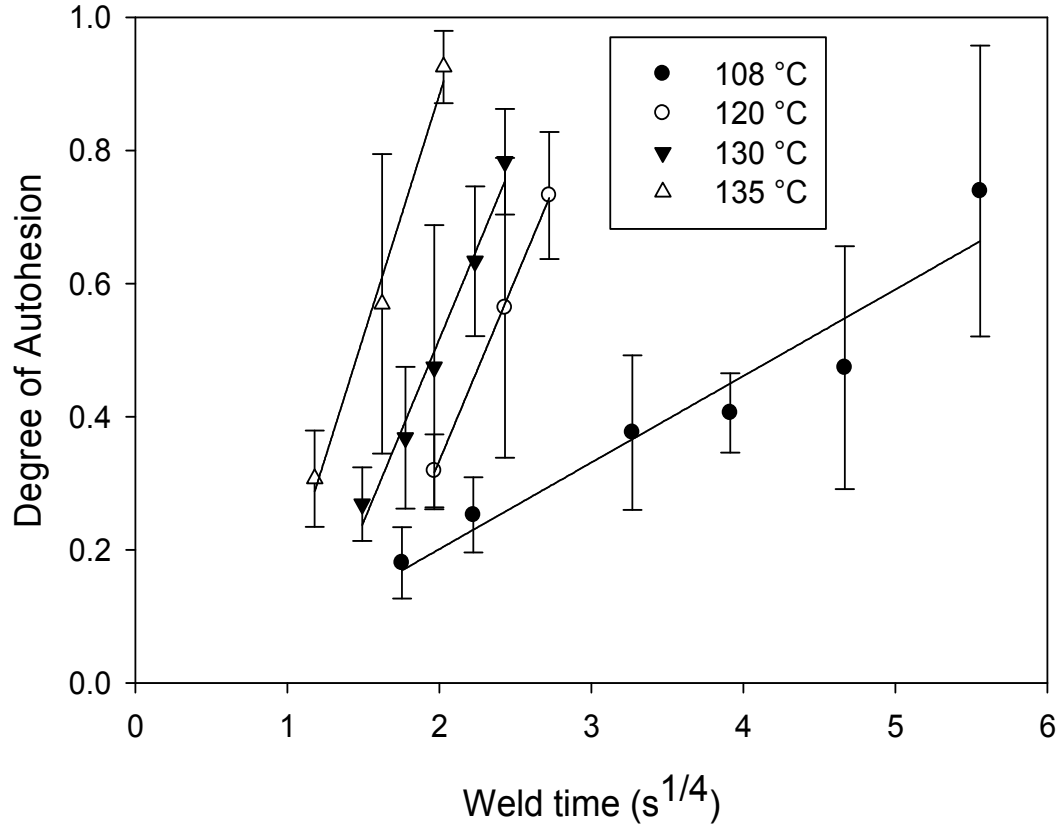

Figure 10 Degree of autohesion as a function of the fourth root of weld time for 0.1 mm thick PLA films at 0.33 MPa

By plotting the natural logarithms of the slopes of the trend lines from Figure 10 as a function of the inverse of the welding temperature at steady state, it is possible to calculate the activation energy E_a of Eq. 8 and the extension of this plot to the intersection with the ordinate corresponds to the natural logarithm of the material parameter K_0.

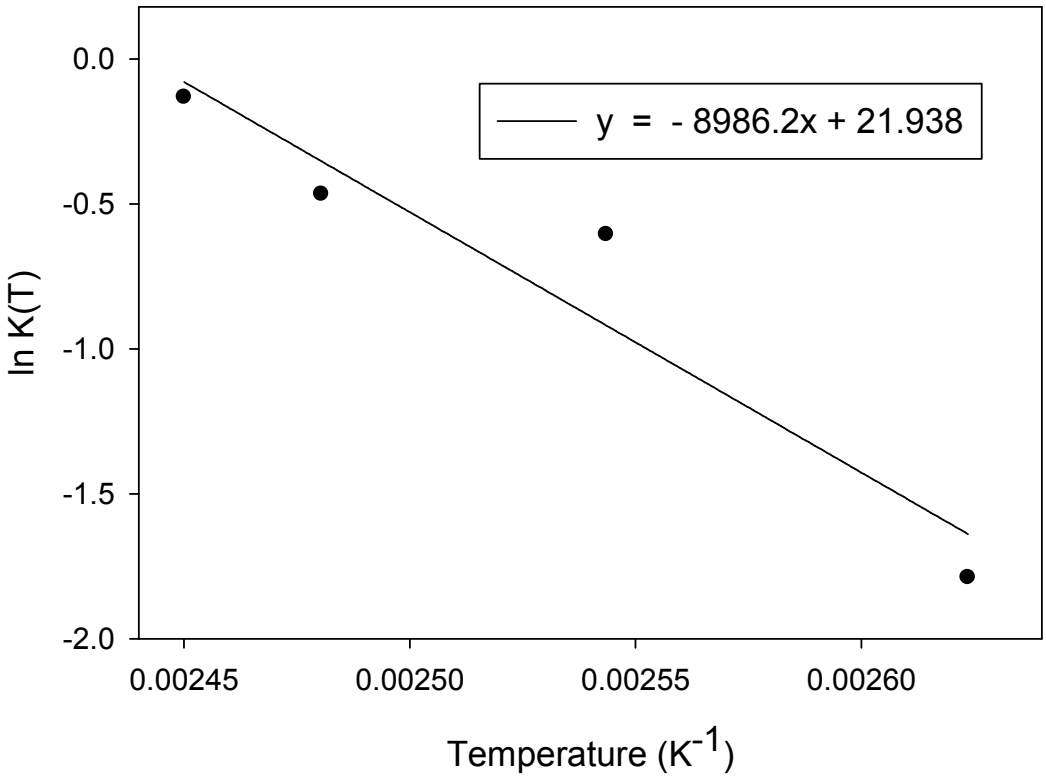

Figure 11 Natural logarithm of slopes vs. inverse temperature (*K(T)*) of Figure 10

With the slope and intersection shown in Figure 11 the activation energy E_a is calculated as 74.8 kJ mol^{-1}, and $K_0 = 3.37*10^9$.

Using these experimental values of E_a and K_0 the degree of autohesion was calculated from Eq. (9) for welds with varying temperatures (non-top hat) for increasing weld times of 1.25, 1.875 and 2.5 s. Figure 12 compares the degree of autohesion based on theoretical calculations using the previously mentioned approach and experimental values. The experimental and calculated data ($\Delta t = 0.105$ s) are in good agreement when the calculation for the degree of autohesion was calculated with an estimated $\ln(K_0)=20.35$ ($K_0 = 6.88*10^8$ s$^{-1/4}$) instead of the value of $\ln(K_0) = 21.94$ ($K_0 = 3.37*10^9$ s$^{-1/4}$). When the original material parameter ($K_0 = 3.37*10^9$ s$^{-1/4}$) was used to estimate the degree of autohesion the calculated and experimental values were not in good agreement

and only through experimental varying this value was it possible to generate good agreement. There is no decisive understanding for this apparent shift factor, but it may be related to a temperature dependent activation energy as report in previous work [13].

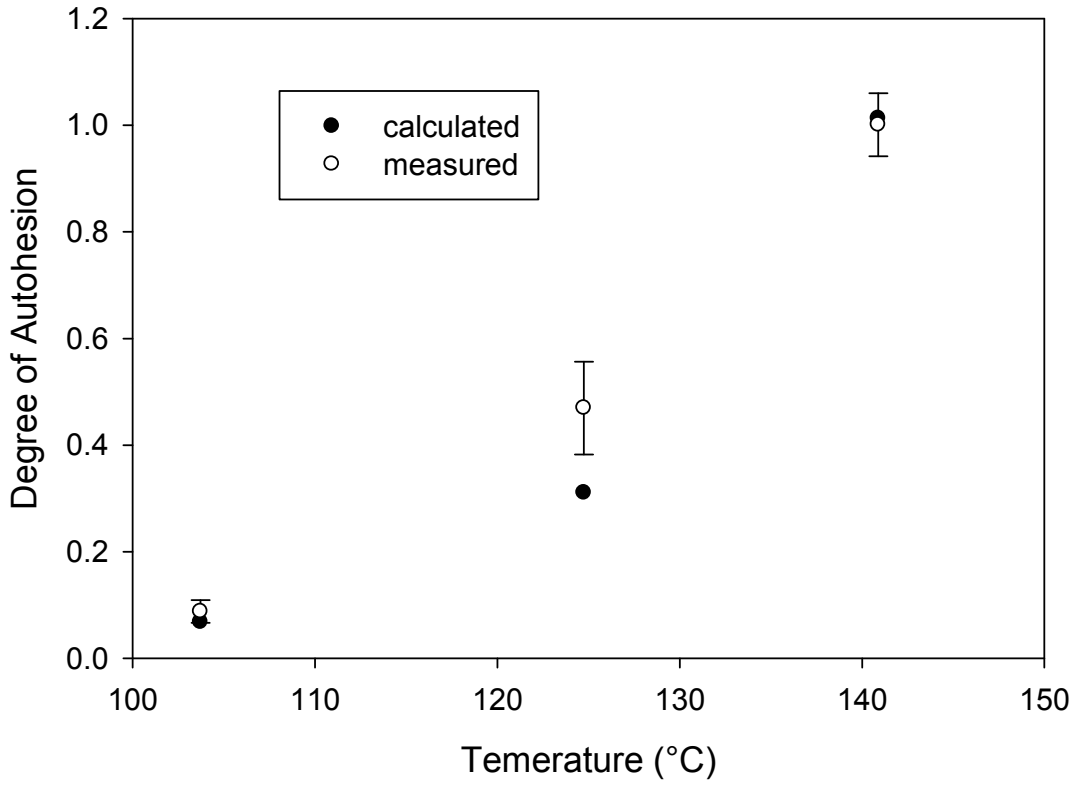

Figure 12 Degree of autohesion measured and calculated

3.2 Effect of Contact Pressure

The effect of pressure on the degree of autohesion was examined by doubling (0.66 MPa) and tripling (0.99 MPa) the initial pressure value that was used in the previous experiments. The slopes of the degree of autohesion measurements were taken to plot the $\ln(K(T))$ as a function of T^{-1} to calculate the activation energy at the various pressures.

Figure 13 shows the degree of autohesion that was measured for a pressure of 0.66 MPa. As expected with the higher pressure the weld time to achieve a measurable D_{Au} is relatively short compared to the initial lower pressure. In addition, the lowest possible temperature at which welding can be achieved is lower compared to the initial lower pressure. It is seen from Figure 10 and Figure 13 that the rate of degree of autohesion development (rate of welding) is proportional to weld pressure and time as expected. For example, at 120 °C and a pressure of 0.33 MPa a degree of autohesion of 0.75 can be achieved in approximately 60 s while the same degree of autohesion at 0.66 MPa only requires a weld time of approximately 10s.

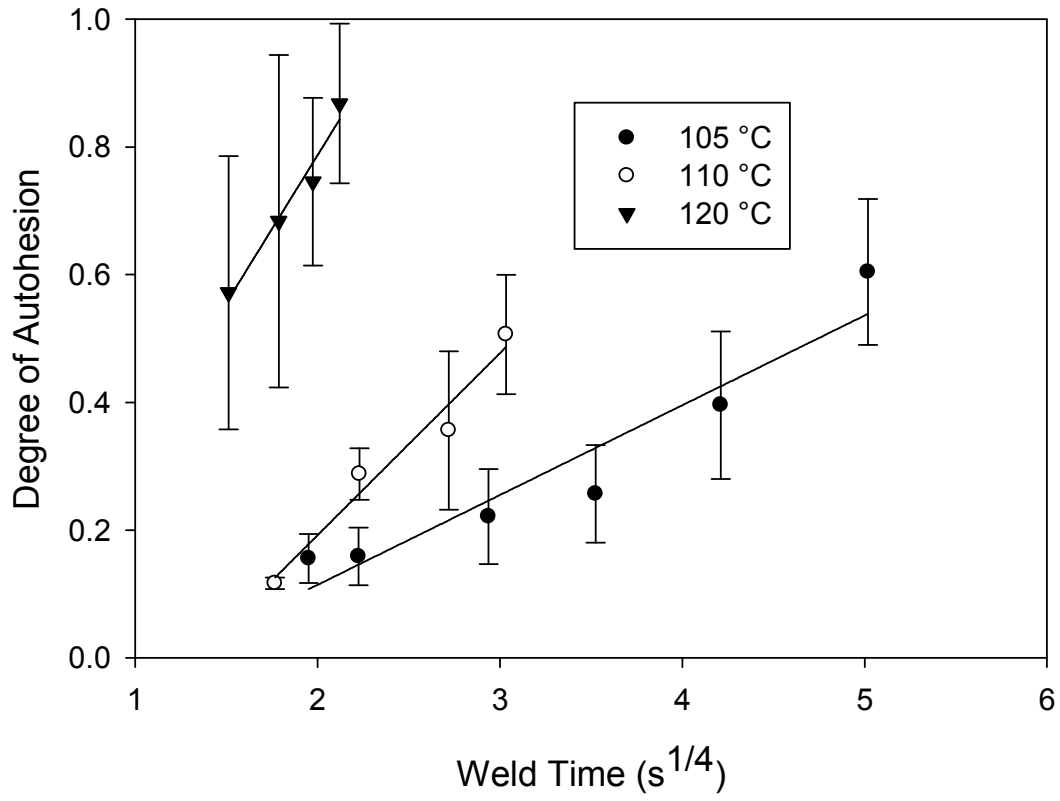

Figure 13 Degree of autohesion as a function of the fourth root of weld time for 0.1 mm thick PLA films at 0.66 MPa pressure

Figure 14 shows the degree of autohesion at a pressure of 0.99 MPa. It can be seen that at lower temperatures (90°C) the weld time is excessively long (~1000 s) to achieve a measurable degree of autohesion, while it is relatively short (13 s) at elevated temperatures. In summary, the degree of autohesion at the lower temperature (90°C) appears to be disproportionally low compared to the other temperatures. This large dependence on temperature suggests that there critical temperature value at which the diffusion rate increases suddenly and that this critical temperature is approximately 90°C as below this temperature welding was not possible.

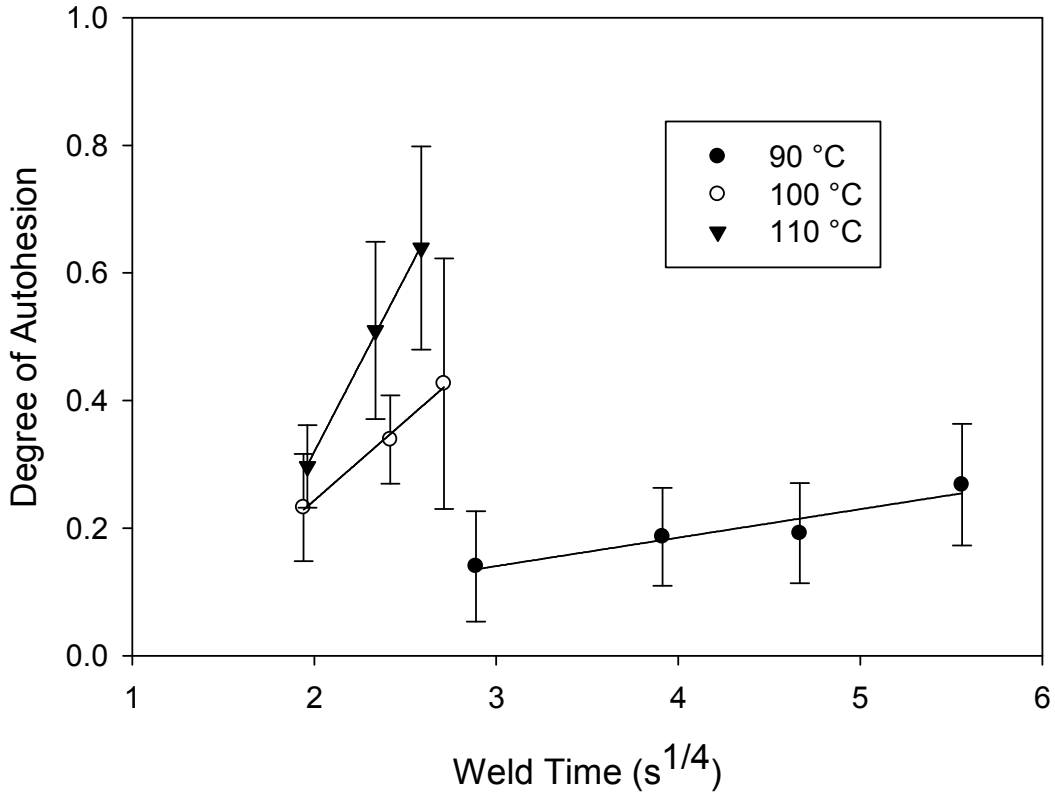

Figure 14 Degree of autohesion as a function of the fourth root of weld time for 0.1 mm thick PLA films at 3 times the initial compaction pressure.

Figure 15 shows the ln(K(T)) as a function of T^{-1} plots for all three pressures. With increasing pressure the slope of the graphs decreases which suggests an increase in the

activation energy for diffusion. This is most likely the result of reduced free volume and reduced molecular freedom of movement after surface matching.

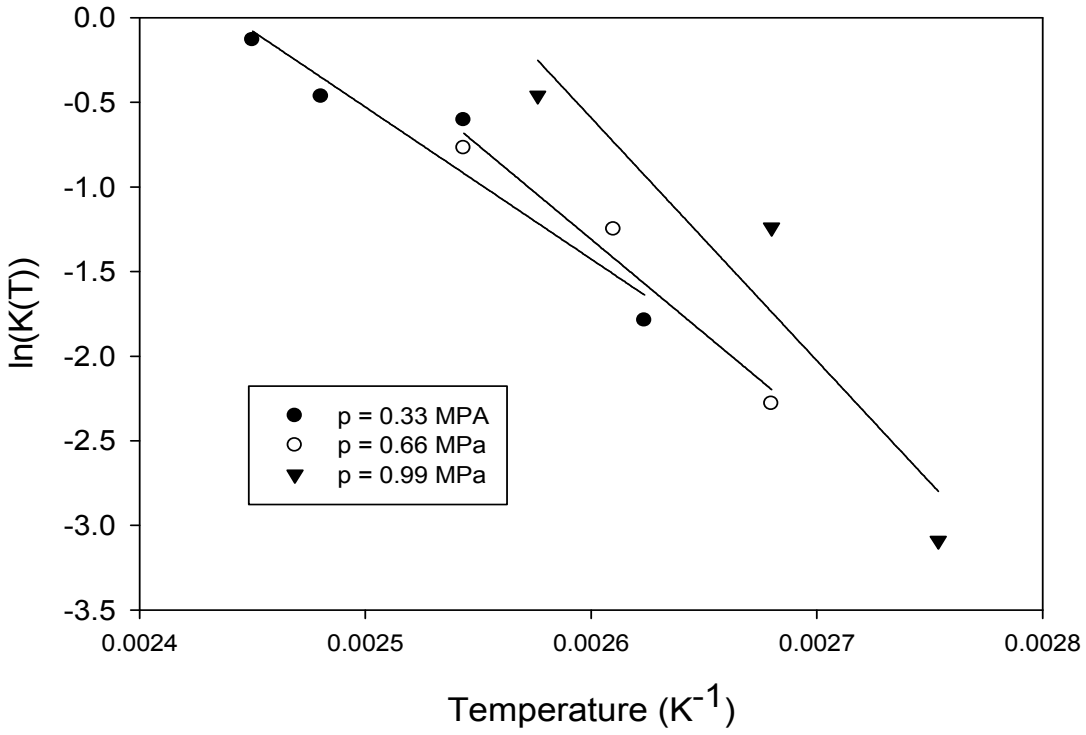

Figure 15 Natural log of K(T) vs. T^{-1} as a function of time for different contact pressure.

Table 3 details the activation energy from the slopes and K_o values and intersections with the ordinate of the graphs in Figure 15. The calculations show that for increasing pressure the activation energy increases too.

Table 3 Activation energy and K_0 values for increasing contact pressure

Pressure [MPa]	slope	ln(K_0)	E_a [kJ/mol]	K_0 [$s^{-1/4}$]
0.33	-8986.4	21.94	74.71	3.37E+9
0.66	-10484	25.95	87.16	1.86E+11
0.99	-14523	45.28	119.69	4.64E+14

Figure 16 shows an asymptotic increase in degree of autohesion (D_{Au}) with increasing contact pressure measured after a contact time of 25 s at a contact temperature of 115 °C. The asymptotic characteristic indicates that the D_{Au} will reach a saturation pressure above which a further increase in pressure has little effect on the diffusion rate.

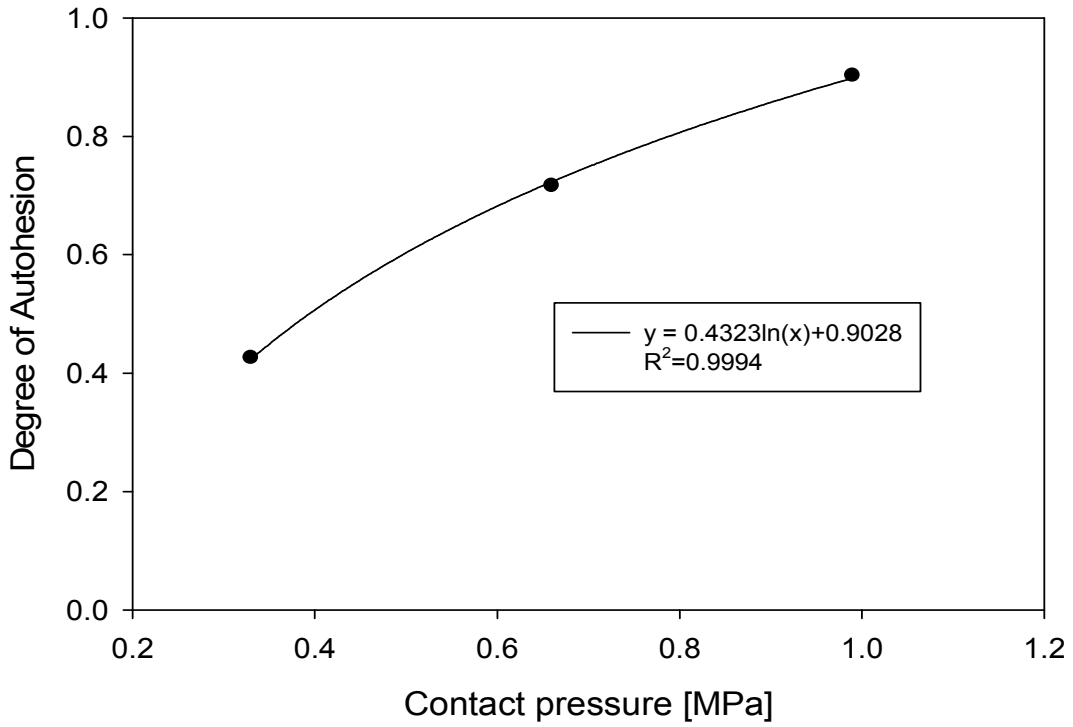

Figure 16 Degree of autohesion for increasing contact pressure at 25s contact time and 115 °C interface temperature

3.3 Time Temperature Superposition

Figure 17 shows the temperature shift factor a_T for all three pressures calculated according to Eq. (10) and Eq. (12). The reference temperature for each pressure was assumed to be lowest temperature at which welding could be achieved and was 108, 105 and 90°C for 0.33, 0.66 and 0.99 MPa respectively. The data points represent the shift factors calculated as defined Eq. (10) and 12 respectively. While both shift factors are in relatively good agreement for a pressure of 0.33 MPa in a temperature range between 108 °C of 135 °C, it can be seen that the two shift factors are diverge at the 0.66 and 0.99 MPa pressures. This suggests that the activation energy for diffusion is constant at the lower pressure and given temperature range, but at the higher pressures becomes temperature dependent as previously mentioned.

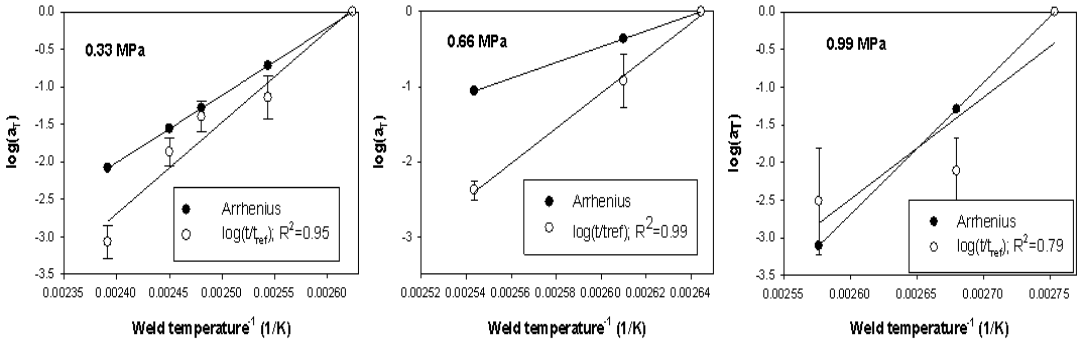

Figure 17 Arrhenius shift factor loga_T for 0.33, 0.66 and 0.99 MPa contact pressure

4 Conclusions

The activation energy for diffusion was calculated from the slope of the regression lines in Figure 15 whereby the graph was plotted from the slopes of increasing interfacial strength at increasing weld time at 4 different temperatures. The constant K_0 is the exponent of the number read from the graph in Figure 15 where the graph intersects with

the ordinate, assuming the graph is linear. Because of this exponential relation, small deviations in the graph would cause a large deviation of the calculated number of K_0.

The time temperature superposition reasonably predicts the weld/diffusion behavior for temperature a range between 108 and 135 °C at a contact pressure of 0.33 MPa. However, with higher temperatures or pressures the time temperature superposition requires a separate shift factor.

Future work should focus on developing models for temperature activation energy.

5 Acknowledgements

Acknowledgements go to 'Branson Ultrasonics Coorporation' for donation of equipments, 'Bi-Ax International Inc.' for donation of PLA samples, the Iowa State University Center for Crops Utilization Research (C.C.U.R.) and the USDA Bio-Preferred Program.

References

1. Y.H. Kim, R.P. Wool, *Macromolecules,* **16**, (1983)

2. R.P. Wool, K.M. O'Connor, *J. Appl. Phys.*, **52** (1981)

3. I.L. Woo, G.S. Springr, *J. Compos. Mater.*, **21** (1987)

4. Y.M. Boiko, G. Guerin, V.A. Marakhin, R.E. Prud'homme, *Polymer,* **42** (2001)

5. R. P. Wool, *Polymer Interfaces, Structure and Strength,* Hanser Publications, Munich Germany (1995)

6. R.S. Blackburn (ed.), *Biodegradable and Sustainable Fibres, Chapter 6 "Poly(lactic acid) fibres"* CRC Press. (2005)

7. T. Oswald, E. Baur, S. Brinkmann, K. Oberbach, E. Schmachtenberg, *International Plastics Handbook,* Hanser Publications, Munich Germany (2006)

8. A. Harper, *Modern Plastics Handbook,* McGraw-Hill Professional, New York (2000)

9. P.H. Dara, A.C. Loos, *Thermoplastic Matrix Composites Processing Model,*Virginia Cetner for Composite Materials and Structures

10. Y.M. Boiko, R.E. Prud'homme, *Macromolecules,* **31** (1998)

11. M.J. Shim, S.W. Kim, *Mater. Chem. Phys.*, **48** (1997)

12. K. Jud, H.H. Kausch, J.G. Williams, *J. Mater. Sci.*, **16** (1981)

13. D. Grewell, A. Benatar, *Polym. Eng. Sci.,* **48** (2008)

14. J.R. Fried, *Polymer Science and Technology*, Prentice Hall PTR, New Jersey (1995)

15. W.K. Goertzen, M.R. Kessler, *Mater. Sci. Eng.*, A, **412** (2006)

16. M. Tajvidi, R.H. Falk, J.C. Hermanson, *J. Appl. Polym. Sci*., **97** (2005)

Chapter 5: Comparison of processing costs and direct carbon footprint of selected bio-plastics and petrochemical plastics

Julius Vogel – Department of Mechanical Engineering, Iowa State University

David Grewell, Ph.D. - Department of Agricultural and Biosystems Engineering, Iowa State University

Robert P. Anex, Ph.D. – Biological Systems Engineering, The University of Madison Wisconsin

A paper submitted to *The International Journal of Life Cycle Assessment*

Abstract

Background, aim, and scope: Recently, there has been an increased interest in bio-based plastics due to environmental concerns as well as fluctuating oil prices. Bio-based plastics, defined here are plastics that are fully or partially produced from renewable feedstock. However, the manufacturing of products from bio-based plastics may result in more energy consumption, waste and emissions than traditional plastics. This study examines the 'Carbon Footprint' of bio-plastics such as zein - a corn based protein polymer, soy protein isolate (SPI) – a soy bean based protein polymer, polylactic acid (PLA) and compares these materials with petroleum based plastics with similar mechanical properties and potentially similar applications such as polyethylene (PE) and polystyrene (PS).

Materials and methods: This analysis includes the energy input as well as the CO_2-equivalent emissions and the costs of producing these plastics from a cradle-to-grave

perspective. This includes all steps in production, ranging from raw material acquisition, material processing, manufacturing of products to their final disposal. The costs of manufacturing include the production facility as well as material costs and is calculated in terms of costs per unit ($/kg) and costs per part ($/part). In addition, this model covers all common end-product treatment options when applicable, including their beneficial effects such as energy and emissions savings through recycling, energy recovery from waste incineration and landfill gas recovery, as well as non-beneficial effects such as the cost of landfill.

Results and discussion: The results showed that bio-plastics are preferable compared to petrochemical plastics in terms of energy consumption and CO_2-equivalent emission generation. The comparison of the manufacturing costs showed that the protein based bio-plastics (zein and SPI) are more expensive because of their relatively high feedstock price. In addition, PLA is more expensive compared to petrochemical plastics and less expensive compared to SPI and zein plastics. However, it was shown that by increasing the production capacity, the relative difference between the costs of bio- and petrochemical-plastics decreased. By using this approach, the maximums in energy input as well as emissions output during the entire life cycle of a plastic can be identified, giving the opportunity to identify the product phases where cost reductions and GHG reductions can be most beneficial.

Conclusions: This model is a tool for comparing the greenhouse gases and economics of bio- and petroleum based plastics. It can estimate the CO_2 emissions of bio-plastics as well as their commercial drawbacks.

Recommendations and perspectives: The results indicate that comparing biodegradable plastics with non biodegradable plastics can help decision makers to replace petroleum

based plastic products with bio-degradable plastic products, by comparing the energy input, emission output and cost associated during their entire life cycle. In addition, as non-food grade feedstock for zein and SPI plastics become available these studies should be revised.

Keywords: Carbon Footprint • Energy consumption • Emission generation • Cradle to grave analysis • Life cycle costs • Life cycle analysis • Biodegradable plastics • Economic engineering approach • Parameterization models

1 Background, aim, and scope

While the first plastics were derived from biomass resources, they were progressively replaced as of the 1930's by petrochemical polymers. Recently, there has been a return in the interest of bio-based plastics due to environmental concerns as well as fluctuating prices for oil and gas. In principle, biodegradable polymers can also be manufactured from petrochemical raw materials. However, bio-based plastics, defined here are plastics that are fully or partially produced from renewable feedstock. This paper compares two common petrochemical plastics, polystyrene (PS) and polyethylene (PE) with bio-based plastics with similar properties and possibly similar applications, namely PLA and SPI or zein respectively. While others (Patel et al. 2003, ESTO 2005, Akiyama et al. 2002, Kumar et al. 2002, Shapouri & McAloon 2001) have reported a portions of these results, this paper comprehensively and directly compares these plastics in terms of energy usage, generation of green house gases and costs. The use of agricultural products such as soybeans and corn as a feedstock for biodegradable polymers has been demonstrated. It has been shown that vegetable proteins can be denatured with selected solvents and processing to directly produce polymers (Pandey et al. 2005, Vlad et al. 2007). These

polymers, which are not dependent on diminishing fossil fuels, have the advantage of being both renewable and biodegradable. Because of their bio-degradability, bio-based plastics in particular, have the potential to replace traditional plastics in applications ranging from packaging, to disposable road signs, to drug delivery, while they do not significantly impact the environment. Various publications report the life cycle analysis of bio-plastics compared with those of petroleum plastics. Greenhouse gas emissions and energy consumption from cradle to grave of PLA compared to PP as a packaging material on a functional unit base are reported by (Bohlmann 2004), the savings in energy consumption and emissions generation for the production of raw materials for plastics from bio based feedstock instead petroleum based are reported by (Hermann et. al. 2007). However, currently there is limited definition of their environmental and economical justification. Based on reported numbers for energy consumption as well as emissions generation of the production of plastics and their raw materials, the goal of this project is to develop an economical as well as ecological model of various bio-plastics and compare these models to the costs of conventional petrochemical plastics. The aim is to accelerate the development of new bio-plastic products and increase their acceptance by the industry and the consumer. The main difference in this paper compared to existing publications is that plastics are compared in terms of their 'Carbon Footprint' as well as commercial costs.

2 Materials and model

2.1 Research design

The construction of the comparison consisted of five steps:

Identification of plastics: Three biodegradable polymers and two petroleum based polymers were chosen for this study. These were protein derived plastics from corn and soy such as zein and SPI, PLA and two petroleum derived plastics (HDPE and PS). These petroleum plastics were selected because they can potentially be replaced by the chosen bio-plastics in certain applications such as packaging because of comparable mechanical properties. In more detail, SPI and zein plastics can potentially replace HDPE in some applications and similarly PLA can potentially replace PS and HDPE in some applications.

Tabulation of impact data: The life cycle steps of each plastic were identified, and data on the energy consumption and greenhouse gas emissions reported as CO_2-equivalent directly related to their life cycle steps was collected from published sources.

End-of-life product treatment: The end-of-life product treatment options for each plastic were identified and included in the life cycle model as an economical or environmental beneficial or non beneficial effect.

Tabulation of costs: The costs of processing plastic parts/products of the above mentioned plastics were calculated per part ($/part) or per unit ($/kg) following the 'Economic Engineering Approach' as detailed in (Middleton et al. 2001).

Comparison of plastics-impacts: The various plastics were compared based on their specific energy consumption, greenhouse gas emission, and cost of processing. The comparison of the bio-plastics with the petro-plastics is based on the functional unit of 1 kg of plastic pellets, which is then hypothetically processed into 1 kg of a plastic product. All energy as well as emission related numbers are related to this functional unit.

2.2 Assumptions of the LCA

The analysis included the life cycle costs of the plastics from a cradle-to-grave perspective divided into the 4 phases: 1. Raw material acquisition; 2. Manufacturing of products; 3. Use/Consumption; 4. Disposal.

Raw material acquisition: The model included the energy and material inputs as well as emissions generated during their acquisition and processing. While the energy inputs, as well as the emissions for the production of electricity, can vary based on the local energy production facilities, in this study, the U.S. average fuel mix (fuel consumption for the production of electricity and heat) was assumed for the energy input and the emissions are referred to as CO_2-equivalent. The cost of the feedstock material of zein, SPI and PLA includes all agricultural activities in the production of corn grains and soy beans. The agricultural activities are combined in the harvesting costs and comprises of the energy consumption and CO_2-eqivalent generation.

Manufacturing of products: The production of the bio-materials includes all processing steps to separate the protein and starch from the grains. The energy consumption and emission generation of each processing step are detailed and shown as the production costs for each material as well as processing costs and CO_2-equivalent emissions. The acquisition of raw material for the petrochemical industry and the production of petrochemical plastics are based on well document sources such as (RMIT 1998, Worrel et al. 2000, Harding et al. 2007). While (Worrel et. al. 2000) reports the energy consumption and emission generation of the production of feedstock chemicals as well as their polymerization process to produce petro-plastics such as PE or PS in the U.S. chemical industry, (Harding et al. 2007) reports the energy input and CO_2-equivalent emissions for the production of PP and PE compared to the biological plastic PHB.

Use/Consumption: The life cycle step of use and consumption of plastic products would include the energy consumed and the CO_2-equivalent created during the phase of a plastic product when it reaches the end consumer to its disposal.

Disposal: The disposal costs of plastic material include the costs to remove the final product from the consumer and the costs of waste abatement. It is assumed that the 'End Product Treatment' would be one of: (1) recycling, (2) energy recovery through municipal solid waste incineration (MSWI) or methane recovery, or (3) landfilling, as it is depicted in Fig. 1 and detailed below.

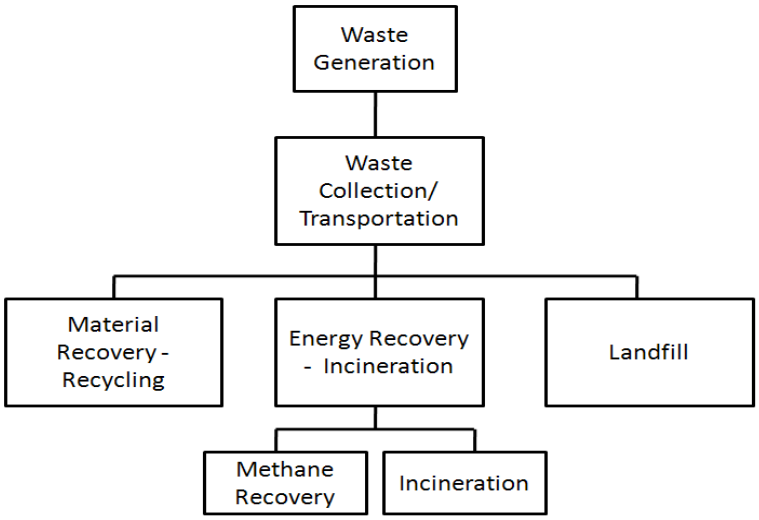

Fig. 1 Solid waste flow diagram

(1) Because recycled material can offset the production of new material it can represent a beneficial factor of the 'end of life phase'. There are two common models for recycling: 'open-loop' and 'closed-loop' recycling. Open loop recycling, as detailed by (Ekvall & Tillman 1997), can be considered as a cascade of material life cycles. The material passes through the steps of material production, product manufacturing and product use. However, because material recovery for recycling includes sorting, washing, and possibly

melting, only high value plastics that are produced in large volumes are normally recycled. Even the presence of small amounts of contaminants can be detrimental for a recycling batch. In addition to energy saving, recycling reduces the volume of material sent to landfills. Twelve percent (12%) of the total municipal solid waste (MSW) generated in 2005 in the U.S. was plastic waste (USEPA 2006). However, because recycled plastics cannot be used for food and medical applications, they are limited to applications such as commodity bottles, carpets and clothing (www.earth911.org). The advantages of recycling have been demonstrated in a study by (McDougall et al. 2001) where the emission and energy consumption of producing LDPE bags from a recycled plastic and a virgin resin was compared. The results showed that both energy consumption and CO_2 emissions are lower for the recycled material. In more detail, the reduction of CO_2 emissions and energy consumption during the production of LDPE bags from recycled films collected at supermarkets was approximately 46% and 38% respectively. It was shown by (Korhonen & Dahlo 2007) that a reduction in the emissions of 1.4 - 1.7 tons of CO_2/(ton of plastic) produced is possible by recycling plastic. The amount of energy and CO_2-emissions required for recycling plastic varies between studies, however recycling compared to using virgin plastics has been shown to be less energy demanding, it does not consume additional raw materials such as natural gas or crude oil, it emits less greenhouse gases and it reduces the occupation of landfill space. Currently the recycling rate of plastics in the U.S. is 30% (EPA 2008). Fig. 2 shows a proposed flow chart for a 'closed loop' recycling model. The recycling rate 'r' is defined as that fraction of the total initial plastic which is recycled. The amount of non-recycled plastic which is further treated in landfill or incineration facilities is defined as '1-r'. The energy required for the production of the virgin material resin and the emission generation is defined as 'E_v' and 'CO_{2v}' respectively. The energy consumption and

emissions for the production of recycled plastic is defined as 'E_{rec}' and 'CO_{2rec}'. The recycled plastic is assumed to be mixed with the virgin material in a weight ratio given by the recycling rate. The beneficial effect of recycling plastic can be expressed as a reduction of the energy demand and CO_2 emissions during its production.

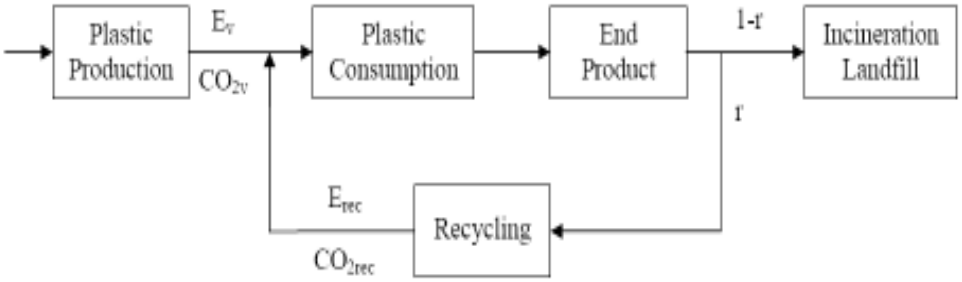

Fig. 2 Flow chart of recycling as end product treatment

The energy demand of producing recycled plastic can be defined by Eq. 1:

$$E_{rec} = e \cdot E_v \quad (1)$$

where: E_{rec}: average energy consumption to produce recycled plastic (MJ/kg); e: ratio of energy consumption for production of recycled material to virgin material (based on (Korhonen & Dahlo 2007), e=0.62 for LDPE); E_v: energy consumption to produce virgin material (MJ/kg). The CO_2 emission savings can be calculated in a similar manner, with the corresponding values for the ratio of CO_2 emission for the production of recycled and virgin materials as detailed in Eq. 2.

$$CO_{2\,rec} = c \cdot CO_{2\,v} \quad (2)$$

where: CO_{2rec}; average CO_2 emission of producing a recycled plastic resin per kg; c: ratio of CO_2 emission for production of recycled material to virgin material (based on

(Korhonen & Dahlo 2007), c=0.54); CO_{2v}: CO_2 emissions for production of virgin plastic material. The specific energy savings (MJ/kg) for resin production, which includes virgin and recycled material, can be determined using Eq. 3.

$$E_{sav} = E_v - \left(E_{rec} \cdot r + E_v \cdot (1-r)\right) \quad (3)$$

The reduction in CO_2 emissions can be determined using Eq. 4.

$$CO_{2\,sav} = CO_{2v} - \left(CO_{2\,rec} \cdot r + CO_{2v} \cdot (1-r)\right) \quad (4)$$

The energy and emission savings of recycling can be shown as a function of number of parts that are produced from recycled instead of virgin material to directly compare those two environmental impacts in terms of CO_2-equivalent categories in the life cycle of plastics.

(2) To model the energy recovery from incineration and methane production, it is assumed that 7% to 17% of all MSW in the U.S is combusted for energy generation. In 2005 approximately 34 million metric tons of solid waste was combusted releasing approximately 20.9 million tons of CO_2-equivalent. Plastics constitute approximately 12% wt. of the municipal solid waste and generate 13.9 million tons of CO_2-equivalent (EPA 2007). The average heat value of municipal solid waste ranges from 10-14 MJ/kg and the amount of electricity generated from burning one ton of municipal solid waste ranges between 0.5-0.6 MWh (USDE 2005). However, in a study by (Profu 2004) it was reported that the incineration of MSW can produce 3 MWh/ton of electric energy and heat recovery in Sweden. In contrast, only 0.5 MWh of energy was generated when only electricity is produced based on plants in Great Britain. The combination of heat and

electricity production from waste incineration, can recover as much as 90% of the stored energy from waste (Profu 2004). The combustion of plastic can offset the CO_2 production to an equal energy content from fossil fuels. Because the energy recovery (0.5 to 3 MWh/ton) from waste incineration depends of the efficiency of the incineration facility, a 'high' and 'low' scenario are defined to bound the range to account for varying amounts of energy that can be recovered from a given feedstock. In the low scenario, it is assumed that with the lowest efficiency 0.5 MWh can be recovered and up to 3 MWh can be recovered per ton of waste in a 'high' scenario. These assumptions are used to calculate the beneficial effect of energy recovery through waste incineration.

The reduction of CO_2 emissions resulting from waste incineration was based on the national fuel average for the electricity production. According to the 'Electrical Power Annual 2008' (USDE 2008) 0.85 tons of CO_2-equivalent are emitted per MWh electricity produced which correlates to 0.425 and 2.55 tons of CO2-equivalent in the 'low' and 'high' scenario. The amount of CO_2-equivalent from the incineration of fossil fuels prevented by incinerating waste is defined in Eq. 5.

$$CO_{2\,MSWI} = CO_{2\,FFI} \cdot E_{MSWI} \qquad (5)$$

where: CO_{2MSWI}: amount of CO_2-equivalent prevented through incineration of municipal solid waste; CO_{2FFI}: CO_2-equivalent emissions/MWh from fossil fuel incineration on a national fuel average; E_{MSWI}: electricity produced per ton MSW incinerated. It is important to note that the heat value of plastic (42 MJ/kg for HDPE) is significantly higher than that of municipal solid waste (10-14 MJ/kg). The energy recovered is limited by the given average heat value of MSW and the efficiency of the waste incineration facility. The relative heat content of MSW added by a plastic in percent is defined as h_i.

Thus, the heat energy recovered and the emissions saved are defined in Eq. 6 and Eq. 7 respectively.

$$E_{MSWI,i} = E_{MSW} \cdot \eta \cdot h_i \quad (6)$$

$$CO_{2\,MSW,i} = CO_{2\,FFI} \cdot E_{MSWI} \cdot h_i \quad (7)$$

where: EMSW: average heat content of municipal solid waste; hi: percentage contribution to the heat value of MSW from each plastic; η: incineration facility efficiency. The financial impact of plastic incineration is calculated as detailed in Eq. 8.

$$C_{MSWI} = E_{MSWI} \cdot h_i \cdot c_E \quad (8)$$

where: C_{MSWI}: financial benefit from MSWI incineration; c_E: cost of electricity

Because bio-plastics such as SPI and zein are currently not produced in quantities that would significantly contribute to energy recovery from waste incineration (450 t.p.a. zein were produced in 1997), in this model it was assumed that they have no energy value but can be added in future models. PLA is produced in larger quantities compared to zein and SPI. NatureWorks produced 140,000 t.p.a. in 2001 and Hycail (NED) plans the construction of a plant capable of producing between 25,000 and 150,000 t.p.a. (ESTO 2005). However, the heat value of PLA in MSW is too insignificant to contribute to energy recovery from waste incineration.

Recovering landfill gas that is generated during the microbial decomposition of waste has several beneficial effects. Methane from U.S. landfills contributes to 3.8% of the global greenhouse gas emissions. The amount of greenhouse gasses generated throughout the

lifetime of a typical landfill has been estimated to be between 39 and 500 m3/ton of landfill (Williams 2005). Annual rates of gas production for typical solid waste landfills are estimated to be between 6 - 8 m^3/ton/year, but 25 m^3/ton/year has also been observed. Landfill gases constitutes approximately 40-50% of methane, 50-60% CO_2 and numerous trace components. Thus, the gas from landfill has a caloric value of only 15-22 MJ/kg compared to 37 MJ/kg for natural gas (Williams 2005, Spokas et. al. 2005). As previously noted, methane is 25 times higher than CO_2 in terms of greenhouse effects (IPCC 2007). Thus, by burning the captured methane, it can be converted to less potent CO_2 and water, as well as release energy. Thus, energy production and greenhouse gas reduction are synergetic when capturing methane from landfills. With existing technology, approximately 60-90% of the landfill gas can be recovered. In some landfill sites the recovery rate is 98.1% during summer months (Spokas et. al. 2005). It is important to note the total methane released from landfills in 1995 was 7.6 million tons corresponding to a CO_2-equivalent of 159 million tons. This amount of methane also corresponds to $4.7 \cdot 10^{11}$ MJ of energy. Currently, 14% of all methane generated in landfills is recovered which corresponds to $5.7 \cdot 10^{10}$ MJ (EPA 2007, EPA 2000).

However, according to a report on greenhouse gas emissions published by the U.S. Department of Energy, approximately 2.8 million tons of methane from landfill gasses were recovered for energy production in the U.S. in 2005 (EPA 2007). According to a 'Landfill Methane Outreach Program' by the United States Environmental Protection Agency, the electrical energy potential produced from this amount of methane is 1,400 MW. Combustion of this methane would eliminate the emission of 60 million tons of CO_2. To be able to predict the methane generation for each biodegradable plastic, its half life time in landfill as well as its amount of organic carbon needs to be determined. With

the rate of methane generation, its relative amount in the waste stream and the total amount of the waste stream going to landfill, the methane production for each biodegradable plastic in MSW can be predicted.

(3) The landfilling costs can vary locally, depending of population density, availability of landfill space, as well as other variables. With increasing amounts of solid waste and a decreasing acceptance of landfills in densely populated areas, the cost of landfilling has increased. The average tipping fee (cost to drop one truck load of waste in landfill) for landfills has raised from $36 in 1988 to more than $150 in 1992. In New York City, transferring and transporting waste generated costs of $240 per ton in 2002 (Porter 2002). Based on these statistics, the costs of landfilling can be assumed to be approximately $0.24/kg.

Independent of the waste treatment method, emissions are generated during the collection and transportation of waste from the end consumer to the treatment facility. The collection system requires a specific amount of energy and creates a specific amount of emissions and financial costs for transporting the mass of collected waste a specific distance. Assuming a truck collection system, it was shown by (Dornburg et al. 2005) that 0.00125 GJ/Mg/km are required for the collection system. In addition, 0.096 kg of CO_2-equivalent is emitted and costs of $0.05 are generated. Based on these assumptions, and further assuming the average distance a truck needs to drive is approximately 50 km, this would require 0.0625 MJ/kg of energy resulting in the emission of 0.0048 kg /kg (CO_2/waste) and costs of $0.025/kg.

3 Results

3.1 Life cycle costs and impact of plastic production

3.1.1 Zein

The total energy cost of corn grain production is 2.5 MJ/kg for all agricultural activities including the CO_2 balance of the corn grain production, which is -1.32 kg/kg (CO_2/corn). This includes the CO_2 absorption during the growth of the corn, which is -1.47 kg/kg (CO_2/corn) and the CO_2 emission produced by all agricultural activities, which is 0.15 kg/kg (CO_2/corn) (Akiyama et al. 2002).

According to a net energy balance of the ethanol production in nine states of the U.S., the average energy used for transporting corn from local storage facilities to ethanol plants is 0.234 MJ/kg corn (Shapouri & McAloon 2001). In addition to that the cost of fertilizing corn was estimated in a study by (Wang 2002) indicating that for 33.5 kg of corn, 1 kg 'anhydrous ammonia fertilizer' at a price of $1.10/kg is used.

As previously mentioned, zein is typically produced with a corn wet milling process, whereby it appears as a co-product as defined by (PAS 2050). Because there is limited data that correlates energy streams to individual co-products in an ethanol wet milling or dry milling plant, it is difficult to allocate the energy consumption to zein production. According to the net energy balance of the ethanol production in the nine major corn producing states in the U.S., 34% of the energy required for the ethanol production in the wet milling process is used for the co-products, such as corn gluten meal, from which zein is extracted by distillation. This correlates to 6.5 MJ/kg (17,799 Btu/gl) of ethanol produced (Shapouri & McAloon 2001). Assuming 10.23 liter (2.7 gallons of ethanol), 0.77 kg corn oil, 1.36 kg corn gluten meal with a protein content of 60% and 5.9 kg gluten feed can be produced from a bushel of corn (25.4 kg), the energy allocated for the

co-products is 2.23 MJ/kg. The utility costs for steam and electric power for zein extraction from corn gluten for a plant producing approximately 6,955 tons of zein annually (15.3 million pounds of zein annually), is estimated to be $317,000. This is based on a power consumption of 1,702 MW to produce 21,109,090 kg steam with an energy requirement of 1.88 MJ/kg steam (850 Btu/lb steam). Thus the energy cost for zein extraction in a wet milling plant is $0.044/kg zein which corresponds to emissions of 1.54 kg/kg (CO_2/zein) (Leland).

Currently the market price for zein is approximately $8-10/kg depending on grade and purchased quantity. This feedstock price is relatively high compared to petroleum based plastics such as PE which is approximately $1-2/kg. The energy consumption for the raw material acquisition and production of zein is detailed in Fig. 3 and shown on a ‘high’ and ‘low’ assumption. The ‘high’ and ‘low’ assumptions are defined in order to bound the range of possible energy and CO_2 equivalent allocated to the production of zein and SPI which is different from the high and low assumption for the recovery of energy and emissions from waste incineration.

In the ‘high’ assumption all energy of the agricultural activities and the wet milling process is allocated for only zein production and the energy used for producing the co-products is neglected. In the low-assumption, it is assumed that the energy consumption is allocated to all products of the wet milling process proportionally to their weights.

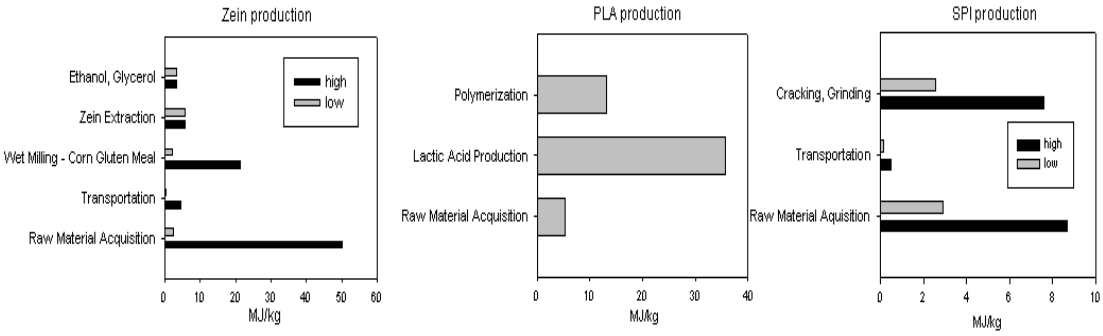

Fig. 3 Energy consumption of zein, PLA and SPI production

This approach is used because there is no published data on energy consumption for the individual co-products of wet milling plants. The majority of the energy in the high-assumption is required for the agricultural harvesting of the corn. Because corn only contains 5% (wt.) zein, the energy required to produce 1 kg of zein requires the acquisition of 20 kg of corn, assuming a 100% efficiency of the zein extraction. Thus, 50 MJ/kg zein is required for raw material acquisition in a high-assumption model. Similarly, the transportation cost of corn is 0.23 MJ/kg, which correspond to 4.6 MJ/kg of zein. The energy consumption for the co-products of the wet milling process is 2.23 MJ/kg. Assuming that zein is 10.7% wt. of the wet milling co-products, this corresponds to 21 MJ/kg of zein, assuming the balance of the co-products have no value. Extraction of zein from corn gluten meal requires 5.9 MJ/kg. In addition, solvents and plasticizers such as ethanol and glycerol must be added to produce zein plastics. The corresponding energy for ethanol and glycerol production is detailed in Fig. 3. The energy demand for the production of ethanol is 11.6 MJ/kg (Shapouri & McAloon 2001). Glycerol is a co-product of the bio-diesel production. The energy allocated for glycerol production is assumed to be 10% of the bio-diesel process, which requires approximately 11 MJ/kg of bio-diesel (Ahmed et al. 1994). Because it is assumed that 10% and 20% of zein on a

weight base of ethanol and glycerol are needed, the energy demand for their production is included in the overall energy consumption of zein plastic products. Because zein is biodegradable it is assumed that it will contribute to methane production in landfills due to microbial decomposition. The environmental benefit of methane recovery would be the amount of methane prevented that reaches the atmosphere, the offset of emissions through the electricity production by incinerating the collected methane and the financial benefit from selling the electricity produced from the incinerated methane.

3.1.2 Soy Protein Isolate (SPI)

The agricultural activities for the production of soy beans require 2.9 MJ/kg of energy with emissions of 0.19 kg CO_2/kg. The growth of the soy plants absorbs 2.84 kg CO2/kg soy bean oil. SPI is extracted from soy beans after several process steps that convert the beans into soy-meal. Because the primary use of soy beans is the production of soybean oil, which is then processed into biodiesel and food grade oil, SPI is derived as a co-product of this process. Soy beans are received at crushing mills in their natural form. Further processing includes crushing to reduce the particle size for improved efficiency of oil extraction. Before crushing the soy beans, they are cleaned and dried. Drying is one of the most energy consuming process steps of the soy bean flaking. Drying, cleaning, and storing require 0.08 MJ/kg (21.3 kWh/ton) of soybeans. In addition 1.11 MJ/kg soy beans (266,275 kcal/ton) are required for the production of the steam that is used for the drying process. In total, this treatment results in an energy consumption of 1.19 MJ/kg dried soy beans.

After the beans are dried, they are cracked and their hulls removed before they are flaked. This causes additional electricity consumption of 21.6 kWh, and energy consumption for steam production of 41,431 kcal per ton, resulting in a total energy consumption of 0.624

MJ/kg soy flakes. After crushing, the oil is extracted from the soy flakes. Most plant designs use an integrated heat system, making it possible to recover the heat from other processes for the evaporation of the hexane, which is used as a solvent to separate the soluble part of the soy bean from the insoluble, the energy demand for this process step being relatively low with 0.0129 MJ/kg which is 3.6 kWh per metric ton. The solvent containing flakes is separated in a de-solventizer-toaster, which removes the hexane by contacting the flakes with open steam. The meal is then ground and prepared for final shipment. Energy requirements for this process are 19.96 kWh per ton for electricity and 133,074 kcal per ton of energy for the steam production. This results in an energy consumption of 0.632 MJ/kg soy meal. In total, 0.53 kg/kg (CO_2/soy meal) are generated from these processes for the electricity and steam production (Sheehan et al. 1998). Additional energy requirements for the recovery of the solvent, as well as the waste treatment, results in an additional 0.075 MJ/kg of soybeans processed. The life cycle steps with their corresponding energy consumption are detailed in Fig. 3. The crushing of soybeans yields 76% soy meal, 17% soybean oil, and 7% waste. The protein content of the soy meal is approximately 44%. Thus, the energy consumption for this process is approximately 16.75 MJ/kg SPI. The energy consumption is shown in 'high' and 'low' assumptions, as it was detailed for the production of zein. However, the life cycle inventory for SPI is incomplete, as the data for energy consumption and emission generation for the process step that yields pure soy protein isolate is not available to our knowledge. For producing SPI, the protein part of the soy meal can be extracted with warm water at a pH of approximately 8.5. The soluble protein fraction is separated from the insoluble part by centrifugation (Kumar et al. 2002). These process steps cause additional energy consumption as well as emissions that need to be added to the final energy and emission balance in future studies. Because SPI plastic is currently not

commercially available, large scale recycling would interrupt the existing recycling systems of traditional plastics. Thus, landfilling is assumed to be the only option of waste treatment. The cost of landfill is assumed to be $0.24/kg. Because SPI is biodegradable it can be assumed that it will contribute to methane production in landfill due to microbial decomposition.

3.1.3 Polylactic acid (PLA)

PLA is a commercially available biodegradable plastic based on corn starch. It has superior mechanical properties compared to zein and SPI plastics. Detailed life cycle inventories of PLA can be found in (ESTO 2005). The energy consumption and emission generation were reported to be at least 19 MJ/kg and 1.0 kg CO_2 lower for PLA compared to a non degradable counterpart with similar properties and applications. The energy requirement to produce PLA is 54 MJ/kg. End product treatment options for PLA are landfilling, and landfilling with methane recovery as detailed for zein and SPI and will be assumed to be the same as for zein and SPI plastics. Recycling is a possible end product treatment option, but because of the relatively low amount of PLA used, recycling is not yet applicable. The benefits of solid waste incineration of PLA are calculated with an estimated contribution of 0.1% to the heat value of waste and shown in Table 2.

3.1.4 Polyethylene (HDPE)

Data sources for the life cycle inventory of PE were (RMIT 1998, Worrel et al. 2000, Harding et al. 2007). In (RMIT 1998) nine different life cycle inventories of PE were compared which show that the energy consumption for PE for the raw material acquisition and polymerization is between 62 and 72 MJ/kg. In addition the energy for the polymerization was found to be between 2.8 and 13.6 MJ/kg depending of the process and feedstock energy allocation. In a ‘Cradle to Grave Analysis’ for plastic production

conducted by (Gerngross and Slater 2000) the total energy requirements for HDPE production was found to be 80 MJ/kg (49 MJ for feedstock energy and 31 MJ for process energy). The greenhouse gas emission of the HDPE production is estimated to be 1.8 kg/kg (CO_2/plastic) from cradle to factory gate. Additionally 3.1 kg CO_2-equivalent are chemically stored in the polymer. In total, 4.9 kg CO_2-equivalent are set free during the raw material acquisition and production of this plastic. Considering the option of energy recovery through incineration of plastic waste, the total amount of CO_2 emissions is 2.8 kg/kg (CO_2/plastic), because a part of CO_2 would be saved when PE is burned for electricity production instead of fossil fuels (Patel et al. 2003). In an environmental life cycle comparison of the production of a biodegradable plastic with typical petrochemical plastics, it was shown that for LDPE and HDPE, 80 MJ/kg and 81MJ/kg of energy are required from cradle to grave (Akiyama et al. 2002). In addition, it was reported that 1.9 and 1.8 kg/kg (CO_2/plastic) are emitted for LDPE and HDPE from cradle to factory gate (USDE 2007). Because polyethylene is a widely used plastic material with an existing infrastructure of recycling facilities, material recovery is a typical end product treatment option. Assuming a recycling rate of r=0.3, an energy coefficient of energy consumption of recycled compared to virgin material production of e=0.62, and a CO_2 emission coefficient of recycled compared to virgin material production of c=0.54 as reported in (Korhonen & Dahlo 2007), the energy saved and emission prevented can be calculated according to eq. (3) and (4). The results for energy and emission saving through recycling are shown in a case study for different recycling, energy and emission saving rates in Table 1. The degradation process of polyethylene is relatively time-consuming compared to the biodegradable materials and takes several hundred years until it is completed. Thus, landfill and MSWI are two options of waste abatement for HDPE. The landfill costs are assumed to be approximately $240/ton of waste but can vary locally. The energy

recovered by incineration can be estimated based on the assumption that 5.4% of the energy content of MSW is from HDPE and that each kg waste burned can produce 0.5-0.6 kWh of electricity (USDE 2007). Based on these assumptions, through the incineration of HDPE for electricity production, the reduction in CO_2-emissions, the fiscal benefit of HDPE incineration and the energy recovery per kg waste burned are shown in (PAS 2050).

3.1.5 Polystyrene (PS)

Polystyrene has cradle to grave energy requirements of 87 MJ/kg. The greenhouse gas emissions generated during the production of PS are reported as 2.5 kg CO_2/kg (ESTO 2005, CRMD 2006). A detailed life cycle inventory of PS can be found in (Boustead 2006). End product treatment options for PS are landfillling, recycling and energy recovery through incineration, while the contribution to the heat value of MSW is approximately 4% (USDE 2007). The results of energy consumption, emission generation, costs, energy and emission saving through recycling are detailed in Fig. 1 to Fig. 7 and Table 1 and Table 2.

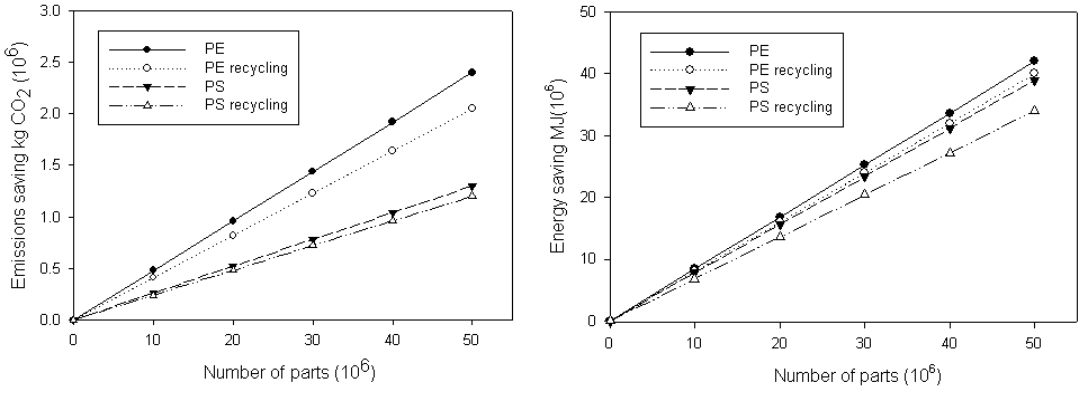

Fig. 4 Energy and emission savings as a function of number of produced parts recycled

3.2 Processing Costs

The costs of manufacturing include: (1) the costs of extrusion and (2) the cost-estimate of a net-shape forming processes such as injection molding. The cost of manufacturing is calculated by using an 'Economic Engineering Approach'. This approach includes three basic aspects: (1) costs of a processing plant; (2) estimating manufacturing rate and parameters; and (3) calculation of the processing costs 'per part' ($/part) or 'per unit' ($/kg). However, because SPI and zein need to be extruded and pelletized before they can be shaped into a product, these additional processing costs must be included into their cost per part calculation. The final cost of extrusion is calculated on a per mass basis ($/kg) according to eq. (9).

$$C_{unit} = \frac{C_{equip} + C_{el} + C_{maint}}{M} \qquad (9)$$

where: C_{unit}: cost of material on a 'per unit' ($/kg) base; C_{equip}: cost of process equipment including a mixer, extruder and pelletizer; C_{el}: cost of electricity to produce one unit of plastic product; C_{maint}: maintenance cost; M: amount of material. The final cost of injection molded parts are calculated on a per part basis ($/part) according to eq. (10):

$$C_{part} = C_{proc} + C_{mat} + C_{tool} \qquad (10)$$

where: C_{part}: cost of one part ($/part); C_{proc}: cost of processing one part; includes a injection molding machine, a grinder, the cost to run the equipment which includes maintenance cost, cost of electricity; C_{tool}: cost of a injection molding tool; C_{mat}: cost of material on a 'per unit' base. With all required equipment related to a production process

such as injection molding, the cost per part was calculated for each plastic type as it is shown in Fig. 5.

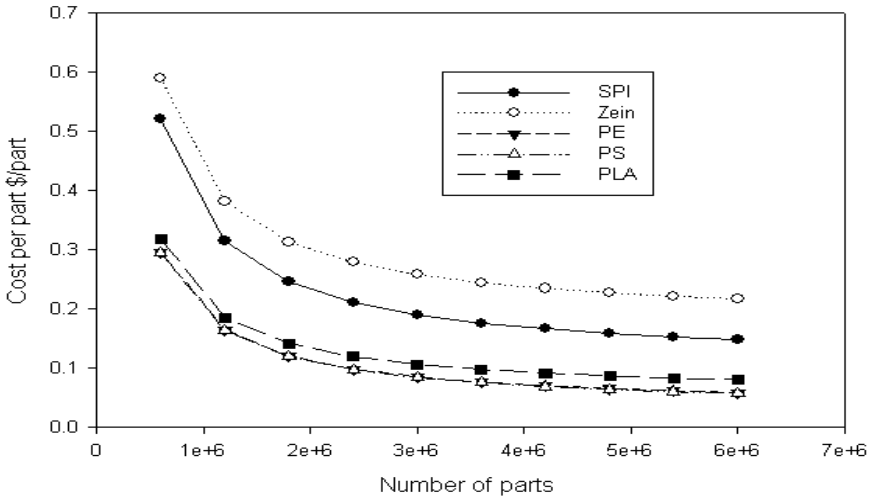

Fig. 5 Cost per part

Fig. 5 shows the corresponding costs structure of a high- and low production volume for PE and zein. It can be seen, that the cost structure changes as the production volume increases. On a ‘low’ production volume of PE parts, the ‘Material costs‘ are the major contributor to the cost per part, while on a ‘high’ production volume the ‘Processing costs‘ are most expensive. However for the bio-plastic zein the cost structuree is different. While the ‘Processing costs‘ are most expensive on a ‘low’ production volume, the cost structure inverts for the ‘high’ production volume. As the number of parts produced increases the ‘Material costs‘ become the dominating cost factor.

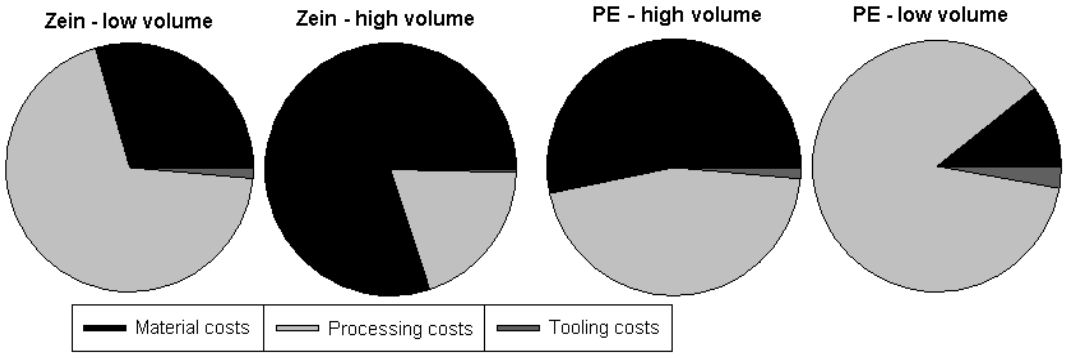

Fig. 6 Cost structure showing the relative costs of on a low and high production volume

4 Discussion

The energy demand and emissions generated during the production of the plastics are detailed in Fig. 7. It is seen that the energy consumption and emissions are relatively low for SPI and zein in the 'low' model. However, in the 'high' assumption model, the production of zein consumes significantly more energy. The energy consumption of the production of SPI is also relatively high in the 'high' assumption model, but still significantly lower compared to zein. This difference is because the protein content of soy beans (34%) is higher than corn grains (5%). It is important to note that the energy consumption of the protein extraction from spy meal was not included because of a lack of information about that process. The recovery of energy and emission savings through waste incineration depend of the heat content as well as the average amount of each plastic in solid waste. Assuming that bio-plastics will play a more important role in the future, their beneficial effect of the end product treatment can be calculated once their contribution to the energy content of solid waste as well as their beneficial effect of recycling has been determined.

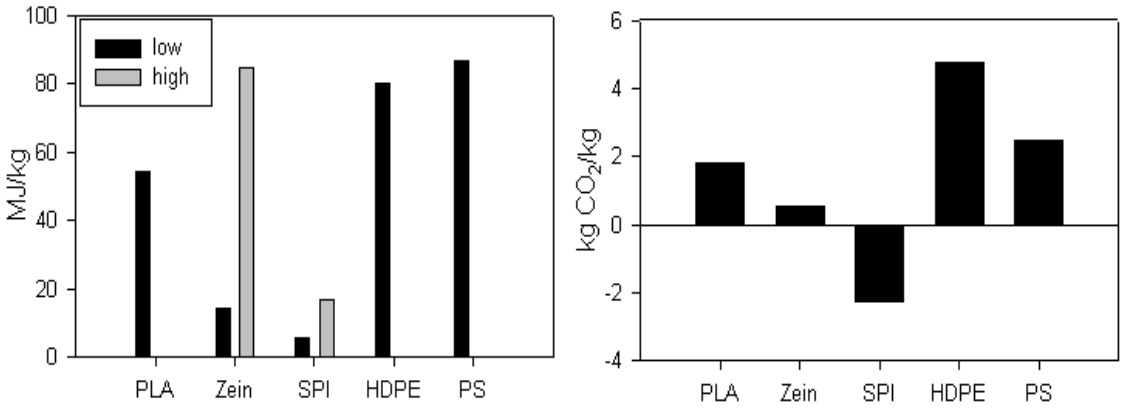

Fig. 7 Energy consumption with high and low assumption for zein and SPI and CO_2-emissions of plastic production

Table 1 details one of several sensitivity analysis that was conducted on our model to validate its predictions. In this analysis, the reduction in energy consumption and GWP is calculated for a given energy and emission saving rate as well as recycling rate following Eq. (1) to (4). For an increasing recycling rate the energy consumption and GWP is reduced. For increasing emission and energy saving rate the GWP and the energy consumption are increased.

Table 1 Sensitivity analysis of recycling; r - recycling rate, c - emissions, e - energy saving rate

Energy saving [MJ/kg] CO_2 savings [kg/kg]		r=0.1		r=0.3		r=0.5		r=0.7	
		PS	PE	PS	PE	PS	PE	PS	PE
Energy	e=0.1	7.83	7.2	23.49	21.6	39.15	36	54.81	50.4
CO_2	c=0.15	0.221	0.41	0.66	1.22	1.11	2.04	1.55	2.86
Energy	e=0.4	5.22	4.8	15.66	14.4	26.1	24	36.54	33.6
CO_2	c=0.45	0.143	0.26	0.43	0.79	0.72	1.32	1	1.85
Energy	e=0.7	2.61	2.4	7.83	7.2	13.05	12	18.27	16.8
CO_2	c=0.75	0.065	0.12	0.19	0.36	0.33	0.6	0.46	0.84

Table 2 details a sensitivity analysis for an increasing incineration efficiency of MSWI comparing PE, PS, PLA and zein. It is important to note that the contribution to the heat value of waste of zein and PLA is not known and estimated to be 0.001 and 0.1% because

of the low amount of these materials in the solid waste stream. The energy and emission savings are calculated with Eq. (5) and (6), the fiscal benefit with Eq. (7). The table shows that the materials which contribute most to the heat value of waste also have the highest potential of energy and emissions saving through incineration. For example, because zein and PLA do not contribute a significant amount of heat energy to the value of waste, there is also less potential energy saved and emissions avoided.

The cost analysis shows that the limiting factor of bio-plastics remains to be the high feedstock price. By increasing their production capacity the relative costs of bio-plastics can be decreased, making them more competitive to established petroleum based plastics. In detail, the 'cost per part' model shows that the protein based plastics are initially relatively expensive. However, a tenfold increase in their production capacity reduces the piece price to approximately one third at fixed unit price for the materials (see Fig. 5) and also reduces the absolute difference in the price structure. Comparing the relative cost structure of parts produced in high and low volumes from zein and PE as shown in Fig. 6, it is seen that the material price of zein is a major cost factor on the high production volume resulting in approximately 80% of the cost of one part, while it is only 55% for PE.

Table 2 Sensitivity analysis of MSWI for increasing incineration efficiency, 12MJ/kg average heat value of MSW

	PE			PS			PLA			Zein		
Contribution to heat value of MSW [%]	4.2			1.6			0.1			0.001		
Incineration efficiency [%]	0.25	0.35	0.45	0.25	0.35	0.45	0.25	0.35	0.45	0.25	0.35	0.45
Energy recovery [MJ/kg]	0.13	0.18	0.23	0.05	0.07	0.09	0.003	0.004	0.005	0.00003	0.00004	0.00005
Emission recovery [kg CO_2/kg]	0.03	0.045	0.006	0.01	0.02	0.03	0.008	0.001	0.001	0.000008	0.000011	0.00001
Fiscal benefit [$/kg]	0.0028	0.004	0.005	0.001	0.002	0.002	0.00007	0.00009	0.0001	$6.6*10^{-7}$	$9.33*10^{-7}$	0.000001

5 Perspectives

The 'Carbon Footprint' of plastics in general can be improved by factors, such as an increase in the recycling rate which would decrease the CO_2 emissions and energy consumption of the plastic production. The high price for zein and SPI will prevent their commercial breakthrough as long as they are not competitive to petroleum based plastics. Until now zein and SPI have appeared only as co-products of the ethanol and bio-diesel industry. With an increasing production of corn ethanol and bio-diesel from soy beans, large quantities of non-food grade zein and SPI will be available with an expected decrease of their price. Thus, finding new applications as well as improvements in the material science of bio plastics should be promoted.

Acknowledgement

USDA - Office of Energy Policy and New Uses and USDA - Bio-Preferred program

References

Ahmed I, Decker J, Morris D (1994), How much energy does it take to make a gallon of soydiesel, Institute for Local Self Reliance, Minneapolis

Akiyama M, Takeharu T, Yoshiharu D (2002) Environmental life cycle comparison of Polyhydroxyalkanoates produced from renewable carbon resources by bacterial fermentation, Polym. Degrad. Stab. vol. 80: 183-194

Bohlmann GM (2004) Biodegradable packaging life-cycle assessment, Environ. Prog. 23(4): 342-346

Boustead I (2006) Eco-profiles of the European Plastics Industry, Polystyrene, Plastics Europe

CRMD - Canadian Raw Materials Database- Life cycle inventory of the manufacture of general purpose polystyrene (2006) http://crmd.uwaterloo.ca/crmd/data.html

Dornburg V, Faaij A, Patel M, Turkenburg W (2006) Economics and GHG emission reduction of a PLA bio-refinery system - Combining bottom-up analysis with price elasticity effects, Resour. Conserv. Recycl. 46 (4): 377-409

EPA (2000) U.S. Environmental Protection Agency, Landfill Methane Recovery

EPA (2007) U.S. Environmental Protection Agency, Inventory of U.S. Greenhouse Gas Emissions and Sinks

EPA (2008) U.S. Environmental Protection Agency, Municipal Solid Waste (MSW), www.epa.gov/garbage/recycle.htm#figures

EPA U.S. Environmental Agency, Benefits of LFG Energy, www.epa.gov/lmop/benefits.htm

ESTO (2005) European Science and Technology Observatory, Institute for Prospective Technological Studies, Techno-economic feasibility of large-scale production of bio-based polymers in Europe, EUR 22103 EN

Ekvall T, Tillman AM (1997) Open-loop recycling: Criteria for allocation procedures, Intl. J. Life Cycle Assess. 2(3): 155-162

Gerngross TU, Slater SC (2000) How green are plastics, Scientific American, 283:36

Harding KG, Dennis JS, von Blottnitz H, Harrison STL (2007) Environmental analysis of plastic production processes: Comparing petroleum-based polypropylene and polyethylene with biologically-based poly-hydroxybutyric acid using life cycle analysis, J. Biotechnol. 130: 57-66

Hermann B, Blok K, Patel M (2007) Producing bio-based bulk chemicals using industrial biotechnology saves energy and combats climate change, Environ. Sci. Technol. 41(22): 7915-7921

IPCC (2007) Internationa Panel on Climate Change, IPCC Fourth Assessment Report: Climate Change 2007, www.ipcc.ch

Korhonen M, Dahlbo H (2007), Reducing greenhouse gas Emissions by recycling plastics and textiles into products, The Finnish Environment Institute

Kumar R, Choudhary V, Misha S, Varma I, Matttison B (2002) Adhesives and plastics based on soy protein products, Ind. Crops Prod. 16, 155-172

Leland, Email communication with Dickey Leland, Agricultural Research Service, U.S. Department of Agriculture

McDougall F, White P, Franke M, Hindle P (2001) Integrated solid waste management: A life cycle inventory, 2nd Edition, Blackwell Science Ltd.

Middleton M, Elam E, Holt G, Laird W (2001), Preliminary estimates of the cost of extrusion processing of cotton gin by-product as a livestock feed, Proceedings of the Beltwide Cotton Conference, 1: 266-270

PAS 2050 (2008) Assessing the life cycle greenhouse gas emissions of goods and services, British Standards BSI

Pandey JK, Kumar AP, Misra M, Mohanty AK, Drzal LT, Singh R (2005) Recent advances in biodegradable nanocomposites, J. Nanosci. Nanotechnol. vol. 5 (4): 497-526

Patel M, Bastioli C, Marini L, Würdinger E (2003), Environmental assessment of bio-based polymers and natural fibers, Utrecht University, Department of Science Technology and Society (STS), Novamont, Novara, Italy, Bavarian Institute of Applied Environmental Research and Technology (BIFA), Augsburg, Germany

Porter R (2002) The economics of waste, RFF press, Washington

Profu (2004) Evaluating waste incineration as treatment and energy recovery method from an environmental point of view, www.profu.se

RMIT (1998), A Life Cycle Inventory project of the PE production in Australia conducted by the Center of Design at the 'Royal Melbourne Institute of Technology' (RMIT) University

Shapouri H, McAloon A (2001) The 2001 net energy balance of corn-ethanol, U.S. Department of Agriculture (USDA), Office of the Chief Economist (OCE), Washington, D.C., Andrew McAloon, USDA/Agricultural Research Service (ARS), Wyndmoor, PA. 19038

Sheehan J, Camobreco V, Duffield J, Graboski M, Shapouri H (1998) Life cycle inventory of biodiesel and petroleum use in urban bus, US Department of Agriculture, US Department of Energy

Spokas K, Bogner J, Chanton JP, Morcet M, Aran C, Graff C, Golvan, YM, Hebe I (2006) Methane mass balance at three landfill sites: what is the efficiency of capture by gas collection systems, Waste Management 26(5): 516-525

USDE (2005) U.S. Department of Energy, Renewable Energy Annual 2005, Energy Information Administration

USDE (2007) U.S. Department of Energy, Methodology for Allocating Municipal Solid Waste to Biogenic and Non-Biogenic Energy, Energy Information Administration Office of Coal, Nuclear, Electric and Alternate Fuels

USDE (2008) Electric Power Annual 2008, U.S. Department of Energy, Energy Information Administration, Office of Coal, Nuclear, Electric and Alternate Fuels, DOE/EIA-0348

USEPA (2006) Municipal solid waste in the United States: 2005 Facts and figures, United States Environmental Protection Agency, Office of Solid Waste

Vlad M, Srinivasan G, Grewell D, Jane J (2007) Improvement of the mechanical properties of soy protein isolate-based plastics through formulation and processing, Int. Polym. Proc. vol. 12(5) 489-496

Wang M, (2005) Energy and greenhouse gas emissions effects of fuel ethanol, Center for Transportation Research, Argonne National Laboratory

Williams PT (2005) Waste Treatment and Disposal, John Wiley and Sons, Chichester, England

Worrel E, Phylipsen D, Einstein D, Martin N (2000) Energy Use and Energy Intensity of the U.S. Chemical Industry, Energy Analysis Department, Environmental Energy Technologies Division, Ernest Orlando Lawrence Berkeley National Laboratory, LBNL-44314

General Conclusions

Ultrasonic as well as impulse welding of PLA are effective welding processes when the proper parameter combinations are chosen. It was demonstrated that in both processes, the weld time had the strongest impact on the weld factor. While ultrasonic welding can be completed with cycle times as short as 0.15 s, significantly more time is required to create the same weld strengths in impulse welding. In detail impulse welding requires approximately 0.5 s and for film thicknesses at 25 µm and 4 s for 300 µm thick films.

Thermal and optical characterization of the material shows, that heat treatment of PLA 'erased' the physical aging and increases the weld strength as well as the base strength of the material. The annealing process also allows the polymer chains to form spherulites in the weld zone that increase the crystallinity of the material.

In ultrasonic cutting of PLA is was shown that the angle of the cutting blade effects cutting process. In general it can be reasoned that the smaller the angle the higher the cutting efficiency. In addition it was shown that ultrasonic welding and cutting simultaneously is possible.

By calculating the activation energy of diffusion in PLA it was possible to identify a predictive equation that can be used to calculate the degree of welding. However, because the predictive equation is only applicable in a narrow temperature range at one pressure, the effect of temperature, time and pressure on the diffusion in PLA during the welding process was not fully understood. Future research should focus on the effect and interrelation of combinations of all three parameters on the diffusion process.

A holistic energetic as well as emission related model for plastic parts covering the entire life cycle from material production to waste disposal was introduced that allows the user to compare bio-plastics to petroleum based from a environmental point of view. This approach allows different user groups ranging from material supplier, manufacturer of plastic parts to end of life management to compare bio-plastics to their petrochemical counterparts in terms of energy consumption, greenhouse gas emissions and costs throughout their entire life cycle. In addition to that the life cycle energy and emissions of zein and SPI, which are relatively new bio-plastics were collected.